NON-INVASIVE MONITORING OF INTRACRANIAL PRESSURE USING TRANSCRANIAL DOPPLER ULTRASONOGRAPHY

Danilo Augusto Cardim

Supervisor: Professor Marek Czosnyka

St. Catharine's College

University of Cambridge

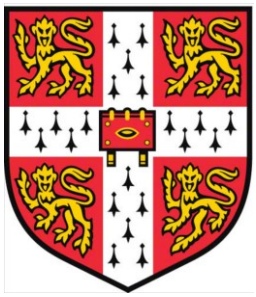

September 2017

This dissertation is submitted for the degree of Doctor of Philosophy

Preface

This dissertation is the result of my own work and includes nothing which is the outcome of work done in collaboration except as declared in the Preface and specified in the text.

This dissertation is not substantially the same as any that I have submitted, or, is being concurrently submitted for a degree or diploma or other qualification at the University of Cambridge or any other University or similar institution except as declared in the Preface and specified in the text. I further state that no substantial part of my dissertation has already been submitted, or, is being concurrently submitted for any such degree, diploma or other qualification at the University of Cambridge or any other University or similar institution except as declared in the Preface and specified in the text.

This dissertation does not exceed the word limit of 60,000 words.

The choices we make, not the chances we take, determine our destiny.

Dedicated to my mother,

Célia

TABLE OF CONTENTS

SUMMARY

Intracranial pressure (ICP) is an important monitoring modality in the clinical management of several neurological diseases carrying the risk of fatal intracranial hypertension (ICH). However, this parameter is not always considered due to its invasive assessment. In this scenario, a non-invasive estimation of ICP (nICP) may be essential, and indeed it has become a Holy Grail in Clinical Neurosciences: extensively searched, albeit never found. This thesis is devoted to the assessment, applications and development of transcranial Doppler (TCD)-based non-invasive methods for ICP and cerebral perfusion pressure (CPP) monitoring.

The thesis is divided into three sections:

I) The accuracy of existing TCD-based nICP estimators in various scenarios of varying ICP (traumatic brain injury (TBI), rise of ICP during plateau waves, and rise in ICP induced by infusion of cerebrospinal fluid (CSF) during infusion test). The estimators of nICP consisted of a mathematical black box model, methods based on non-invasive CPP, and a method based on TCD pulsatility index.

II) The feasibility of the best performing nICP estimator in clinical practice, including patients with closed TBI and brain midline shift, patients with acute liver failure during liver transplant surgery, and patients during non-neurosurgical surgery in the beach chair position.

III) The description and assessment of a novel methodology for non-invasive assessment of cerebral perfusion pressure (nCPP).

The accuracy studies indicated that the black box model had the best performance to estimate ICP in TBI patients, and the overall confidence interval for ICP prediction presented by the TCD-based nICP methods was estimated around 10 mmHg. During infusion tests, ICP changes were estimated with only moderate correlations, and vasogenic components of ICP, like increases in cerebral blood volume, were better estimated with TCD-based nICP methods than the component related to increased CSF circulation during infusion test. During plateau waves, the nICP methods were remarkably accurate to replicate relative changes in ICP in the time domain, presenting correlations with direct ICP ranging from 0.62-0.80. Furthermore, they presented high performance to rule out intracranial hypertension and identify ICP changes of vasogenic origin during plateau waves, presenting prediction abilities around 80%.

For the feasibility studies, only the black box estimator was assessed since it provided the best estimation performance. It could identify an interhemispheric pressure gradient in TBI patients with closed head injury presenting midline shift, demonstrating that a greater CPP at the site of brain expansion was the driving force generating the pressure gradient. In patients with acute liver failure, different patterns of cerebral haemodynamics could be identified non-invasively during transplant surgery using a TCD-derived multiparameter approach englobing nICP, nCPP, and other cerebral haemodynamics parameters. The results indicated normal ICP and decreasing CPP during the procedure and an alteration of cerebral blood flow autoregulation. Also applying a multiparameter approach, the assessment of patients undergoing surgery in the beach chair position demonstrated significant cerebral haemodynamics changes in individuals with no indications of previous neurological impairment. The findings suggested that this surgical setting caused an alteration of cerebral haemodynamics, especially decrease in estimated CPP and impairment of cerebral autoregulation.

The new method of nCPP estimation was based on spectral arterial blood volume accounting. It could identify changes in CPP across time reliably in conditions of decreasing and increasing CPP. It also presented a reasonable prediction ability to detect changes in CPP, with values around 70% for positive prediction power.

These findings support the use of TCD-based nICP methods in a variety of clinical conditions requiring management of intracranial pressure and brain perfusion. Moreover, the low costs associated with nICP methods, since TCD is a widely available medical device, could contribute to its widespread use as a reliable alternative for ICP monitoring in everyday clinical practice. New methodologies should be tried and further developed (such as machine learning, artificial intelligence) since the absolute accuracy of estimation still needs improvement.

ACKNOWLEDGEMENTS

I would like to thank my supervisor Professor Marek Czosnyka. I am indebted and grateful for the opportunity of having me under his supervision, and for his many efforts and time invested in this project and my academic career. Here, I would also like to thank Professor Sérgio Mascarenhas, for his early mentorship in my life and for providing me with support and inspiration in my academic career.

I am grateful to Dr Peter Smielewski, for providing me with fundamental support regarding research software used for the development of this thesis and for contributing to my studies with constructive ideas.

I would also like to thank Dr Bernhard Schmidt for his fundamental support on the development of this thesis and for critically reviewing my studies.

I would like to thank Dr Zofia Czosnyka for teaching me how to conduct cerebrospinal fluid infusion tests and for contributing to my studies. I would also like to thank for her kind support over these years.

I would like to thank my colleagues from the Brain Physics Laboratory for their friendship and for the many fruitful collaborations and discussions over the years, Chiara Robba, Joseph Donnelly, Manuel Cabeleira, Xiuyun Liu, Brenno Cabella, Cristine Sortica, Georgios Varsos, Dr Christina Haubrich, Aphroditi Lalou, Leanne Calviello, Dr Maxwell Damian.

I am grateful for the constant support and encouragement from my friends Samuel Beserra, Ligia Kiyuna, Dr Gustavo Frigieri and Ligia Gomiero.

I would like to thank the Cambridge Commonwealth, European & International Trust, University of Cambridge for the financial support.

Finally, I would like to thank my family, Célia, Valter, Adélia, Ana Carolina, Lucas, Manuela, Evandro, for understanding my absence and for their constant motivation and support in the search for my dreams and goals in life. ***Muito obrigado***!

LIST OF PUBLICATIONS

This is a current list (September, 2017) of manuscripts and presentations which have resulted from the work performed during the development of this thesis.

Papers published

Cardim, D., Robba, C., Donnelly, J., Bohdanowicz, M., Schmidt, B., Damian, M., Varsos, G. V, Liu, X., Cabeleira, M., Frigieri, G., Cabella, B., Smieleweski, P., Mascarenhas, S., and Czosnyka, M. (2015). Prospective study on non-invasive assessment of ICP in head injured patients: comparison of four methods. J. Neurotrauma.

Cardim, D., Czosnyka, M., Donnelly, J., Robba, C., Cabella, B.C.T., Liu, X., Cabeleira, M.T., Smielewski, P., Haubrich, C., Garnett, M.R., Pickard, J.D., and Czosnyka, Z. (2016). Assessment of non-invasive ICP during CSF infusion test: an approach with transcranial Doppler. Acta Neurochir. (Wien). 158, 279–87.

Cardim, D., Robba, C., Bohdanowicz, M., Donnelly, J., Cabella, B., Liu, X., Cabeleira, M., Smielewski, P., Schmidt, B., and Czosnyka, M. (2016). Non-invasive Monitoring of Intracranial Pressure Using Transcranial Doppler Ultrasonography: Is It Possible? Neurocrit. Care.

Cardim, D., Schmidt, B., Robba, C., Donnelly, J., Puppo, C., Czosnyka, M., and Smielewski, P. (2016). Transcranial Doppler Monitoring of Intracranial Pressure Plateau Waves. Neurocrit. Care , 1–9.

Manuscripts in submission

Cardim, D., Robba, C., Schmidt, B., Donnelly, J., Schmidt, E.A., Bohdanowicz, M., Smielewski, P., Czosnyka, M.: Midline shift in patients with closed traumatic brain injury may be driven by cerebral perfusion pressure not intracranial pressure. **Journal of Neurological Research (2017).**

Cardim, D., Klinck, J., Robba, C., Schmidt, B., Donnelly, J., Schmidt, E.A., Smielewski, P., Czosnyka, M.: Transcranial Doppler non-invasive assessment of intracranial pressure, autoregulation of cerebral blood flow and critical closing pressure during orthotopic liver transplant. **Liver Transplantation (2017).**

Cardim, D., Robba, C., Matta, B., Tytherleigh-Strong, G., Kang, N., Schmidt, B., Donnelly, J., Calviello, L., Smielewski, P., Czosnyka, M. Cerebrovascular assessment of patients undergoing shoulder surgery in beach chair position using a multiparameter transcranial Doppler approach. **British Journal of Anaesthesia (2017).**

Cardim, D., Varsos, G.V., Uryga, A., Kaczmarska, K., Robba, C., Calviello, L., Bohdanowicz, M., Kasprowicz, M., Schmidt, B., Smielewski, P., Steiner, L.A., Czosnyka, M.: Spectral cerebral blood volume accounting for non-invasive estimation of changes in cerebral perfusion pressure using transcranial Doppler ultrasonography. **Physiological Measurement (2017).**

Conference presentations

Cardim, D., Cabella, B., Donnelly, J., Robba, C., Czosnyka, M., Garnett, M., Pickard, J.D., Czosnyka, Z.: Non-invasive assessment of ICP during infusion test using Transcranial Doppler Ultrasonography. Fluids and Barriers of the CNS 09/2015; 12 (Suppl 1): P6.

Cardim, D., Schmidt, B., Robba, C., Donnelly, J., Cabella, B., Liu, X., Cabeleira, M., Bohdanowicz, M., Smielewski, P., Czosnyka, M.: Transcranial Doppler Non-invasive Assessment of ICP During Intracranial Hypertension of Vasogenic Origin. 16th International Symposium on Intracranial Pressure and Neuromonitoring, Cambridge, MA, USA, 2016.

Cardim, D., Robba, C., Tytherleigh-Strong, G., Donnelly, J., Smielewski, P., Schmidt, B., Matta, B., Czosnyka, M.: The Effects of the Beach-chair Position on Cerebral Haemodynamics and Non-invasive ICP in Patients Undergoing Shoulder Surgery. 16th International Symposium on Intracranial Pressure and Neuromonitoring, Cambridge, MA, USA, 2016.

Co-authored publications

Robba, C., Cardim, D., Tajsic, T., Pietersen, J., Bulman, M., Donnelly, J., Lavinio, A., Gupta, A., Menon, D., Czosnyka, M. Ultrasound non-invasive measurement of intracranial pressure in neurointensive care: a prospective observational study. PLOS Medicine 07/2017 14(7): e1002356.

Robba, C., Cardim, D., Donnelly, J., Bertuccio, A., Bacigaluppi, S., Bragazzi, N., Cabella, B., Liu, X., Matta, B., Lattuada, M., Czosnyka, M.: Effects of pneumoperitoneum and Trendelenburg position on intracranial pressure assessed using different non-invasive methods. British Journal of Anaesthesia 09/2016.

Robba, C., Cardim, D., Sekhon, M., Budohoski, K., Czosnyka, M. Transcranial Doppler: a stethoscope for the brain - neurocritical care use. Journal of Neuroscience Research (in press).

Robba, C., Bacigaluppi, S., Cardim, D., Donnelly, J., Bertuccio, A., Czosnyka, M.: Non-invasive assessment of intracranial pressure. Acta Neurologica Scandinavica 10/2015.

Liu, X., Maurits, N.M., Aries, M.J.H., Czosnyka, M., Ercole, A., Donnelly, J., Cardim, D., Kim, D.J., Dias, C., Cabeleira, M., Smielewski, P: Monitoring of optimal cerebral perfusion pressure in traumatic brain injured patients using a multi-window weighting algorithm. Journal of Neurotrauma 05/2017.

Liu, X., Donnelly, J., Czosnyka, M., Aries, M.J.H., Brady, K., Cardim, D., Robba, C., Cabeleira, M., Kim, D.J. Haubrich, C., Smielewski, S.: Cerebrovascular Pressure Reactivity Monitoring Using Wavelet Analysis in Traumatic Brain Injury Patients: A Retrospective Study. PLOS Medicine 07/2017 14(7): e1002348.

Donnelly, J., Czosnyka, M., Adams, H.A., Robba, C., Steiner, L.A., Cardim, D., Cabella, B., Liu, X., Ercole, A., Hutchinson, P., Smielewski, P.: Individualising thresholds of cerebral perfusion pressure using estimated limits of autoregulation. Critical Care Medicine, Volume 45(9), September 2017, p 1464–1471.

Cabella, B., Donnelly, J., Cardim, D., Liu, X., Cabeleira, M., Smielewski, P., Haubrich, C., Hutchinson, P. Kim, D.J. Czosnyka, M.: An Association Between ICP-Derived Data and Outcome in TBI Patients: The Role of Sample Size. Neurocritical Care 11/2016.

Donnelly, J., Czosnyka, M., Harland, S., Varsos, G.V., Cardim, D., Robba, C., Liu, X., Ainslie, P.N., Smielewski, P.: Cerebral haemodynamics during experimental intracranial hypertension. Journal of Cerebral Blood Flow & Metabolism 03/2016; 37(2).

Robba, C., Bragazzi, N.L., Bertuccio, A., Cardim, D., Donnelly, J., Sekhon, M., Lavinio, A., Duane, D., Burnstein, R., Matta, B., Bacigaluppi, S., Lattuada, M., Czosnyka, M.: Effects of Prone Position and Positive End-Expiratory Pressure on Non-invasive Estimators of ICP: A Pilot Study. Journal of Neurosurgical Anesthesiology 02/2016.

Robba, C., Bacigaluppi, S., Cardim, D., Donnelly, J., Sekhon, M., Aries, M.J.A., Mancardi, G., Booth, A., Bragazzi, N.L., Czosnyka, M., Matta, B.: Intraoperative non-invasive intracranial pressure monitoring during pneumoperitoneum: a case report and a review of the published cases and case report series. Journal of Clinical Monitoring and Computing 09/2015.

Robba, C., Donnelly, J., Bertuetti, R., Cardim, D., Sekhon, M., Aries, M.J.A., Smielewski, P., Richards, H., Czosnyka, M.: Doppler Non-invasive Monitoring of ICP in an Animal Model of Acute Intracranial Hypertension. Neurocritical Care 08/2015; 23(3).

DISTINCTIONS

This is a current list (September, 2017) of scholarship and grants that have been awarded for the work performed as part of this thesis.

Scholarship

Cambridge Commonwealth, European & International Trust Scholarship, University of Cambridge (2014-2017).

Grants

1. St. Catharine's College, Travel and Research Grant, University of Cambridge (2015);

2. St. Catharine's College, Travel and Research Grant, University of Cambridge (2016);

3. NIHR Brain Injury Healthcare Technology Cooperative, Cambridge, UK, Travel Grant (2016).

LIST OF FIGURES

LIST OF TABLES

LIST OF EQUATIONS

Equation 2.1, page 29

Cerebral blood flow velocity derived from transcranial Doppler ultrasonography

$$v = \frac{(c \times f_d)}{2 \times f_0 \times \cos\theta} \quad (cm/s)$$

Equation 3.1, page 40

Non-invasive cerebral perfusion pressure estimation per Aaslid et al. [67]

$$nCPP_{Aaslid} = (FV_m/f1) \times a1 \ \ (mmHg)$$

Equation 3.2, page 41

Linear regression determined for $nCPP_{Aaslid}$ estimation

$$CPP = 1.1\ nCPP_{Aaslid}\text{-}5 \ \ (mmHg)$$

Equation 3.3, page 43

Non-invasive cerebral perfusion pressure estimation per Edouard et al. [74]

$$nCPP_{Edouard} = \left(\frac{FV_m}{FV_m\text{-}\ FV_d}\right) \times (ABP_m\text{-}ABP_d) \ \ (mmHg)$$

Equation 4.1, page 67

Transcranial Doppler-derived pulsatility index per Gosling et al.[49]

$$PI = \frac{FV_s\text{-}FV_d}{FV_m} \ \ (a.u.)$$

Equation 4.2, page 68

Critical closing pressure per Varsos et al.[81]

$$CrCP = ABP\text{-}\ \frac{ABP}{\sqrt{(CVR \cdot C_a \cdot HR \cdot 2\pi)^2 + 1}} \ \ (mmHg)$$

Equation 4.3, page 68

Non-invasive approximation of cerebrovascular resistance

$$CVR = \frac{ABP}{FV} \ \ (mmHg/(cm/s))$$

Equation 4.4, page 68

Compliance of the cerebral arterial bed

$$C_a = \frac{C_a BV1}{a1} \text{ (cm/mmHg)}$$

Equation 4.5, page 69

Diastolic closing margin

$$DCM = ABP_d\text{-}CrCP \text{ (mmHg)}$$

Equation 4.6, page 69

Non-invasive cerebral perfusion pressure estimator based on the diastolic cerebral flow velocity, per Czosnyka et al. [69]

$$nCPP_{FV_d} = ABP \times \frac{FV_d}{FV_m} + 14 \text{ (mmHg)}$$

Equation 4.7, page 70

Non-invasive cerebral perfusion pressure estimator based on critical closing pressure, per Varsos et al.[76]

$$nCPP_{CrCP} = ABP \times \left[0.734\text{-} \frac{0.266}{\sqrt{(CVR \cdot C_a \cdot HR \cdot 2\pi)^2 + 1}}\right]\text{-}7.026 \text{ (mmHg)}$$

Equation 4.8, page 70

Non-invasive intracranial pressure estimator based on the concept of critical closing pressure

$$nICP_{CrCP} = ABP\text{-}\, nCPP_{CrCP} \text{ (mmHg)}$$

Equation 4.9, page 70

Non-invasive intracranial pressure estimator based on pulsatility index

$$nICP_{PI} = 4.47 \times PI + 12.68 \text{ (mmHg)}$$

Equation 7.1, page 149

Mathematical expression of cerebrovascular impedance based on cerebrovascular resistance, compliance and frequency

$$Z(j\omega) = \frac{\frac{CVR}{j\omega \cdot C_a}}{CVR + \frac{1}{j\omega \cdot C_a}} = \frac{CVR}{j\omega \cdot CVR \cdot C_a + 1} \text{ (mmHg/(cm}^3\text{/s)}$$

Equation 7.2, page 150

Modulus of impedance, derived from Equation 7.1

$$|Z(\omega)| = \frac{CVR}{\sqrt{CVR^2 \cdot C_a \cdot \omega^2 + 1}} \text{ (mmHg/(cm}^3\text{/s)}$$

Equation 7.3, page 151

Non-invasive cerebral perfusion pressure estimator based on the spectral volume accounting method ($nCPP_s$)

$$\mathrm{CPP} = \frac{\mathrm{a1}}{\mathrm{sPI}} \times \sqrt{(\mathrm{CVR} \cdot \mathrm{C_a})^2 \cdot \mathrm{HR}^2 \cdot (2\pi)^2 + 1} \quad (\mathrm{mmHg})$$

Equation 7.4, page 152

Estimated changes of pulsatile cerebral blood volume over one cardiac cycle

$$\Delta\mathrm{CBV}(\mathrm{t}) = \int_{\mathrm{t_0}}^{\mathrm{t}} \left(\mathrm{CBF_a}(\mathrm{s}) - \mathrm{CBF_v}(\mathrm{s})\right) \mathrm{ds} \quad (\mathrm{cm^3})$$

Equation 7.5, page 152

Estimated changes of cerebral arterial blood volume over one cardiac cycle according to the continuous flow forward model

$$\Delta\mathrm{C_aBV_{CFF}}(\mathrm{t}) = \int_{\mathrm{t_0}}^{\mathrm{t}} (\mathrm{CBF_a}(\mathrm{s}) - \mathrm{mean\ CBF_a})\, \mathrm{ds} \quad (\mathrm{cm^3})$$

Equation 7.6, page 153

Estimated changes of cerebral arterial blood volume over one cardiac cycle according to the pulsatile flow forward model

$$\Delta\mathrm{C_aBV_{PFF}}(\mathrm{t}) = \int_{\mathrm{t_0}}^{\mathrm{t}} \left(\mathrm{CBF_a}(\mathrm{s}) - \frac{\mathrm{ABP(s)}}{\mathrm{CVR}}\right) \mathrm{ds} \quad (\mathrm{cm^3})$$

Equation 7.7, page 153

Compliance of the cerebral arterial bed according to the continuous flow forward model

$$\mathrm{C_{aCFF}} = {}^{\mathrm{C1_{CFF}}}/_{\mathrm{a1}} \quad (\mathrm{cm/mmHg})$$

Equation 7.8, page 153

Compliance of the cerebral arterial bed according to the pulsatile flow forward model

$$\mathrm{C_{aPFF}} = {}^{\mathrm{C1_{PFF}}}/_{\mathrm{a1}} \quad (\mathrm{cm/mmHg})$$

Equation 7.9, page 154

Non-invasive approximation of cerebrovascular resistance used for $nCPP_s$ estimation

$$\mathrm{CVR_1} = \frac{\mathrm{ABP}}{\mathrm{FV}} \quad (\mathrm{mmHg/(cm/s)})$$

Equation 7.10, page 154

Cerebrovascular resistance according to the "resistance area product" method

$$\mathrm{CVR_2} = \frac{\mathrm{a1}}{\mathrm{f1}} \quad (\mathrm{mmHg/(cm/s)})$$

Equation 7.11, page 155

Amplitude of the first harmonic of heart frequency according to the continuous flow forward model

$$C1_{CFF} = \frac{f1}{\omega_{HR}}$$

Equation 7.12, page 155

Amplitude of the first harmonic of heart frequency according to the pulsatile flow forward model

$$C1_{PFF} = \frac{(f1\text{-}a1/CVR)}{\omega_{HR}}$$

LIST OF ABBREVIATIONS

A **ABP**, arterial blood pressure

ABP_d, diastolic arterial blood pressure

ABP_s, systolic arterial blood pressure

ACA, anterior cerebral artery

ALF, acute liver failure

ARI, autoregulation index

ArLD, alcohol-related liver disease

AUC, area under the curve

B **BCP**, beach chair position

BMI, body-mass index

C **C_a**, compliance of the cerebral arterial bed

C_aBV, cerebral arterial blood volume

CBF, cerebral blood flow

CFF, continuous flow forward model

CI, confidence interval

CO_2, carbon dioxide

COx, correlation index between ABP and regional cerebral oxygen saturation

CPP, cerebral perfusion pressure

CPP_{opt}, optimal cerebral perfusion pressure

CrCP, critical closing pressure

CSF, cerebrospinal fluid

CT, computed tomography

CVR, cerebrovascular resistance

D **DCM**, diastolic closing margin

E **EEG**, electroencephalogram

$ETCO_2$, end-tidal carbon dioxide concentration

F **FFT**, fast Fourier transformation

FV, cerebral blood flow velocity

FV_d, diastolic cerebral blood flow velocity

FV_s, systolic cerebral blood flow velocity

G **GCS**, Glasgow coma scale

H **HCC**, hepatocellular carcinoma

HCV, hepatitis C virus

HR, heart rate

I **ICA**, internal carotid artery

ICH, intracranial hypertension

ICP, intracranial pressure

INPH, idiopathic normal pressure hydrocephalus

IQR, interquartile range

K **KSR**, kernel spectral regression

L **LP**, lumbar puncture

M **MAD**, mean absolute difference

MCA, middle cerebral artery

MRI, magnetic resonance imaging

MS, midline shift

Mx, mean flow cerebral autoregulation index based on cerebral perfusion pressure

Mxa, mean flow cerebral autoregulation index based on arterial blood pressure

N **NA**, not available

NASH, non-alcoholic steatohepatitis;

NCCU, Neurosciences Critical Care Unit

nCPP, non-invasive cerebral perfusion pressure

$nCPP_s$, spectral non-invasive cerebral perfusion pressure

nICP, non-invasive intracranial pressure

$nICP_{BB}$, non-invasive intracranial pressure based on the black box method

$nICP_{FVd}$, non-invasive intracranial pressure based on the diastolic cerebral blood flow velocity method

$nICP_{CrCP}$, non-invasive intracranial pressure based on the critical closing pressure method

$nICP_{PI}$, non-invasive intracranial pressure based on the pulsatility index method

NM, not measured

NPV, negative predictive value

O **OLT**, orthotopic liver transplant

ONSD, optic nerve sheath diameter

OR, odds ratio

P **$PaCO_2$**, partial pressure of carbon dioxide

PCA, posterior cerebral artery

PE, prediction error

$PECO_2$, pressure of expired carbon dioxide

PFF, pulsatile flow forward model

PI, pulsatility index

PPV, positive predictive value

PRx, pressure reactivity index

PSC, primary sclerosing cholangitis

R **R**, correlation coefficient

R^2, coefficient of determination

R_{CSF}, resistance to cerebrospinal fluid outflow

REC, research ethics committee

RI, resistance index

ROC, receiver operating characteristic

$rSCO_2$, regional cerebral oxygen saturation

S **SAH**, subarachnoid haemorrhage

SCA, state of cerebral autoregulation

SD, standard deviation

SDE, standard deviation of the error

SJO_2, jugular bulb venous blood oxygen saturation

SVM, support vector machine

T **TBI**, traumatic brain injury

TCD, transcranial Doppler ultrasonography

W **WT**, cerebrovascular wall tension

1 AIMS AND HYPOTHESES

This thesis is devoted to transcranial Doppler-based methods for non-invasive intracranial pressure and cerebral perfusion pressure monitoring. The structure of the thesis consists of 10 chapters containing a comprehensive literature review of the existing methods for non-invasive intracranial pressure and cerebral perfusion pressure based on transcranial Doppler ultrasonography, the presentation of clinical material used for the author's original projects and a method for non-invasive monitoring. The results are divided into three parts: I) accuracy of non-invasive intracranial pressure estimation; II) clinical feasibility of non-invasive monitoring; III) novel method for non-invasive cerebral perfusion pressure monitoring based on spectral arterial blood volume accounting.

Hypotheses

In the course of the thesis project, the following hypotheses were formulated and subsequently tested:

Hypothesis I: Transcranial Doppler-based non-invasive monitoring methods can reliably estimate intracranial pressure with a finite error.

Transcranial Doppler ultrasonography consists of a technique with several possibilities for non-invasive estimation of cerebral haemodynamics, including different methods for the assessment of intracranial pressure. Nevertheless, many of these methods have not been systematically compared in various clinical conditions presenting disturbed cerebral haemodynamics and increased intracranial pressure. To address this issue, this part of the thesis focuses on determining which transcranial Doppler approach offers the best reliability to assess intracranial pressure non-invasively in comparison with the standard invasive technique.

Hypothesis II: Transcranial Doppler-based non-invasive monitoring can be used as a clinically feasible method to assess intracranial pressure and disturbed cerebral haemodynamics.

In many clinical conditions, the assessment of intracranial pressure and cerebral haemodynamics using invasive methods cannot be performed. This part of the thesis focuses on assessing the feasibility of TCD-based non-invasive intracranial pressure monitoring in clinical conditions in which invasive monitoring was not considered or unachieved.

Hypothesis III: Cerebral perfusion pressure dynamics can be estimated using a model-based non-invasive method derived from transcranial Doppler and arterial blood pressure monitoring.

A novel model-based method for cerebral perfusion pressure monitoring using transcranial Doppler-derided cerebral arterial blood volume accounting has been proposed in this thesis. This part of the thesis focuses on testing the performance of the method to replicate and predict changes in direct cerebral perfusion pressure.

2 INTRODUCTION

2.1 Intracranial pressure monitoring

The concept of intracranial pressure (ICP) was first described in 1783 by the Scottish anatomist Alexander Monro, who described the skull as a rigid structure containing an incompressible brain and stated that a constant drainage of venous blood is required to allow continuous arterial supply [1,2]. These assumptions were later confirmed in autopsy studies by George Kellie of Leith [3], whose findings were postulated as the Monro-Kellie doctrine. The doctrine was modified throughout the years with contributions of Vesalius (description of fluid-filled brain ventricles), François Magendie (establishment of the concept of cerebrospinal fluid – CSF [4]), George Burrows (the reciprocal relationship between the volumes of CSF and blood [5]). However, Harvey Cushing, in 1926 [6], formulated the classic explanation of the doctrine: with an intact skull, the volume of the brain, blood, and CSF are constant; an increase in one component will cause a decrease in one or both of the other elements.

On the basis of the Monro-Kellie doctrine, intracranial pressure can be described as the summation of at least four elements, driven by different physiological mechanisms [7]. The first element is associated with arterial blood inflow and volume of arterial blood. The most common phenomenon associated with this element is plateau waves of ICP. The second element of ICP is associated with venous blood outflow. Obstructions to the outflow of blood lead to elevation of ICP (like venous compression due to inadequate head position, but also venous thrombosis). The third component is related with cerebrospinal fluid (CSF) circulation derangements, as commonly seen in ‘acute hydrocephalus’ after traumatic brain injury (TBI) or subarachnoid haemorrhage (SAH). In neurocritical care, this component is commonly eradicated by extraventricular drainage. Finally, the fourth element relates to increasing brain volume (oedema) or volume of contusion (like haematoma). Osmotherapy or surgical decompression are therapeutical measures used to eradicate these complications. In clinical practice, it is important not only to monitor the absolute value of ICP but also to recognise which component is responsible for the pattern of intracranial hypertension observed, as different measures are appropriate for controlling different components [8].

ICP monitoring is one of the standard protocols that can guide patient management undergoing neurocritical care [9]. In association with mean arterial blood pressure (ABP), ICP monitoring provides the knowledge of cerebral perfusion pressure (CPP = ABP - ICP), interpreted as the main force maintaining cerebral blood flow (CBF). However, ICP/CPP are not commonly considered in many clinical conditions outside neurocritical care settings or in non-specialized centres. The invasiveness of the standard methods for ICP monitoring (epidural, subdural, intraparenchymal and intraventricular monitors) and their associated risks to the patient (like infections, brain tissue lesions, haemorrhage) contribute to this scenario. Because of such complications, ICP monitoring has been prevented in a broad range of diseases, for instance in patients with risk of coagulopathy, as well as when invasive monitoring is not considered or outweighed by the risks of the procedure. Another downside is related to costs and availability, since invasive monitoring is an expensive technique, requires trained personnel and neurosurgical settings. The average cost of intraparenchymal microtransducer is around US$ 600, additionally to US$ 6,000-10,000 for the display monitor [10], which makes it inaccessible in low to middle-income regions. Provided that knowledge of ICP can be crucial for the successful management of patients in many sub-critical conditions, non-invasive estimation of ICP may be helpful when indications for invasive ICP monitoring are not met and when it is not immediately available or contraindicated.

Several methods for non-invasive assessment of ICP have been described so far: transcranial Doppler ultrasonography (TCD) to measure cerebral blood flow velocity indices [11]; skull vibrations [12]; skull deformation [13,14]; brain tissue resonance [15]; transcranial time of flight [16]; venous ophthalmodynamometry [17]; optic nerve sheath diameter assessment (ONSD) [18]; tympanic membrane displacement [19,20]; otoacoustic emissions [21]; magnetic resonance imaging (MRI) to estimate intracranial compliance [22]; ultrasound-guided eyeball compression [23], and recordings of visual evoked potentials [24].

Most of these methods are better suited for one-point assessment of the instant value of ICP rather than continuous monitoring. TCD, on the other hand, has been widely explored as a tool for non-invasive ICP monitoring [25–39] due to its ability to detect changes in CBF with ample time resolution.

2.2 Principles of transcranial Doppler ultrasonography

Transcranial Doppler ultrasonography (TCD) technique is based on the phenomenon called Doppler effect, observed by the physicist Christian Andreas Doppler in the 19th century. Reid and Spencer popularised this principle applied to imaging of blood vessels in the 1970's [40]. The application of TCD in clinical practice was first described by Rune Aaslid and collaborators in 1982 [41], as a technique applying ultrasound probes for dynamic monitoring of CBF and vessel pulsatility in the basal cerebral arteries.

The Doppler effect states that when a sound wave with a certain frequency strikes a moving object, the reflected wave changes its frequency (the Doppler shift, f_d) directly proportionally to the velocity of the reflector. When translated to medical applications, this principle has been applied to monitor erythrocyte motion inside an insonated blood vessel by measuring the difference in ultrasound frequencies between emission and reception [41]. The equation derived from this principle is the basis for calculating cerebral blood flow velocity (FV, in cm/s) with TCD:

Equation 2.1

$$v = \frac{(c \times f_d)}{2 \times f_0 \times \cos\theta} \tag{2.1}$$

where c is the speed of the incident wave, f_0 is the incident pulse frequency, f_d is the Doppler shift and θ is the angle of the reflector relative to the ultrasound probe [42].

TCD relies on pulsed wave Doppler to image vessels at multiple insonation depths. The received echoes generate an electrical impulse in the ultrasound probe and is processed to calculate f_d and v, yielding a spectral waveform with peak systolic velocity (FV_s) and end diastolic velocity (FV_d) values (Figure 2.1).

Figure 2.1. Representation of the systolic (FV_s) and diastolic (FV_d) components of the spectral cerebral blood flow (CBF) velocity (FV) waveform.

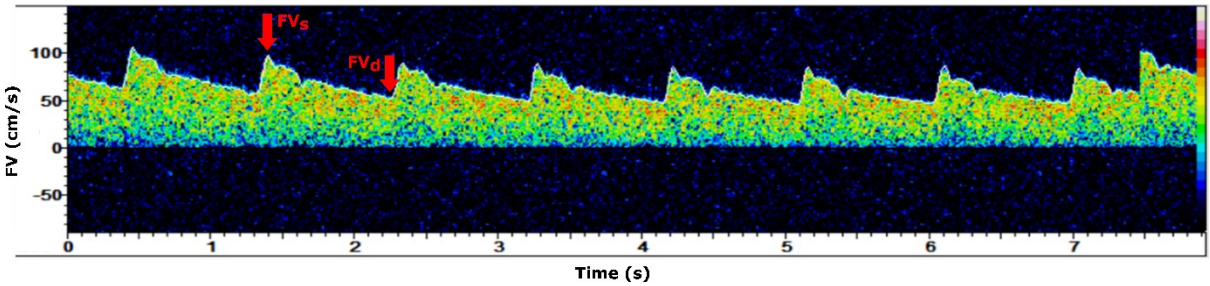

2.3 Assessment of cerebral circulation using transcranial Doppler

The use of low-frequency ultrasound probes (≤2 MHz) allows insonation of basal cerebral arteries through different acoustic windows in the skull. These are regions presenting thin bone layers, through which ultrasound waves can be transmitted. There are four acoustic windows: transtemporal, transforaminal, transorbital and submandibular (Figure 2.2). The transtemporal window is the most frequently used, anatomically located above the zygomatic edge between the lateral canthus of the eye and auricular pinna. Through this window, it is possible to insonate the circle of Willis, specifically middle (MCA), anterior (ACA), posterior cerebral arteries (PCA), and terminal internal carotid artery (ICA) [43]. Artery insonation is subject to probe angle, depth and appropriate acoustic window. However, inadequate transtemporal windows have been reported in 10-20% of patients [44,45], associated with patient age, female sex, and other factors affecting the bone thickness [46].

In clinical practice, the MCA is the most frequently assessed artery. It is responsible for the greatest blood inflow to the brain (80%) [47,48]; thus MCA measurement may represent the global blood flow. CBF represents the blood supply to the brain in a given period, and global changes in this parameter can be monitored continuously and non-invasively with TCD-derived FV [49]. However, FV is only proportional to CBF when vessel cross-sectional area and angle of insonation are constant. The velocity detected by the probe as a fraction of the actual velocity depends on the cosine of the angle of insonation (Equation 2.1).

Figure 2.2. Schematic representation of the acoustic windows for transcranial Doppler ultrasonography.

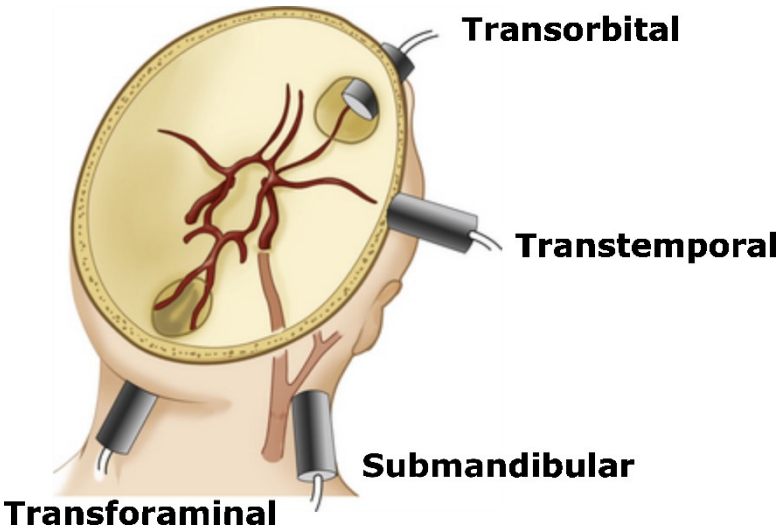

Consequently, at an angle of zero degrees, the erythrocytes' velocities are equal (cosine of θ = 1), whereas, at 90 degrees, no detection of velocity is possible. Anatomically, MCA insonation at the transtemporal acoustic window only allows signal capture at narrow angles (<30 degrees), which approximates the detected velocity to the actual velocity (87% to 100%) [50].

Non-invasive estimation of ICP and CPP

TCD waveform analysis has been explored as a technique for non-invasive estimation of ICP (nICP) and CPP (nCPP). TCD-derived nICP/nCPP methods are based on the relationship between ICP/CPP and indices derived from cerebral blood flow velocity.

Applications of TCD for nICP and nCPP monitoring are conceivable if one considers the insonated compliant MCA as a biological pressure transducer, whose walls can be deflected by transmural pressure (equivalent to CPP), modulating the FV pulsatile waveform accordingly [39].

Next chapter presents a comprehensive literature review of the existing methods for nICP and nCPP assessment based on transcranial Doppler ultrasonography.

3 LITERATURE REVIEW

This chapter is based on work published in *Neurocritical Care* [39]*:*

Cardim, D., Robba, C., Bohdanowicz, M., Donnelly, J., Cabella, B., Liu, X., Cabeleira, M., Smielewski, P., Schmidt, B., and Czosnyka, M. (2016). Non-invasive Monitoring of Intracranial Pressure Using Transcranial Doppler Ultrasonography: Is It Possible? Neurocrit. Care.

3.1 Introduction

TCD-based nICP continuous monitoring methods are mainly based on approximate semi-quantitative relationships between ICP and cerebrovascular dynamics assessed with TCD. They can be divided into three categories: I) methods based on the TCD-derived pulsatility index (PI); II) methods based on the calculation of nCPP; and III) methods based on mathematical models.

The existing non-invasive ICP methods based on TCD waveform analysis present a considerable variability in their reported accuracy inter and intra-categories. Considering the wide range of applications of TCD as a technique for nICP monitoring, this review presents TCD-based methods and their documented clinical or experimental applications with measures of accuracy in comparison to standard invasive methods for ICP monitoring.

3.2 Methods

Works from 1985 to 2017 were found on PUBMED database using the keywords ‘transcranial Doppler non-invasive intracranial pressure’, in a total of 97 studies. The inclusion criteria were the use of transcranial Doppler as a tool for non-invasive ICP with clinical or experimental applications of such methods. Excluded papers consisted of works on other TCD applications

than non-invasive ICP estimation, or absence of clinical or experimental applications in papers describing TCD-based methods for non-invasive ICP estimation. Selected articles were then subdivided into the categories above. Only available full-length articles in the English language were considered. The total number of articles considered was 36; some articles presented assessments in more than one category. Works derived from this thesis were not considered in this review but will be subsequently presented in the following results chapters.

Main findings for each nICP category are presented in Table 3.1, Table 3.2 and Table 3.3. Sections in results present major attributes of the nICP categories.

3.3 Results

3.3.1 Methods based on the correlation between ICP and PI ($nICP_{PI}$)

Methods based on TCD-derived pulsatility index rely on the observation that ICP and PI are positively correlated. PI describes quantitatively and qualitatively morphological changes in the TCD waveform resulting from varying CPP. It is represented by the difference between systolic and diastolic flow velocities divided by the mean velocity, initially described by Gosling in 1974 [51] (Equation 4.1).

PI has been reported as inversely proportional to mean CPP, directly proportional to pulse amplitude of ABP and non-linearly proportional to the compliance of the cerebral arterial bed (C_a), cerebrovascular resistance (CVR) and heart rate (HR) [52]. In Gosling's original work, normal PI values were reported between 0.5-1.19 [51]. Proximal stenosis or occlusion may lower PI below 0.5 due to downstream arteriolar vasodilation, whereas distal occlusion or constriction may increase PI above 1.19 [53]. A PI less than 0.5 may also indicate an arteriovenous malformation as the resistance in proximal vessels is reduced due to continuous distal venous flow [54].

More recently, a larger study including more than 350 healthy individuals has reported normative values for TCD assessment of arteries in the circle of Willis [55]. Normal PI values

have been reported as 0.82±0.16 and 0.81±0.13 for distal and proximal MCA, respectively. Being a ratio, PI is not affected by the angle of insonation and therefore may be a sensitive parameter for early detection of intracranial hemodynamic changes [55].

Table 3.1. summarises the studies which demonstrated a relationship between PI and ICP, either positive or inexistent.

Table 3.1. Modified from Cardim et al. [39]. nICP methods based on TCD-derived pulsatility index ($nICP_{PI}$).

Method	Author	Study purpose	Sample size and disease	Invasive ICP monitoring	nICP method accuracy and correlation measures with ICP	Sensitivity (%)	Specificity (%)	AUC
$nICP_{PI}$	Steiger[56]	Investigate PI in TBI patients and compare them to healthy volunteers.	9, TBI	NA	PI analysis revealed values from 1.5 to 2.0 in control subjects, showing a gradual increase in patients with post-traumatic brain oedema. PI values ≥3 were associated with severe intracranial hypertension.			
	Chan et al.[57]	Examine the relationships between FV, SJO_2, and alterations in ABP, ICP, and CPP.	41, TBI	Subdural	Rises in ICP or drops in ABP were associated with a reduction in FV, particularly with FVd falling more than FV_s. PI was strongly correlated with ICP (R=0.9*).			
	Homburg et al.[58]	Investigate the PI-ICP relation as to evaluate TCD as an alternative to invasive ICP.	10, TBI	Epidural	Correlation between PI and ICP was R=0.82.			
	Martin et al.[59]	Assess PI in three distinct haemodynamic phases (hypoperfusion, hyperaemia and vasospasm).	125, TBI	Intraventricular/Intraparenchymal	Higher PI values were found in all hemodynamic phases during the first 2 weeks after injury (on day 0, compared to days 1 through 3 and days 4 through 14 post-trauma).			
	McQuire et al.[60]	Investigate the incidence of early abnormalities in the cerebral circulation after TBI by relating the results of CT scan with TCD-PI.	22, TBI	NM	10 patients presented increased PI in conditions indicative of ICH (space-occupying hematomas or brain swelling indications on CT).			

Moreno et al.[61]	Investigate the correlation between TCD, ICP and CPP in TBI patients.	125, TBI	NA	Correlation between PI and ICP was R^2=0.69. Elevated PI (≥1.56) was predictive of poor outcome.		
Rainov et al.[62]	Investigate a possible relationship between PI, RI, FV and ICP changes in adult patients with hydrocephalus.	29, Hydrocephalus	Epidural	PI in patients with elevated ICP before shunting was significantly increased. Preshunting ICP and PI were not correlated (R=0.37).		
Asil et al.[32]	TCD was compared with clinical examination and neuroradiologic findings.	18, stroke and MCA infarction	NM	Increases in PI were correlated with midline shift as an indication of elevated ICP (R=0.66*).		
Bellner et al.[27]	Investigate the relationship between ICP and PI in neurosurgical patients.	81, (SAH, TBI and other intracranial disorders)	Intraventricular	Correlation between PI and ICP was R=0.94* (ICP = 10.93 x PI – 1.28). In the ICP range of 5-40 mmHg, the correlation formula is: ICP = 11.5 x PI – 2.23 (R^2=0.73*). In this interval, SD for $nICP_{PI}$ was ±2.5 mmHg in the ICP range of 5-40 mmHg. 95% CI of ±4.2 mmHg.	88 (threshold of 10 mmHg) 83 (threshold of 20 mmHg)	69 (threshold of 10 mmHg) 99 (threshold of 20 mmHg)
Voulgaris et al.[33]	Investigate TCD as a tool for detection of cerebral haemodynamics changes.	37, TBI	Intraparenchymal	The overall correlation between ICP and PI was R=0.64*. For ICP ≥20 mmHg, the correlation was R=0.82*. PI allows early identification of patients with low CPP and risk of cerebral ischemia.		

Behrens et al.[63]	Validate TCD as a method for ICP determination INPH	10, INPH	Intraparenchymal	Correlation between PI and ICP was R^2=0.22* (ICP=23 x PI + 14). 95% CI for a mean ICP of 20 mmHg was −3.8 to 43.8 mmHg. PI is not a reliable predictor of ICP.			
Figaji et al.[28]	Examine the relationship between PI and ICP and CPP in children with severe TBI.	34 children, TBI	NM	Marginal correlation between PI and ICP of R=0.36*. No significant relationships between PI and ICP when differences within individuals or binary examination of PI (PI <1 and ≥1) were considered. PI is not a reliable non-invasive indicator of ICP in children with severe TBI.	25 (threshold of 20 mmHg)	88 (threshold of 20 mmHg)	
Brandi et al.[64]	Assess an optimal nICP and nCPP following TBI using TCD.	45, TBI	Intraventricular	Bellner's equation resulted in nICP similar to measured ICP, with nICP of 10.6±4.8 and ICP of 10.3±2.8 mmHg.			
Tude Melo et al.[65]	Evaluate the accuracy of TCD in emergency settings to predict intracranial hypertension and abnormal CPP in children with TBI.	117 children, TBI	Intraparenchymal	PI ≥1.31 was observed in 94% of cases with initially elevated ICP, and 59% of those with normal initial ICP values. TCD is an excellent first-line examination to screen children who need urgent treatment and continuous invasive ICP monitoring.	94 (for detecting initial ICH)	95 (for detecting initial ICH)	
Zweifel et al.[66]	Assess PI as a diagnostic tool for nICP and nCPP estimation.	290, TBI	Intraparenchymal	Correlation between PI and ICP was R=0.31*. 95% prediction interval > ±15 mmHg. The value of PI to assess nICP is insufficient.			0.62 (ICP ≥15 mmHg) 0.74 (ICP ≥35 mmHg)

De Riva et al.[52]	Assess the relationship between PI and CVR in situations where CVR increases (mild hypocapnia) and decreases (plateau waves of ICP) in TBI patients.	345, TBI	Intraparenchymal	Correlation between PI and ICP in such situations was R=0.70*. 95% CI of ±21 mmHg.			
Wakerley et al.[38]	Assess the correlation between PI with CSF pressure.	78, miscellaneous intracranial disorders	LP	Correlation between PI and ICP (CSF pressure) was R=0.65*. Binomial logistic regression indicated a strong significant relationship between raised ICP and PI (OR: 2.44; 95% CI: 1.57-3.78).	81.1	96.3	0.84 (threshold ≥20 cmH_20)
Wakerley et al.[37]	Present a case where TCD serves as an effective tool for nICP monitoring.	Case-report, Sagittal Sinus Thrombosis	NM	Increasing ICP was associated with rapid elevations of PI. On recording day 4, PI was reported to be 1.93 (considering a normal range of 0.6-1.2). ICP was deemed elevated according to clinical status (level of consciousness, headache) and papilledema.			
O'Brien et al.[67]	Determine the relationship between PI, FV_d and ICP in children with severe TBI.	36 children, TBI	Intraventricular/Intraparenchymal	**Initial 24 h post-injury** Correlation between PI and ICP was R=0.6*. **Beyond 24 h post-injury** Correlation between PI and ICP was R=0.38*.	**Initial 24 h post-injury** 100 (threshold ≥20 mmHg for PI of 1.3) **Beyond 24 h post-injury** 47 (threshold ≥20 mmHg for PI of 1.3)	**Initial 24 h post-injury** 82 (threshold ≥20 mmHg for PI of 1.3)	

Robba et al.[68]	Assess PI as a nICP estimator in rabbits submitted to the infusion of artificial CSF solution into the subarachnoid space.	Experimental (28 New Zealand rabbits)	Intraparenchymal	Correlation between PI and ICP was R=0.54*. R considering changes of nICP and ICP in time domain was 0.36±0.47. 95% CI of ±38.56 mmHg.	0.62 (≥20 mmHg) 0.66 (≥40 mmHg)

*Correlation coefficient is significant at the 0.05 level.

ABP, arterial blood pressure; AUC, area under the curve; CI, confidence interval; CT, computerized tomography; CSF; cerebrospinal fluid; FV_d, diastolic flow velocity; ICH, intracranial hypertension; INPH, idiopathic normal pressure hydrocephalus; LP, lumbar puncture; MCA, middle cerebral artery; NA, not available; NM, not measured; NPV, negative predictive value; OR, odds ratio; PPV, positive predictive value; R correlation coefficient; R^2, coefficient of determination; ; RI, resistance index; SAH, subarachnoid haemorrhage; SD, standard deviation; SJO_2, jugular bulb venous blood oxygen saturation; TBI, traumatic brain injury.

3.3.2 Methods based on nCPP estimation

The second approach for nICP monitoring was primarily intended for nCPP estimation. However, non-invasive ICP can be calculated based on the assumption that **nICP = ABP - nCPP**. There are four methods described in the literature (Table 3.2).

Aaslid et al. [69] (***$nICP_{Aaslid}$***)

Aaslid et al. (1986) [69] were the pioneers in developing a mathematical model for non-invasive estimation of CPP based on Transcranial Doppler waveform analysis. Supported by the knowledge that increased ICP was related to decreasing component of the flow waveform in the internal carotid artery [70], the authors deemed feasible that less evident changes in the flow pattern could be detected by more refined methods of waveform analysis. TCD, in such perspective, could be used to obtain an estimate of ICP. Considering CPP as the driving force for flow through the cerebral vascular bed and the main factor for determining pulsatile dynamics, the flow will be approximately proportional to CPP [69].

During increases in ICP, the proportion of the systolic to the diastolic CPP increases as ICP approaches the diastolic ABP. Consequently, the pulsatile component of CPP increases proportionally to its mean value and this would also be reflected in the FV waveform. Thus, the ratio between mean FV (FVm) and pulsatile amplitude of FV ($f1$) would be expected to be related to CPP. The simplest approach, in this case, would be to use this ratio as an index for CPP. However, it does not consider changes in the ratio caused by variations in the amplitude of ABP waveform. Such limitation was solved by multiplying the ratio described above by the amplitude of the first harmonic of ABP ($a1$) [69]:

Equation 3.1

$$nCPP_{Aaslid} = (FV_m/f1) \times a1 \ \ mmHg \tag{3.1}$$

This method was validated in patients with supratentorial hydrocephalus undergoing ventricular infusion tests. ABP (radial artery), ICP (ventricular pressure) and FV were measured. The linear regression determined for nCPP estimation considering all cases was:

Equation 3.2

$$CPP = 1.1\, nCPP_{Aaslid} - 5\, mmHg \quad (3.2)$$

In the individual case, there was a strong correlation between nCPP and CPP, R=0.93 to 0.99. The standard deviation (SD) between nCPP and CPP was 8.2 mmHg at 40 mmHg, while the mean deviation was only 1 mmHg. Overestimation occurred in two cases, 10 and 18 mmHg respectively. Underestimation was present in other two cases, 9 and 8 mmHg respectively. For the six remaining cases, the estimates were within ±5 mmHg of measured CPP. The method could differentiate correctly between low (<40 mmHg) and normal (>80 mmHg) CPP in all patients. At higher levels of CPP, the estimates presented with low accuracy, showing correct differentiation between CPPs of 70 and 100 mmHg in 80% of the cases.

In another attempt of assessment, Czosnyka et al. [71] reported that although sufficiently sensitive to detect changes of CPP over time, this method presented limited accuracy, showing a 95% prediction error (PE) of ±27 mmHg.

Considering studies on animal experimentation, Robba et al. [68] assessed this method in rabbits submitted to intracranial hypertension (ICH) through the infusion of artificial CSF solution into the subarachnoid space. ICP was increased to 70-80 mmHg, and the overall correlation between mean values of $nICP_{Aaslid}$ and ICP was of 0.53 ($p<0.05$). The ability to detect increased ICP above 20 and 40 mmHg was calculated using receiver operating characteristic analysis (ROC), revealing areas under the curve (AUC) of 0.66 and 0.77, respectively. Considering only changes in time between nICP and ICP, averaged correlation was 0.61±0.35. The 95% confidence interval (CI) for ICP prediction was 59.60 mmHg.

Czosnyka et al. [71] **(*$nICP_{FVd}$*)**

Some studies have demonstrated that certain patterns of the TCD waveform, like a decrease in FV_d, reflect impaired cerebral perfusion caused by a CPP decrease [71,72] (Figure 3.1). Czosnyka et al. [71] described this relationship as Equation 4.6.

The correlation between nCPP and measured CPP in TBI patients was R=0.73; $p<0.001$. In 71% of the examinations, the estimation error was below 10 mmHg, and in 84% of the examinations, the error was less than 15 mmHg. The method had a high positive predictive

value (94%) for detecting low CPP (<60 mmHg). Estimated CPP was highly specific for detecting changes in measured CPP over time, caused either by increases in ICP (plateau waves) or systemic hypotension. In six patients presenting plateau waves, nCPP compared with measured CPP had an average goodness-of-fit coefficient R^2 of 0.82. Furthermore, nCPP was very sensitive to detecting decreases in ABP below 70 mmHg (in 10 patients) with an average goodness-of-fit coefficient R^2 of 0.92. A good correlation was found between the average measured CPP and nCPP when day-by-day variability was assessed in a group of 41 patients (R=0.71).

The accuracy of this method in TBI patients was prospectively assessed by Schmidt et al. [73]. The absolute difference based on daily averages between direct CPP and nCPP was less than 10 mmHg in 89% of measurements and less than 13 mmHg in 92% of measurements. The 95% CI for CPP prediction was ±12 mmHg for CPP varying from 70 to 95 mmHg.

In another independent assessment of this method [74], mean values of nCPP and invasive CPP were 66.10±10.55 mmHg and 65.40±10.03 mmHg, respectively. The correlation between non-invasive and invasive CPP measurements was strongly significant, R=0.92 (p<0.001).

Figure 3.1. Extracted from Cardim et al., 2016 [39]. Systolic and diastolic flow velocities behaviour during a drop of cerebral perfusion pressure during a plateau wave increase of ICP observed in a TBI patient (source: Brain Physics Laboratory TBI Database, University of Cambridge). FV_d component, in this case, indicates inadequate cerebral perfusion.

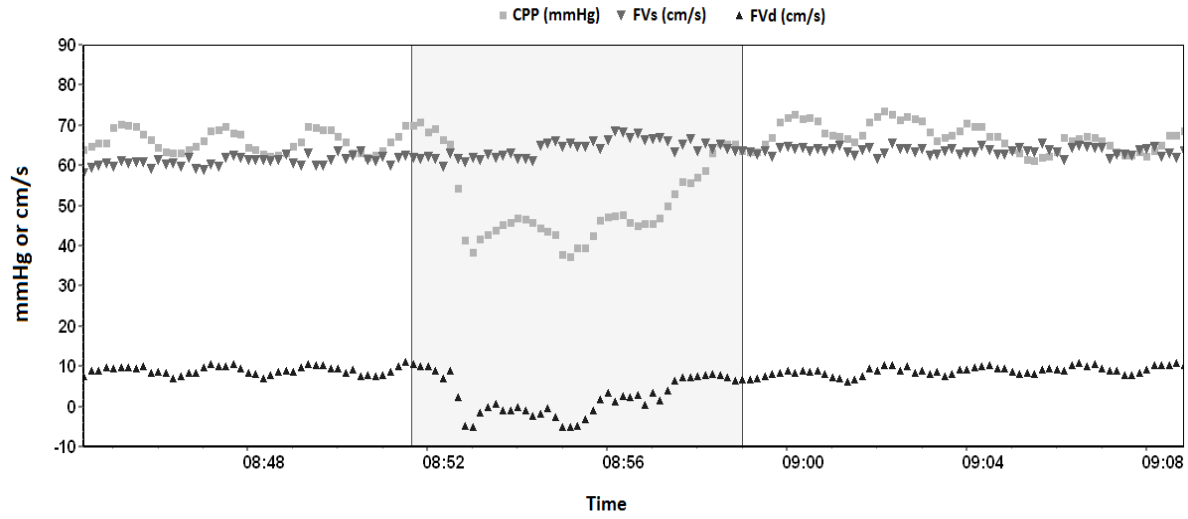

CPP, cerebral perfusion pressure, FV_s, systolic flow velocity; FV_d, diastolic flow velocity, ICP, intracranial pressure; TBI, traumatic brain injury.

In another study [64], the comparison between measured ICP and CPP showed a bias±95% CI of 5.6±17.4 mmHg for nICP and −5.5±20.6 mmHg for nCPP.

In an experimental study[68], during ICP increase to 70-80 mmHg the overall correlation between mean values of nICP and measure ICP was of 0.77 ($p<0.05$). The ability to detect increased ICP above 20 and 40 mmHg was given by AUCs of 0.86 and 0.94, respectively. Considering only changes of nICP and ICP in the time domain, the averaged correlation was 0.85±0.11. The 95% CI was 26.26 mmHg.

More recently, Rasulo et al. [75], compared $nICP_{FVd}$ with invasive ICP in three time frames: immediately before ICP placement, immediately after ICP placement, and 3 hours following ICP positioning. 12 patients (31.6%) presented episodes of ICP >20 mm Hg. The combined AUC for the three time points was 0.96 (95% CI 0.898-1) for ICH prediction. Sensitivity and specificity for the estimated best threshold (24.8 mm Hg) were 100% and 91.2%, respectively. The estimation bias was 6.2 mmHg (95% CI 5.08-7.30).

Edouard et al. [76] ($nICP_{Edouard}$)

This method is based on a non-invasive assessment of CPP using a combination of phasic values of both MCA FV and ABP. It was primarily validated in pre-eclamptic and healthy pregnant women by comparing nCPP with CPP measured at the epidural space [77].

In Edouard and colleagues' prospective study [76], the objective was to assess the adequacy of such method for TBI patients with invasive ICP monitoring, in both a stable state and during a rapid change in cerebrovascular tone following an induced alteration in arterial blood carbon dioxide pressure ($PaCO_2$).

The non-invasive CPP ($nICP_{Edouard}$) was calculated using the following formula:

Equation 3.3

$$nCPP_{Edouard} = \left(\frac{FV_m}{FV_m - FV_d}\right) \times (ABP_m - ABP_d)\ mmHg \quad (3.3)$$

ABP_m and ABP_d represent the mean and diastolic ABP, respectively.

Twenty adults with bilateral and diffuse brain injuries were included in the study and subdivided into two groups. In group A (N=10), the comparison was repeatedly performed under stable conditions. In group B (N=10), the comparison was conducted during a CO_2 reactivity test. nICP was not estimated in this study.

In group A, nCPP and measured CPP were correlated (slope, 0.76; intercept, +10.9; 95% CI, -3.5 to +25.4). The relationship persisted during ICP increase caused by the reactivity test in group B (slope, 0.55; intercept, +32.6; 95% CI, +16.3 to +48.9). However, the discrepancy between nCPP and measured CPP increased as reflected by the increase in bias and variability.

In another study [64], this method was tested for nICP and nCPP estimations, in a cohort of 45 TBI patients. Bias±95% CI for prediction was 6.8±19.7 mmHg and −6.8±45.2 mmHg for nICP and nCPP, respectively.

Varsos et al. [78] (nICP$_{CrCP}$)

The concept of critical Closing Pressure (CrCP) was first introduced by Burton's model, described as the sum of ICP and vascular wall tension (WT) [79]. WT represents the active cerebral vasomotor tone that combined with ICP determines the CrCP. Clinically, CrCP represents the lower threshold of ABP below which blood pressure in the brain microvasculature is inadequate to prevent the collapse and cessation of blood flow [79]. CrCP can be assessed non-invasively using TCD, by comparing the pulsatile waveforms of FV and ABP. Given the association with the vasomotor tone of small blood vessels, CrCP can to provide information regarding the state of cerebral haemodynamics and reflect changes in CPP [79–83] (Figure 3.2).

The conception and assessment of the model for the non-invasive estimator of CPP (nCPP$_{CrCP}$) were performed using a cohort of 280 TBI patients, divided into two subgroups: the formation group with 232 patients (including 455 recordings) and the validation group with 48 patients (including 325 recordings). Equations describing the model are presented in Section 4.2.3 (Equation 4.2, Equation 4.3, Equation 4.4, Equation 4.7, Equation 4.8).

Figure 3.2. Extracted from Cardim et al., 2016 [39]. Representation of the CrCP interaction with ICP and WT in a situation of intracranial hypertension observed in a traumatic brain-injured patient (source: Brain Physics Laboratory TBI Database, University of Cambridge). During the increase of ICP, the CrCP also increases and WT decreases as an effect of preserved autoregulation.

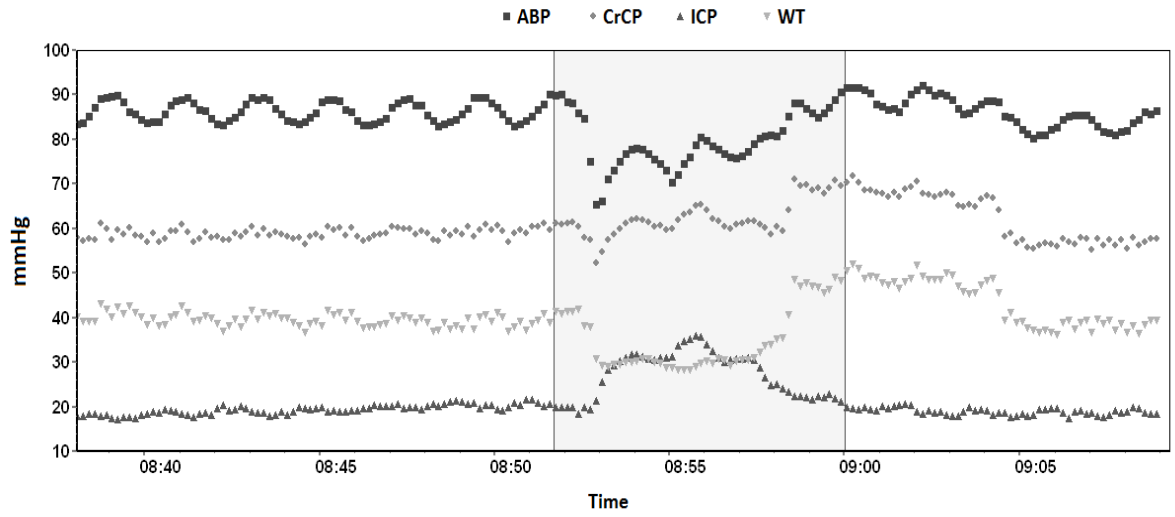

ABP, arterial blood pressure; CrCP, critical closing pressure; ICP, intracranial pressure; WT, wall tension; TBI, traumatic brain injury.

$nCPP_{CrCP}$ was tested against invasive CPP using data from the validation group. $nCPP_{CrCP}$ was correlated with measured CPP ($R=0.85$, $p<0.001$), with a bias of 4.02±6.01 mmHg; in 83.3% of the cases with an estimation error below 10 mmHg. $nCPP_{CrCP}$ prediction analysis at low CPP limits (50, 60, and 70 mmHg) resulted in AUCs greater than 0.8 for all limits. $nCPP_{CrCP}$ was found to be strongly correlated with CPP changes in the time domain (mean $R=0.733$, range 0.231–0.993). For each patient, $nCPP_{CrCP}$ presented a mean difference from CPP of 3.45 mmHg (range -4.69 to 19.03 mmHg), and a mean standard deviation of this difference of 5.52 mmHg (range 1.52–10.76 mmHg). $nCPP_{CrCP}$ could predict CPP between multiple recording sessions with a 95% CI of 1.89–5.01 mmHg.

Table 3.2. Modified from Cardim et al. [39]. nICP methods based on non-invasive cerebral perfusion pressure estimation.

Method	Author	Study purpose	Sample size and disease	Invasive ICP monitoring	nICP/nCPP method accuracy and correlation measures with ICP/CPP	AUC	PPV (%)	NPV (%)
nICP$_{Aaslid}$	Aaslid et al.[69]	Describe and assess a method for nCPP calculation based on FV and ABP.	10, supratentorial hydrocephalus	Intraventricular	SD for nCPP estimation of 8.2 mmHg at 40 mmHg. Able to differentiate between low (≤40 mmHg) and normal (≥80 mmHg) CPP in all cases. Low accuracy (80%) at higher levels of CPP (70-100 mmHg).			
	Czosnyka et al.[71]	Assessment of *nICP$_{Aaslid}$*.	96, TBI	Intraparenchymal	95% PE for nCPP estimation was >27 mmHg. Sensitive to detect changes of CPP over time.			
	Robba et al.[68]	Assessment of *nICP$_{Aaslid}$*.	Experimental (28 rabbits)	Intraparenchymal	Correlation between nICP and ICP was R=0.53*. R in the time domain of 0.61±0.35. 95% CI of ±59.60 mmHg.	0.66 (≥20 mmHg) 0.77 (≥ 40 mmHg)		
nICP$_{FVd}$	Czosnyka et al.[71]	Describe and assess a method for nCPP calculation based on FV (using the concept of FVd) and ABP.	96, TBI	Intraparenchymal	Correlation between nCPP and CPP was R=0.73*. Estimation error was less than 10 and 15 mmHg in 71 and 84% of the cases, respectively. Highly specific for detecting changes over time: R^2=0.82. Averaged correlation considering day-by-day variability between CPP and nCPP was R=0.71.		94 (CPP ≤60 mmHg)	
	Schmidt et al.[73]	Assessment of *nICP$_{FVd}$*.	25, TBI	Intraparenchymal	Error for nCPP estimation was less than 10 and 13 mmHg in 89 and 92% of the cases respectively. 95% CI of ±12 mmHg.			
	Gura et al.[74]	Assessment of *nICP$_{FVd}$*.	47, TBI	Intraparenchymal	Correlation between nCPP and CPP was R=0.92*. Mean values of nCPP and CPP were 66.10±10.55 mmHg and 65.40±10.03 mmHg, respectively.			

	Brandi et al.[64]	Assess an optimal nICP and nCPP following TBI using TCD.	45, TBI	Intraparenchymal	**nICP:** Bias of 5.6 mmHg and 95% CI of ±17.4 mmHg. **nCPP:** Bias of −5.5 mmHg and 95% CI of ±20.6 mmHg.	
	Robba et al.[68]	Assessment of $nICP_{FVd.}$	Experimental (28 rabbits)	Intraparenchymal	Correlation between ICP and nICP was R=0.77*. R in the time domain of 0.85±0.11. 95% CI of ±26.26 mmHg.	0.86 (≥20 mmHg) 0.94 (≥40 mmHg)
	Rasulo et al.[75]	Assessment of $nICP_{FVd.}$	38, acute brain injury	28 intraparenchymal, 10 intraventricular	Bias of 6.2 mmHg and 95% CI of 11.8 mmHg	0.96 (≥20 mmHg)
***nICP*$_{Edouard}$**	Edouard et al.[76]	Describe and assess a method for nCPP calculation based on FV and ABP under stable conditions and during CO_2 reactivity test.	20, TBI	Intraparenchymal	**During normocapnia:** nCPP and CPP were correlated (slope, 0.76; intercept, 10.9; 95% CI, -3.5 to 25.4 mmHg). **During hypercapnia:** nCPP and CPP were correlated, but with increased discrepancy, as reflected in confidence interval (slope, 0.55; intercept, 32.6; 95% CI, 16.3 to 48.9 mmHg).	
	Brandi et al.[64]	Assessment of $nICP_{Edouard}$.	45, TBI	Intraparenchymal	**nICP:** Bias of 6.8 mmHg and 95% CI ±19.7 mmHg. **nCPP:** Bias of -6.8 mmHg and 95% CI ±45.2 mmHg.	

nICP$_{CrCP}$	Varsos et al.[78]	Describe and assess a method for nCPP calculation based on FV (using the concept of CrCP) and ABP.	280, TBI	Intraparenchymal	Correlation between nCPP and CPP was R=0.85*. Bias±SD of 4.02±6.01 mmHg. nCPP estimation error was below 10 mmHg in 83.3% of the cases. **Temporal analysis:** Mean correlation in time domain was R=0.73 (0.23–0.99). Bias of 3.45 mmHg (range: 4.69-9.03 mmHg). Mean SD of 5.52 mmHg (range: 1.52–10.76 mmHg) and 95% CI of the SD of 1.89–5.01 mmHg.	>0.8

*Correlation coefficient is significant at the 0.05 level.

AUC, area under the curve; ABP, arterial blood pressure; CI, confidence interval; FV, cerebral blood flow velocity; NPV, negative predictive value; PPV, positive predictive value; PE, prediction error; R correlation coefficient; R^2, coefficient of determination; SD, standard deviation; SAH, subarachnoid haemorrhage; TBI, traumatic brain injury.

3.3.3 Model-based nICP methods

Black-Box model for ICP estimation ($nICP_{BB}$)

In this model, the intracranial compartment is considered a black-box (BB) system, with ICP being a system response to the incoming signal ABP [25]. This mathematical model originates from systems analysis, which provides a method to describe the transmission characteristics, with input and output signals. The intracranial compartment is indirectly described by a transfer function [84,85] which connects the assumed input signal, ABP, with the output signal, ICP. Two linear models are first established to depict the relationship between ABP and ICP and that between ABP and FV, yielding two coefficients, ***f*** and ***w***, respectively. By applying this linear mapping function, non-invasive ICP estimation can be performed by first estimating ***f*** from the coefficients ***w*** obtained from ABP and FV (TCD characteristics). An estimate of ICP can then be derived from ABP using the calculated ***f***. The output data provides a continuous full waveform of nICP (in mmHg) and constant relationship between FV-ABP (Figure 3.3).

$nICP_{BB}$ was first validated in a cohort of 11 TBI [25]. For each patient, measured and predicted ICP were compared during a time interval of 100 s. As a measure of the simulation's accuracy, the mean of the absolute values of the differences (bias) between measured and predicted ICP values (MAD-ICP) was obtained. To verify the simulation's capability of predicting the mean ICP averaged over one cardiac cycle (ICP_{CC}), the mean of the absolute differences (bias) between measured and predicted ICP_{CC} (MAD-ICP_{CC}) was calculated.

The MAD-ICP was smaller than 3 mmHg in 4 patients and smaller than 5 mmHg in 8 patients, and the maximum MAD-ICP was 7.5 mmHg. The MAD-ICP_{CC} was slightly lower than the MAD-ICP; it was smaller than 3 mmHg in 4 patients and smaller than 5 mmHg in 9 patients, and again the maximum was 7.5 mmHg. On average, the patients' MAD-ICP was 4.0±1.8 mmHg, and the MAD-ICP_{CC} was 3.8±1.9 mmHg. The 95% CI for ICP prediction was smaller than 5 mmHg in 3 patients and smaller than 10 mmHg in 8 patients, and the maximum was 12.8 mmHg. The 95% CI for ICP_{CC} was smaller than 5 mmHg in 4 patients and smaller than 10 mmHg in 11 patients, and the maximum was 11.7 mmHg.

Figure 3.3. Extracted from Cardim et al., 2016 [39]. Schematic representation of the black-box model for nICP estimation. A known transfer function (represented by a linear model) between ABP and FV, alongside modification TCD characteristics, are used as means to continuously find a relationship between ABP and nICP transformations (unknown transfer function – a linear model between ABP and ICP).

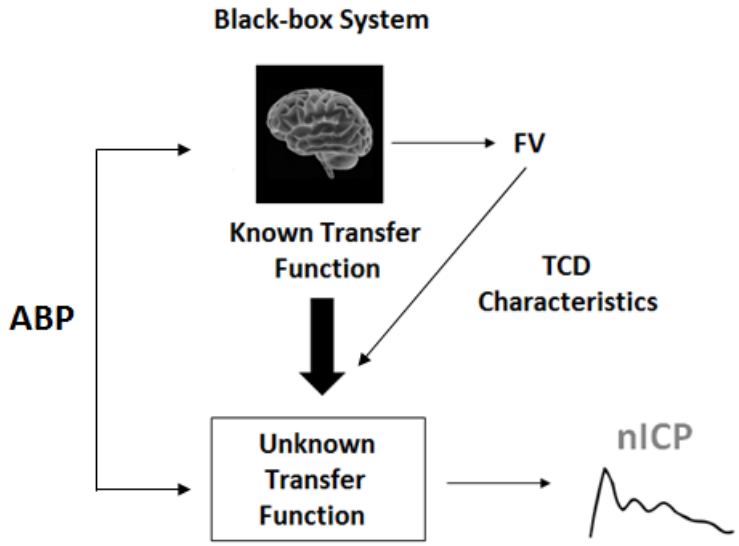

ABP, arterial blood pressure; FV, cerebral blood flow velocity; TCD, transcranial Doppler; nICP, non-invasive intracranial pressure.

In another study, this method was applied in patients with different types of hydrocephalus as an aid to predict the time course of raised ICP during infusion tests, and its suitability for estimating the resistance to cerebrospinal fluid outflow (R_{CSF}) [30]. The mean absolute error (bias) found between actual and simulated R_{CSF} was 4.1±2.2 mmHg minute/ml, considering all types of hydrocephalus (N=21 patients). In this case, the correlation between actual and simulated R_{CSF} was R=0.73 ($p<0.001$). By constructing simulations specific to different subtypes of hydrocephalus arising from several causes, the mean error decreased to 2.7±1.7 mmHg minute/ml, whereas the correlation coefficient increased to R=0.89 ($p<0.001$).

Another clinical application of this method considered nICP during plateau waves of intracranial pressure [26]. The objective of this study was to clarify whether simultaneous changes of FV and ABP could assess such waves non-invasively in a cohort of 17 severely TBI patients. Plateau waves were observed in 7 of them. In both direct ICP and nICP recordings, similar typical plateau shapes of waveforms could be observed. On average, bias (ICP-nICP) was

8.3±5.4 mmHg at the baseline and 7.9±4.3 mmHg at the top of plateau waves. Increases of nICP and direct ICP during plateau waves showed a strong correlation, R=0.98 ($p<0.001$).

This method was also applied to assess the impact of cerebral autoregulation to nICP assessment and investigate the ability of the model to adapt to the state of cerebral autoregulation (SCA), in order to improve the quality of nICP estimation and non-invasive assessment of pressure reactivity of the cerebrovascular system (PRx) [26,31]. The study included 145 patients with acute brain injury (135 TBI and 10 stroke). A FV-CPP relating index (Mx) was calculated as a correlation coefficient of 36 samples of CPP and FV mean values. The positive association between CPP and FV (Mx>0) indicates the passive dependence of blood flow on CPP, and therefore impaired autoregulation. Negative values of Mx implicate active cerebrovascular responses to changes in CPP or ABP, and therefore preserved autoregulation [86]. PRx (pressure reactivity index) works similarly to Mx but takes into account active regulation in cerebral blood volume [87,88].

nICP was calculated from data collected in 197 different recordings of 145 patients. In 167 recordings, the dynamics of FV or ABP met the inclusion criteria for the evaluation of SCA. In these recordings, Mx and PRx were calculated from FV, ABP, and measured ICP; nMx and nPRx were calculated with nICP instead of ICP.

Correlations between Mx and nMx and between PRx and nPRx were significant, R=0.90 and R=0.62 ($p<0.001$), respectively. In 125 recordings of 106 patients, Mx was definite (>0.2 or <-0.2). In 2 of these recordings, the value of nMx was contradictory to Mx. Subsequently, nMx indicated definite SCA in 121 recordings of 104 patients. nMx was contradictory to Mx in 3 cases. The specificity of nMx for Mx estimation was 92% and sensitivity 97%.

The sensitivity of nPRx for predicting PRx values was 61%, and its specificity was 67%. The median ΔICP (bias) (ICP-nICP) was 6.0 mmHg. In 75% of the evaluated recordings, ΔICP was <9.1 mmHg. A paired comparison of nICP assessments with a fixed nICP procedure showed significantly lower ICP estimation errors if the nICP procedure was adapted to SCA (mean errors: 7.6 and 6.9 mmHg; $p<0.005$). Considering only TBI patients, the mean ΔICP was 7.1 mmHg; considering only stroke, it was 4.3 mmHg.

Cerebrovascular dynamics model for estimation of ICP [29,36] ($nICP_{Heldt}$)

This model-based nICP method focuses on the major intracranial compartments and their associated variables: brain tissue, cerebral vasculature and CSF. It continuously estimates and tracks ICP using measurements of peripheral ABP and FV in the MCA. This physiological model of cerebrovascular dynamics is represented by a circuit analogue and provides mathematical limits that relate the measured waveforms to ICP. Patient-specific ICP estimations are produced by an algorithm, with no calibration or training in specific populations needed. Ursino and Lodi [89] initially described the dynamical model of CSF and cerebral blood flow, then modified by many independently working neuroscientists.

The $nICP_{Heldt}$ method was validated in a cohort of 37 TBI patients with severe closed head injury, in a total of 45 recordings. Thirty of these recordings presented bilateral FV monitoring. The correlation coefficient between $nICP_{Heldt}$ and measured ICP was R=0.90 for the total data obtained on the 2665 non-overlapping estimation windows. The bias of $nICP_{Heldt}$ versus measured ICP in this case across all patients was 1.6 mmHg and standard deviation of the error (SDE) of 7.6 mmHg. The overall correlation coefficient with measured ICP (ranging up to 100 mmHg) was strong (R=0.9). However, considering only the bilateral recordings, the correlation dropped to 0.76, despite the smaller SDE of 5.9 mmHg due to the narrower range of ICP variation (few points above 40 mmHg). On a patient-record basis of the 45 estimates, the correlation coefficient was 0.92, reflecting the fact that the average ICP covers a range of about 75 mmHg across these records, whereas the SDE was under 6 mmHg.

The ability of the method to correctly identify elevated ICP was tested for the 2665 data pairs, considering a nICP threshold of 20 mmHg. The estimates presented a sensitivity of 83% and a specificity of 70%. A full receiver operating characteristic was obtained by varying the nICP threshold from 0 to 100 mmHg. This resulted in an AUC of 0.83. This procedure was repeated on a patient-record basis using the threshold of 20 mmHg, and the sensitivity and specificity were 90% and 80%, respectively. In this case, the ROC analysis, also obtained by varying the nICP threshold, had an AUC of 0.88.

Models based on non-linear regressions

Modified nICP$_{BB}$

The previously described black-box model for ICP estimation [25] adopts a linear relationship among ABP, ICP and FV. Xu et al. [90], assuming that the relationships among these three signals are more complex than simple linear models, and consequently not adequate to depict the relationship between $\boldsymbol{f}$ and $\boldsymbol{w}$ coefficients, investigated the adoption of several nonlinear regression approaches. Considering that non-linear regressions, such as support vector machines (SVM)[91], kernel spectral regression (KSR) [92], have been proved to be more powerful for the prediction problem than the linear ones [93,94], the authors proposed the use of these approaches to model the relationship between coefficients $\boldsymbol{f}$ and $\boldsymbol{w}$.

Modified nICP$_{BB}$ showed that the mean ICP error by the non-linear approaches could be reduced to below 6.0 mmHg compared to 6.7 mmHg of the original approach. Moreover, the ICP estimation error by the proposed non-linear kernel approaches was statistically smaller ($p<0.05$) than that obtained with the original linear model.

Data mining

Hu et al. [95] initially proposed an innovative data-mining framework for nICP assessment. The proposed framework explores the rules of deriving ICP from ABP and FV that are captured implicitly by a signal database without using an explicit mathematical model. The main strategy of this framework is to provide a mapping function to quantify the uncertainty of an ICP estimate associated with each database entry, and to use this information to determine the best entry to build an ICP simulation model for an optimal ICP estimation. It achieved significant improvements regarding ICP simulation accuracy. In comparison to nICP$_{BB}$, for example, the proposed method presented a median normalised prediction error for ICP of 39% compared to 51% of nICP$_{BB}$, and its median correlation coefficient between estimated and measured normalised ICP was 0.80 compared to 0.35 of nICP$_{BB}$.

In another work, Kim et al. [96] aimed at adopting a new (linear and non-linear) mapping functions into the previous data mining framework for nICP estimation to demonstrate that the performance of nICP assessment could be improved by utilising proper mapping functions.

The new framework used a database of simultaneously recorded signals (ABP, FV and ICP) and dynamic models of the signals (inputs: ABP and FV, output: ICP). Two types of relevant data are drawn from this database: hemodynamic features and dissimilarity measures. Hemodynamic features are extracted from ABP and FV to capture the characteristic aspects of the cerebral haemodynamic state. Dissimilarity measures are calculated as the distance between actual ICP and its estimates, obtained by simulating the dynamic models in the database. This approach quantifies how closely each dynamic model can estimate actual ICP only using the corresponding ABP/FV signals.

The main strategy of the data mining framework is to formulate a mapping function between haemodynamic features and dissimilarity measures. The results demonstrated that a non-linear mapping function based on kernel spectral regression significantly improves the performance of the proposed data mining framework for nICP assessment in comparison to other linear mapping functions, showing a median ICP estimation error of 4.37 mmHg.

Semisupervised machine learning

As previously seen, FV waveform analysis has frequently been applied for non-invasive ICP assessment. Kim et al. [97] introduced a non-invasive ICH detection method based on the TCD measurement of FV alone to demonstrate its performance both in the supervised and semisupervised learning settings.

ICH detection is a classification problem to differentiate patients with elevated ICP from those with normal (or low) ICP. The traditional approach uses only labelled samples to train a given classifier, referred to as supervised learning. The major drawback of this method is that it cannot utilise unlabelled samples even when useful information learned from them may result in the improvement of classification accuracy.

To address the ambiguity in labelling samples, the authors adopted a new classification approach, a semisupervised learning. With this concept, labelling is not necessary since classifiers can be trained using both labelled and unlabelled samples.

Simulation results demonstrated that the predictive accuracy (AUC) of the semisupervised method could be as high as 92%, while that of the supervised method was only around 82%. AUC of the PI-based method was as low as 59%. A decision curve analysis showed that the

semisupervised ICH detection method was not only more accurate but also clinically more useful than the supervised ICH detection method or the PI-based ICH detection method.

Table 3.3. Modified from Cardim et al. [39]. nICP methods based on mathematical models.

Method	Author	Study purpose	Sample size and disease	Invasive ICP monitoring	nICP method accuracy and correlation measures with ICP	Sensitivity (%)	Specificity (%)	AUC
nICP$_{BB}$	Schmidt et al.[25]	Describe and assess a method for nICP calculation based on FV and ABP using a black box model.	11, TBI	Epidural	Bias of 4.0 mmHg and SDE of 1.8 mmHg. In this cohort, a maximum 95% CI of ±12.8 mmHg was found.			
	Schmidt et al.[30]	This study aimed at predicting the time course of raised ICP during CSF infusion tests and its suitability for estimating the R_{CSF} using *nICP$_{BB}$*.	21, different types of hydrocephalus	Epidural	**Analysis of all records:** Correlation between nR_{CSF} and R_{CSF} was R=0.73*. Bias of 4.1 mmHg and SDE for R_{CSF} prediction of 2.2 mmHg · minute/ml. **Analysis specific to different subtypes of hydrocephalus:** Correlation between nR_{CSF} and R_{CSF} was R=0.89*. Bias of 2.7 mmHg and SDE for R_{CSF} prediction of 1.7 mmHg · minute/ml.			
	Schmidt et al. [26]	Assess *nICP$_{BB}$* during plateau waves of ICP.	17, TBI (Plateau (A) waves observed in 7 patients)	Intraparenchymal	Correlation between nICP and ICP during ICP increase was R=0.98*. **Analysis considering the baseline of plateau waves:** Bias of 8.3 mmHg and SDE of 5.4 mmHg. **Analysis considering the top of plateau waves:** Bias of 7.9 mmHg and SDE of 4.3 mmHg. **Increases of nICP and direct ICP during plateau waves:** R=0.98 ($p<0.001$)			

	Schmidt et al.[31]	This study aimed at investigating the ability of $nICP_{BB}$ to adapt to the SCA, using Mx and PRx as parameters.	145 (135 TBI, 10 Stroke)	Intraparenchymal/ Intraventricular	Correlation between nMx and Mx was R=0.90*. Correlation between nPRx and PRx was R=0.62*. Median bias of 6.0 mmHg **Only TBI:** Bias of 7.1 mmHg. **Only Stroke:** Bias of 4.3 mmHg.	For Mx: 97 For PRx: 61	For Mx: 92 For PRx: 67	
$nICP_{Heldt}$	Kashif & Heldt et al.[36]	Describe and assess a method for nICP calculation based on FV and ABP.	37 (45 TCD recordings in total, 30 bilateral), TBI	Intraparenchymal	**Across all TCD records:** Correlation between nICP and ICP was R=0.90. Bias of 1.6 and SDE of ±7.6 mmHg. Inferred 95% CI of ±14.9 mmHg. **Across bilateral TCD records:** Correlation between nICP and ICP was R=0.76. Bias 1.5 and SDE 5.9 mmHg. Inferred 95% CI of ±11.6 mmHg.	83	70	0.83 (≥20 mmHg)
					On a patient-record basis: Correlation between nICP and ICP was R=0.90 (N=45 recordings).	90	80	0.88 (≥20 mmHg)
Modified $nICP_{BB}$	Xu et al.[90]	Describe and assess a method for nICP calculation based on FV and ABP, using an improved model for $nICP_{BB}$.	23 (14 TBI, 9 Hydrocephalus)	Intraparenchymal/ Intraventricular	Biases for non-linear models were <6.0 mmHg compared to 6.7 mmHg of the $nICP_{BB}$ (linear). Inferred 95% CIs for non-linear models were ≤ ±10.8 mmHg, compared to 10.6 mmHg of the linear model.			

Data mining	Hu et al.[95]	Describe and assess a method for nICP calculation based on FV and ABP based on the concepts of data mining.	9, TBI	Intraventricular	Median correlation between data-mining nICP and ICP was R=0.80.	
	Kim et al.[96]	Describe and assess a method for nICP calculation based on FV and ABP based on the concepts of data mining.	57, TBI	NM	Kernal spectral regression-based method presented a median bias of 4.37 mmHg.	
Semisupervised learning	Kim et al.[97]	Describe and assess a method for nICP calculation based on FV and ABP based on the concepts of semisupervised machine learning.	90 (44 TBI, 36 SAH, 10 NPH)	Intraparenchymal/ Intraventricular	Decision curve analysis showed that the semisupervised method is more accurate and clinically useful than the supervised or PI-based method.	0.92

*Correlation coefficient is significant at the 0.05 level.

Inferred 95% CI was calculated as 1.96 x SDE.

AUC, area under the curve; CI, confidence interval; R correlation coefficient; R^2, coefficient of determination; SDE, standard deviation of the error; R_{CSF}, resistance to cerebrospinal fluid (CSF) outflow; R_{CSF}, nICP-derived R_{CSF}; NPH, normal pressure hydrocephalus; TBI, traumatic brain injury; SAH, subarachnoid haemorrhage; SCA, state of cerebral autoregulation.

3.4 Discussion

The review of the presented methods demonstrates that measures of accuracy for each method varied substantially within and among nICP categories. This variability illustrates the importance and necessity of studies applying the same number of samples, calculation methods and measures of accuracy to compare different nICP methods consistently.

The several degrees of approximation for ICP monitoring (i.e., epidural, subdural, intraparenchymal and intraventricular) could contribute to a misleading interpretation in the validation of nICP methods against different invasive techniques. This is due to the presence of multiple intracranial compartments of variable deformability and ability to transmit pressure. Thus, ICP needs to be considered as an anisotropic parameter rather than a global isotropic pressure equally distributed in all intracranial compartments. Over this concept, each invasive method would then be specific to measuring compartmental pressures according to where they are located in the intracranial system. Under these circumstances, the characteristics of invasive ICP monitoring should also be considered in the standard nICP assessment.

Nevertheless, qualitative-wise, TCD-based nICP methods generally presented a positive degree of agreement and acceptable correlations with measured ICP (or with CPP for nCPP-based methods), with exceptions for PI-based methods. For this category, there is a divergence whether PI can predict ICP reliably, with some studies showing rather weak or even inexistent correlations between these two parameters [8,28,52,62,63,66,98]. Such a controversy might originate from the different conditions in which PI can increase independently of ICP increases. For instance, during a decrease in CPP, PI presents an increasing trend, which can be related to increases in ICP or decreases in ABP (Figure 3.4). The same behaviour occurs during a decrease in $PaCO_2$ or increases in pulsatility of ABP waveform. Instead of assuming its linear relationship with ICP, PI can rather be described as inversely proportional to mean CPP, directly proportional to ABP pulse amplitude and non-linearly proportional to C_a, CVR and heart rate [52].

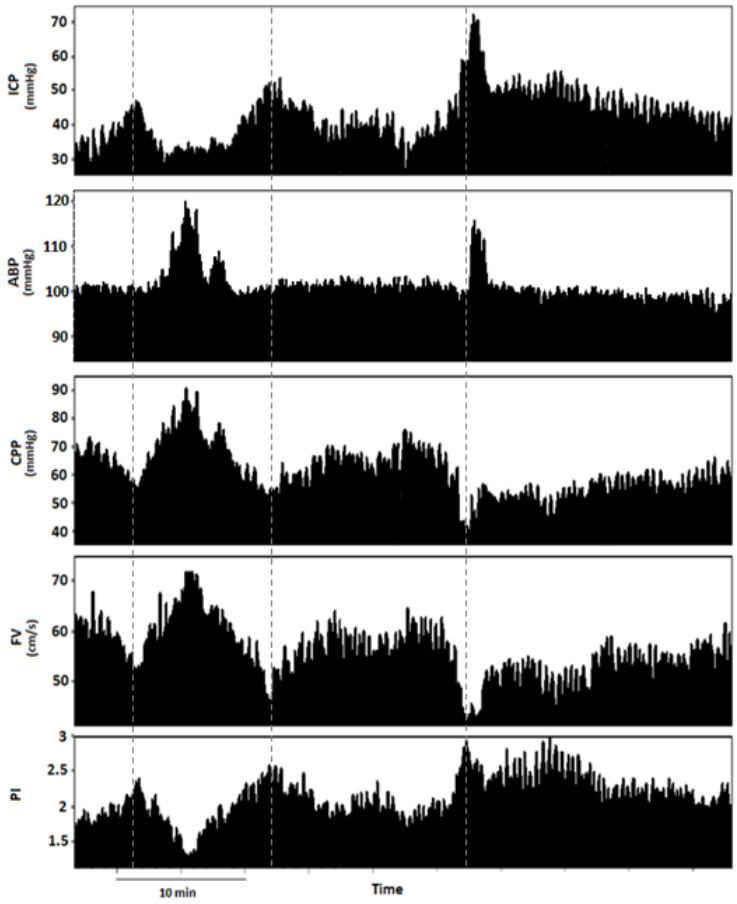

Figure 3.4. Extracted from Cardim et al., 2016 [39]. PI behaviour during drop in CPP observed in a traumatic brain-injured patient (source: Brain Physics Laboratory TBI Database, University of Cambridge). Dashed lines represent periods when PI increased due to increase in ICP, independently of changes in ABP. CPP (mmHg), cerebral perfusion pressure; PI (a.u.), pulsatility index; ICP (mmHg), intracranial pressure; ABP (mmHg), arterial blood pressure; TBI, traumatic brain injury.

The accuracy of the presented methods presented a wide variability for the different method categories (from 4.2 to 59.60 mmHg). Considering the clinically relevant range of ICP about 10 to 20 mmHg, TCD-based methods at the current state of development cannot predict mean values of ICP reliably. Certain factors, like the transmission of cerebrovascular changes to TCD waveform, its linearity, stability in time and calibration coefficients are unknown and could contribute to limiting the accuracy of TCD-based methods. However, accuracy may not be the primary performance measure in every clinical situation, and such downsides may be compensated for by the ability of the method to track changes and trends of ICP over time, rather than its absolute value [39].

3.5 Conclusion

Transcranial Doppler ultrasonography is a versatile technique for nICP estimation. However, the variability in accuracy presented by different methods needs to be clarified in clinical conditions where the use of TCD for non-invasive ICP dynamics monitoring would be relevant. The following chapters of this thesis will present and discuss these applications.

4 MATERIAL AND METHODS

The methodology applied in this thesis can be divided into three categories, including retrospective and prospective studies. Different methodologies have been implemented to: I) the assessment of the accuracy of TCD-based nICP monitoring in comparison to standard ICP invasive methods; II) feasibility studies on the application of nICP monitoring in certain clinical conditions in which ICP monitoring is relevant but not often considered; III) the assessment of a novel method for nCPP estimation presented in this thesis.

Studies in category I consisted of evaluations of the accuracy of TCD-based methods in comparison to a standard invasive method for ICP monitoring. nICP was compared to direct ICP in prospective and retrospective studies. In category II, the feasibility of nICP monitoring was evaluated in prospective and retrospective studies, in clinical conditions which ICP monitoring has not been considered due to risks and complications. Category III includes a retrospective study assessing nCPP estimation in TBI patients.

4.1 Material

Figure 4.1 depicts the organisation of retrospective and prospective studies and materials used in each of them.

4.1.1 Prospective materials

A material including prospectively collected data from TBI patients hospitalised in the Neurocritical Care Unit (NCCU) at Addenbrooke's Hospital, Cambridge, UK, between 2013 and 2015 was utilised in a study devoted to the accuracy of nICP. Patients were sedated, ventilated, and managed in the NCCU with a therapeutic protocol aiming for an ICP <25 mmHg and CPP within 60–70 mmHg. The median pre-intubation Glasgow coma scale (GCS)

score of the patients was 6 (range 3–14). This database included daily recordings of ABP, ICP and FV in the MCA using TCD.

Figure 4.1. Organogram describing the utilisation of retrospective and prospective materials within the study categories.

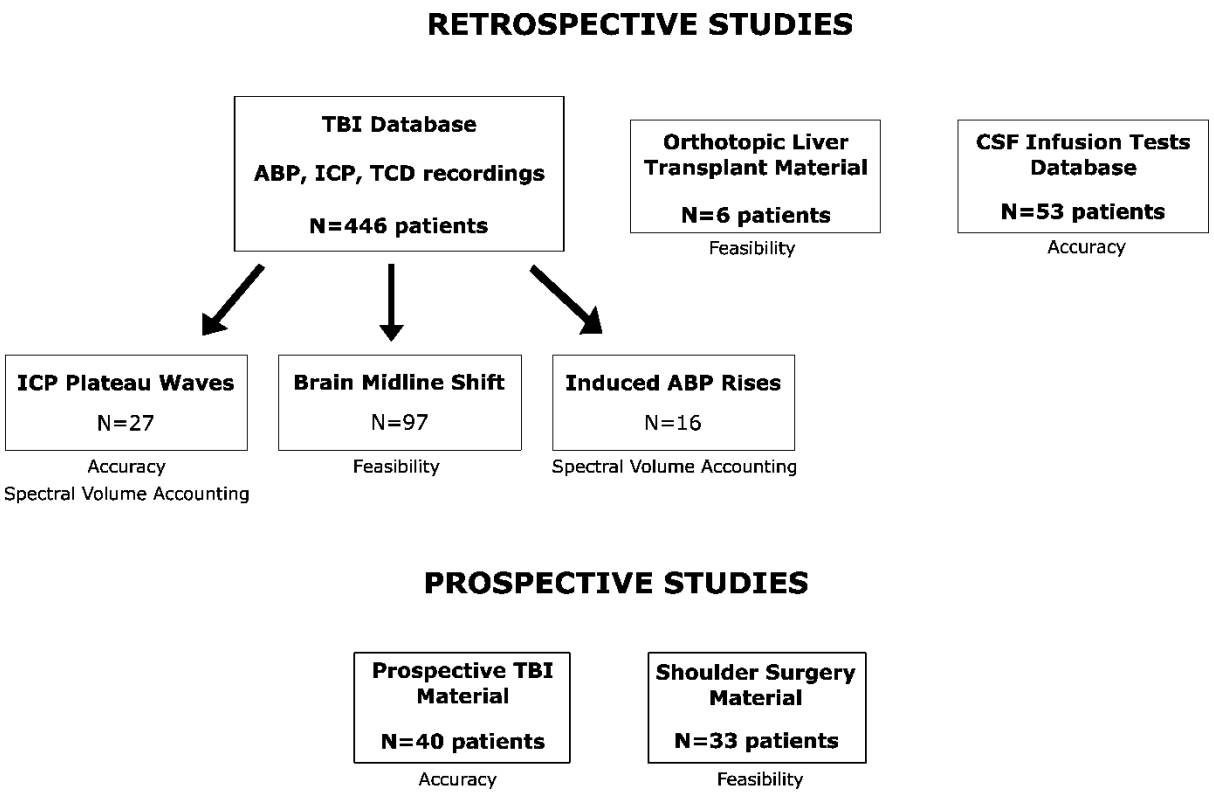

ABP, arterial blood pressure; CSF, cerebrospinal fluid; ICP, intracranial pressure; TCD, transcranial Doppler ultrasonography.

A feasibility study included in category II was based on material consisting of patients admitted to the Department of Trauma and Orthopaedics at Addenbrooke's Hospital, Cambridge, UK, between March 2016 to March 2017. The patients had no history of neurological disease and undertook elective shoulder surgery in the beach chair position. The monitoring modalities included non-invasive ABP and FV in the MCA using TCD.

4.1.2 Retrospective materials

A retrospective database has been prospectively collected since 1992 in the Brain Physics Laboratory, University of Cambridge. It includes patients admitted with traumatic brain injury in the NCCU at Addenbrooke's Hospital, with over 400 patients archived. The monitoring modalities included direct ICP, ABP and FV in the MCA using TCD. This retrospective TBI database was utilised in studies of categories I, II and III.

A second database was collected from 1994 to 1998 and 2006 at Addenbrooke's Hospital, including patients who undertook an infusion test for the investigation of cerebrospinal fluid disturbances. The monitoring modalities included direct ICP (via lumbar puncture), non-invasive ABP and FV in the MCA using TCD. This database was used in a study of category I.

A retrospective material that includes patients undergoing orthotopic liver transplant surgery (OLT) admitted to the Transplant Unit at Addenbrooke's Hospital, Cambridge, UK between December 2002 to March 2003 was used in a study of category II. Inclusion criteria for this study were the presence of chronic hepatic failure requiring OLT and acute liver failure requiring OLT. Exclusion criterion was the contraindication for OLT. The monitoring modalities included ABP and FV in the MCA using TCD.

4.1.3 Ethics approval

TBI data collection was approved by the Institutional Review Board (REC 97/290, 1997). For patients recruited before 1997, the NCCU Users' Committee allowed TCD examinations for the assessment of TBI patients. Further use of the anonymised data was allowed as a part of clinical audits.

The infusion test is a routine clinical investigation in the Hydrocephalus Clinic, Addenbrooke's Hospital, with no ethical approval required. Use of the anonymised data was allowed as a part of clinical audits.

The experimental protocol for OLT data collection and informed consent were approved by the Institutional Review Board (REC 02/308, 2002). Informed consent was obtained from all individual participants included in the study.

The experimental protocol for data collection during shoulder surgery and informed consent were approved by the Institutional Review Board (REC 16/LO/0350, 2016). Informed consent was obtained from all individual participants included in the study.

4.2 Methods

4.2.1 Basic monitoring modalities

Arterial blood pressure

Mean ABP was invasively monitored from the radial artery and calibrated at heart level using a standard pressure monitoring set (Edwards Lifesciences, Irvine, California, USA) with 18-20 G arterial catheters (Insyte-W, BD Medical Systems, Oxford, UK (Figure 4.2). When invasive monitoring was unavailable, ABP was monitored non-invasively using a finger-cuff plethysmograph device (Finapress 2300 (Ohmeda, Englewood, Colorado, USA) or Finometer Pro®, Finapres Medical Systems, Amsterdam, The Netherlands) calibrated either at heart or auditory meatus level.

Intracranial pressure

Invasive ICP monitoring was performed via an intraparenchymal probe inserted in the right cerebral hemisphere (Codman ICP MicroSensor, Codman & Shurtleff, Raynham, Massachusetts, USA, or Direct Pressure Monitor, Camino Laboratories, San Diego, California, USA) for patients requiring neurocritical care (Figure 4.2). In patients investigated for CSF disorders, ICP monitoring was performed via lumbar puncture using one spinal needle (18 G, 3.50 in) inserted between the lumbar L3/L4 or L4/L5 vertebrae, considering the foramen of Monro as the zero-calibration reference.

Transcranial Doppler ultrasonography

Cerebral blood flow velocity measurements were obtained from the middle cerebral artery (either unilateral or bilaterally) by using a TCD ultrasonography system (Neuroguard, Medasonics, Fremont, California, USA; NeuroQ, Deltex; Rimed IntraView or Digi-Lite^{TM}, Israel; or DWL Compumedics, Germany). FV was monitored exclusively from the MCA M1 segment o through the temporal window with a 2-MHz probe. The probe was held in place during the recording using a head band or frame provided by the TCD device manufacturer (Figure 4.2).

Figure 4.2. A representation of simultaneous recordings of ABP, ICP and FV. (A) Full range of recording; (B) representation of the signals waveforms. Source: Brain Physics Laboratory database, University of Cambridge.

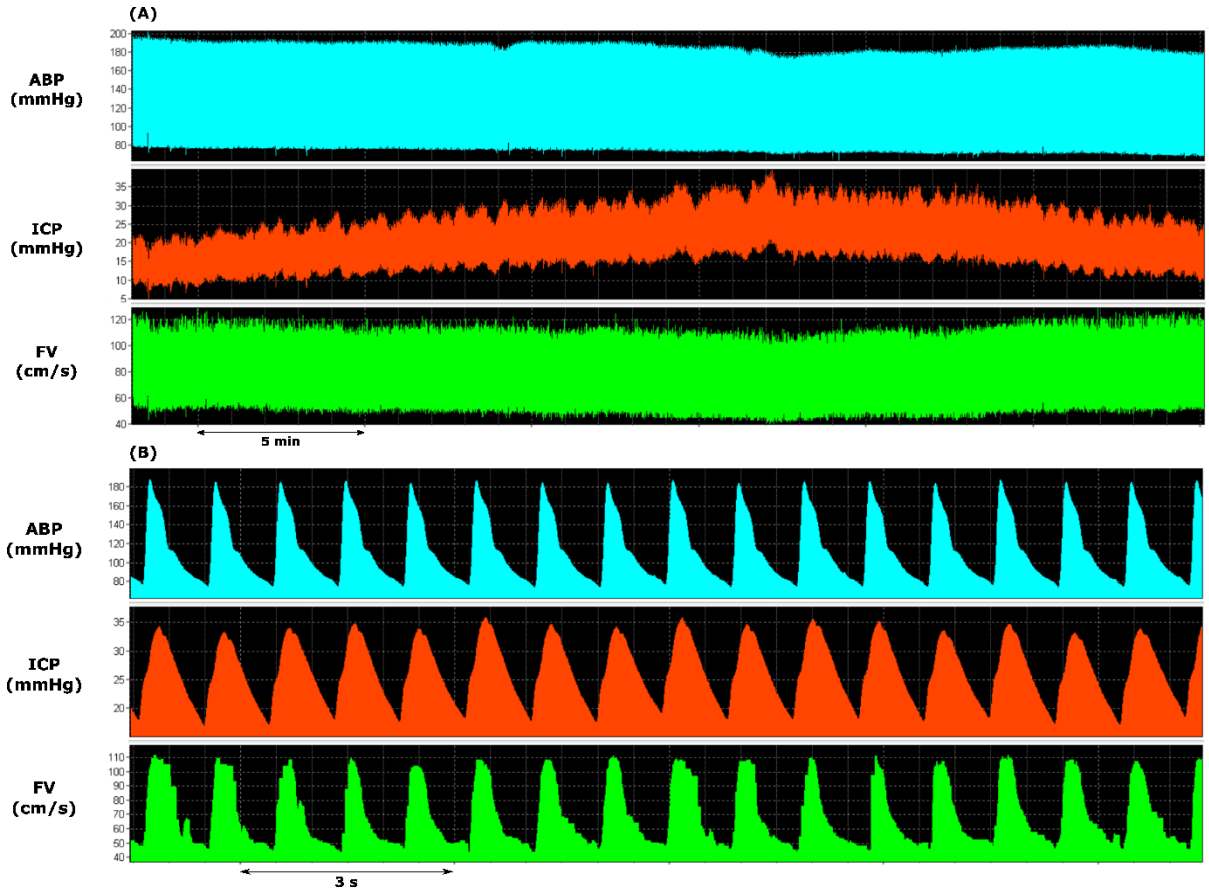

ABP (mmHg), arterial blood pressure; ICP (mmHg), intracranial pressure; FV (cm/s) cerebral blood flow velocity.

4.2.2 Data acquisition

Data were recorded, post-processed and analysed using ICM+ software (Cambridge Enterprise, UK, http://www.neurosurg.cam.ac.uk/icmplus). ABP, ICP and FV waveforms were sampled from an analogue output at 30 or 50 Hz and subsequently digitalised to 100 Hz using an analogue-to-digital converter (DT 2814, Data translation, Marlboro, California, USA).

4.2.3 Derived physiological parameters

Mean values

All data were treated with a moving average filter with a 10-seconds window to obtain the mean values.

Systolic and diastolic components

The maximum and minimum values from a 2-seconds calculation window were treated as the systolic and diastolic values, respectively.

Cerebral perfusion pressure

CPP was calculated as the difference between mean ABP and ICP.

Pulsatility index

TCD-based pulsatility index was calculated according to:

Equation 4.1

$$PI = \frac{FV_s - FV_d}{FV_m} \qquad (4.1)$$

s, systolic; *d*, diastolic; *m*, mean cerebral blood flow velocities (FV, in cm/s).

Critical Closing Pressure

The critical closing pressure of the cerebral circulation was calculated according to Varsos et al. [83].

Equation 4.2

$$\boldsymbol{CrCP = ABP - \frac{ABP}{\sqrt{(CVR \cdot C_a \cdot HR \cdot 2\pi)^2 + 1}}\ (mmHg)} \qquad (\mathbf{4.2})$$

Where:

Equation 4.3

$$CVR = \frac{ABP}{FV} \qquad (4.3)$$

Equation 4.4

$$C_a = \frac{C_aBV1}{a1} \qquad (4.4)$$

CVR (mmHg/(cm/s)) represents cerebral vascular resistance, C_a (cm/mmHg) denotes compliance of the cerebral arterial bed (arteries and arterioles) and *HR,* heart rate given in beat/s. $a1$ represents the pulse amplitude of the first harmonic of the ABP waveform; *f1*, the pulse amplitude of the first harmonic of the FV waveform; C_aBV1, the pulse amplitude of the first harmonic of the cerebral arterial blood volume waveform (C_aBV). The pulse amplitude of first harmonics is determined with fast Fourier transformation (FFT).

Cerebral compliance (C) represents the ability of the brain to adapt to changes in volume (ΔV) inside the cranium in response to changes in pressure (ΔP) to avoid intracranial hypertension. This parameter includes the cerebrovascular arterial compliance (C_a), which describes the change of cerebral arterial blood volume in response to change in ABP [99].

Derived from CrCP and ABP, other indices, such as the diastolic closing margin (DCM) of the brain microvasculature, can be obtained. Previous works have demonstrated that diastolic ABP (ABP_d) below CrCP is associated with the loss of measurable FV during diastole [100], causing

an acceleration of brain ischemia when CPP decreases further. The difference in pressures between ABP_d and CrCP (DCM) represents the force that allows cerebral blood flow circulation during diastole. When DCM is exhausted (≤0 mmHg), vessels will collapse resulting in cessation of cerebral blood flow [100,101].

Equation 4.5

$$DCM = ABP_d - CrCP \ (mmHg) \tag{4.5}$$

Non-invasive intracranial pressure

nICP was calculated using different TCD-based methods. As previously described in Chapter 3, these methods are:

- Black box model ($nICP_{BB}$) (Section 3.3.3):

ABP-nICP transformations for this method were derived from analysis of a retrospective database of patients with traumatic brain injury (N=140).

- $nICP_{FVd}$:

$nICP_{FVd}$ was calculated as the difference between ABP and $nCPP_{FVd}$, according to the relationship described by Czosnyka et al. [71]

Equation 4.6

$$nCPP_{FV_d} = ABP \times \frac{FV_d}{FV_m} + 14 \ (mmHg) \tag{4.6}$$

14 mmHg is the zero compensation factor established in a cohort of TBI patients [71].

- $nICP_{CrCP}$:

$nICP_{CrCP}$ was calculated as the difference between ABP and $nCPP_{CrCP}$ as described in by Varsos et al. [78]:

Equation 4.7

$$nCPP_{CrCP} = ABP \times \left[0.734 - \frac{0.266}{\sqrt{(CVR \cdot C_a \cdot HR \cdot 2\pi)^2 + 1}}\right] - 7.026 \ (mmHg) \quad (4.7)$$

Equation 4.8

$$nICP_{CrCP} = ABP - nCPP_{CrCP} \ (mmHg) \quad (4.8)$$

- $nICP_{PI}$:

nICP estimation based on TCD-derived PI was calculated from the linear regression of known values of ICP and PI obtained from a retrospective cohort of TBI patients (N=292). The regression equation was based on data analysed by Budohoski et al.[102] and given by:

Equation 4.9

$$nICP_{PI} = 4.47 \times PI + 12.68 \ (mmHg) \quad (4.9)$$

Non-invasive cerebral perfusion pressure

nCPP was calculated as the difference between ABP and nICP and according to a novel TCD-based method proposed in this thesis (Chapter 7).

Continuous indices of cerebral autoregulation

Cerebral autoregulation is the ability of the brain to maintain relatively constant blood flow during changes in perfusion pressure or arterial blood pressure. Continuous indices of cerebral autoregulation were calculated from spontaneous fluctuations of ABP and FV. The correlation coefficient methodology as described by Czosnyka et al. [86] was used, in which ABP signal was used for identification of spontaneous fluctuations and treated as the stimulus. Mean FV was

used as a surrogate marker of cerebral blood flow, i.e., the comparator signal. The correlation coefficient between ABP and FV, termed Mxa (mean flow index), was calculated [103]. Mxa close to +1 denotes that slow fluctuations in ABP produce synchronised slow changes in FV, indicating defective cerebral autoregulation. Based on previous studies considering TBI patients, negative values or values less than 0.3 indicate intact cerebral autoregulation, while positive values above 0.3 indicate failure of cerebral autoregulation [104–106]. For Mxa calculation, all signals were time-averaged using a window of 10 s. Subsequently, a moving, linear correlation coefficient between ABP and FV signals were calculated using a 300-seconds window with an update every 10 s [86].

Cerebral autoregulation was also assessed using the autoregulation index (ARI), a dimensionless index ranging from 0 to 9, for which a response of FV to a hypothetical impulse change in ABP is estimated using transfer function analysis of spontaneous fluctuations in ABP and FV [107,108]. An ARI of 9 describes a system in which CBF returns quickly to baseline levels after step changes in ABP; an ARI value of 0 describes a system in which there is no compensatory change in CBF, indicating completely impaired cerebral autoregulation. On this scale, normal autoregulatory capacity is defined as an ARI of 4 to 7, abnormal 3 and below [107,109,110]. ARI was calculated using a plugin developed for ICM+®, performed over a 120 s long-sliding window updated every 10 s. FV changes recorded during the step change in ABP are normalised and compared to 10 grades (0-9) to determine which model response constitutes the best fit, and the grade of that response is returned as ARI [107].

Optimal ABP

A method for individualisation of CPP-oriented management based on the determination of cerebrovascular reactivity (using the pressure reactivity index (PRx)) has been proposed previously [111,112]. PRx is the correlation coefficient between ABP and ICP [113], and studies in TBI populations have indicated that PRx >0.25 is associated with impaired cerebral autoregulation in patients with poor outcome [106]. This methodology was applied to obtain optimal values for ABP, instead of CPP. In this case, only nICP was available, thus the non-invasive PRx (nPRx) was calculated. For nPRx calculation, all signals were time-averaged using a window of 10 s. Subsequently, a moving, linear correlation coefficient between ABP and nICP signals were calculated using a 300-seconds window with an update every 10 s.

4.2.4 Statistical analysis

Statistical analysis was performed using R Studio software (R version 3.4.1) and OriginPro software (version 8, OriginLab Corporation, Wellesley, Massachusetts, USA). The distribution of all data samples was checked for normality using the Shapiro-Wilk test. Depending on the distribution, either parametric or non-parametric statistical tests were used in the analysis.

The analysis included correlations between non-invasive ICP estimators and direct ICP regarding mean values and changes in the time domain. The Bland-Altman method was used to determine the agreement between invasive ICP and the different nICP methods, with their respective bias and 95% confidence interval for prediction. The bias represents the difference between mean values of nICP and ICP; 95% CI is calculated as 1.96 times the standard deviation of the bias. Also, the area under the curve (AUC) of the receiver operating characteristic curve (ROC) was performed to determine the accuracy of the nICP and nCPP methods to predict certain ICP and CPP thresholds. Similarly, where applicable, the ROC analysis was used to calculate the sensitivity and specificity of various thresholds. The predicting ability is considered reasonable when the AUC is higher than 0.7, and strong when the AUC exceeds 0.8 [114]. Statistical differences between ROC curves were verified using the DeLong's test for two correlated ROC curves (R package *pROC* [115]).

The specific statistical methods applied in individual studies are described in the respective chapters.

5 RESULTS AND DISCUSSIONS I: ASSESSMENT OF THE ACCURACY OF TCD-BASED nICP MONITORING METHODS

5.1 A prospective study on non-invasive assessment of ICP in patients with traumatic brain injury

The results presented in this section have been published in *Journal of Neurotrauma* [8]:

Cardim, D., Robba, C., Donnelly, J., Bohdanowicz, M., Schmidt, B., Damian, M., Varsos, G. V, Liu, X., Cabeleira, M., Frigieri, G., Cabella, B., Smieleweski, P., Mascarenhas, S., and Czosnyka, M. (2015). Prospective study on non-invasive assessment of ICP in head injured patients: comparison of four methods. J. Neurotrauma.

Introduction

Chapter 3 highlighted that the existing non-invasive ICP methods based on TCD waveform analysis present with different degrees of agreement for ICP prediction in patients with traumatic brain injury and other clinical conditions.

Considering this issue, this prospective observational study compared a set of TCD-based nICP methods with direct invasive ICP measurements in a single cohort of TBI patients to determine the accuracy of nICP.

Materials and methods

Patient population

This study included prospectively collected data described in Section 4.1.1. This material consisted of 40 patients with traumatic brain injury (32 males (80%), 8 females (20%), population median age 32 years (IQR: 50-21)).

Clinical monitoring and data collection

The implemented clinical monitoring included ABP, ICP and FV as described in Section 4.2.1, in a total of 66 recordings. For FV, the right MCA was chosen because the intraparenchymal ICP probe was inserted on the right side, but for recordings in which right FV was of poor quality and left side was better, this side was chosen.

Four TCD-based nICP methods were assessed in this study, namely: $nICP_{BB}$, $nICP_{FVd}$, $nICP_{CrCP}$ and $nICP_{PI}$. These methods were chosen to contemplate all TCD-based nICP categories described in Chapter 3.

nICP methods and derived physiological parameters were calculated as described in Section 4.2.3.

Statistical analysis

Multiple measurements were considered as independent values. The data were tested for normal distribution using the Shapiro-Wilk test and found to be non-parametric. Statistical comparisons between the mean values of direct ICP and nICP were performed using Student's t-test. The analysis included correlations between non-invasive ICP estimators and measured ICP regarding mean values, with R representing the Pearson correlation coefficient, with the level of significance set at 0.05. Results are presented as mean ± SD. The 95% CI for prediction and bias of the nICP methods were estimated using the Bland-Altman analysis. ROC analysis was performed to determine the ability of the non-invasive methods to predict raised ICP (using a threshold of 17 mmHg). This threshold was chosen due to its proximity to values which would commonly prompt treatment in the clinical setting (normally above 20-25 mmHg [7]). For recordings in which mean ICP changes were greater than 7 mmHg, the averaged correlation in the time domain between ICP and nICP methods was calculated, as well as the correlation between ΔICP and ΔnICP. In this case, "Δ" represents the difference between the maximum and minimum mean value in each recording during ICP changes. Correlations in the time domain are independent of mean values of ICP or nICP and represent the ability of a nICP method to replicate relative changes observed in direct ICP across time.

Results

Table 5.1 presents mean values of the physiological variables assessed in the prospective cohort.

Among the 66 recordings analysed, 8 presented considerable spontaneous changes in ICP (ΔICP) ≥7 mmHg in the time domain. Table 5.2 summarises the averaged correlation coefficients in the time domain between direct ICP and nICP methods. In the same table, correlations between ΔICP and ΔnICP are compared. An example of nICP recording with the four investigated methods is presented in Figure 5.1.

Table 5.1. Physiological variables and nICP estimations assessed, presented and mean ± SD.

ABP	93.74±12.72
ICP	13.57±4.96
CPP	80.17±12.30
$nICP_{BB}$	13.07±4.18
$nICP_{FVd}$	20.91±7.82*
$nICP_{CrCP}$	18.01±2.35*
$nICP_{PI}$	17.68±1.02*

ABP (mmHg), arterial blood pressure; ICP (mmHg), intracranial pressure; CPP (mmHg), cerebral perfusion pressure; $nICP_{BB}$ (mmHg), estimator based on a black-box mathematical model; $nICP_{FVd}$ (mmHg), estimator based on the diastolic cerebral blood flow velocity; $nICP_{CrCP}$ (mmHg), estimator based on the concept of critical closing pressure; $nICP_{PI}$ (mmHg), estimator based on the pulsatility index; SD, standard deviation.

*At the 0.05 level, ICP and nICP are significantly different ($p<0.05$).

Table 5.2. Correlations between non-invasive ICP methods with invasive ICP in the time domain (mean±SD) and between ΔICP and ΔnICP in cases when ΔICP ≥7 mmHg (N=8). Correlation between ΔICP and ΔnICP was not significant in any of the methods.

R (time domain)				R (ΔICP *vs* ΔnICP)			
$nICP_{BB}$	**$nICP_{FVd}$**	**$nICP_{CrCP}$**	**$nICP_{PI}$**	**$\Delta nICP_{BB}$**	**$\Delta nICP_{FVd}$**	**$\Delta nICP_{CrCP}$**	**$\Delta nICP_{PI}$**
0.48±0.40	-0.28±0.69	0.18±0.56	0.61±0.35	0.68	-0.32	0.28	0.19

$nICP_{BB}$ (mmHg), estimator based on a black-box mathematical model; $nICP_{FVd}$ (mmHg), estimator based on the diastolic cerebral blood flow velocity; $nICP_{CrCP}$ (mmHg), estimator based on the concept of critical closing pressure; $nICP_{PI}$ (mmHg), estimator based on the pulsatility index; SD, standard deviation of the mean.

Table 5.3 presents statistical comparisons among nICP methods evaluated. $nICP_{BB}$, $nICP_{FVd}$ and $nICP_{CrCP}$ demonstrated moderate but significant correlations ($p<0.05$) with direct ICP; while $nICP_{PI}$ had poor correlation ($p>0.05$) (Figure 5.2). In regards to Bland-Altman analysis, $nICP_{BB}$ and $nICP_{PI}$ showed biases close to zero, and along with $nICP_{CrCP}$, presented similar 95% CI, close to 10 mmHg. $nICP_{FVd}$ showed greater bias and 95% CI (Figure 5.3). In Figure 5.3 each plot was complemented by the corresponding error histograms.

As observed in Table 5.1, the patient cohort presented a low range of mean ICP values. Consequently, to obtain a consistent ROC analysis, it was necessary to use a threshold reasonably close to, but below critical values for intracranial hypertension treatment. $nICP_{FVd}$ presented the best AUC value (AUC=0.70). Also, Table 5.3 presents results from the arithmetic average of only the best non-invasive ICP estimators ($nICP_{Av}$), i.e., $nICP_{BB}$, $nICP_{FVd}$ and $nICP_{CrCP}$. This method showed slightly improved AUC=0.73 (95% CI: 0.59-0.87) (Figure 5.4), but not statistically significant when compared to $nICP_{FVd}$ ($p=0.48$).

Table 5.3. Correlations between non-invasive methods with invasive ICP (R) (N=66 recordings), bias (±SD), 95% CI for ICP prediction and AUC. The combination of the best performing estimators ($nICP_{Av}$) resulted in better correlation with direct ICP and improved 95% CI and AUC.

Method	R	Bias	95% CI	AUC
$nICP_{BB}$	0.39*	-0.50±5.07	9.94	0.66
$nICP_{FVd}$	0.39*	7.34±7.45+	14.62	0.70
$nICP_{CrCP}$	0.35*	4.44±4.69+	9.19	0.64
$nICP_{PI}$	0.15	4.11±4.90	9.62	0.43
$nICP_{Av}$	0.47*	3.76±4.69+	9.17	0.73

ICP (mmHg), intracranial pressure; $nICP_{BB}$ (mmHg), estimator based on a black-box mathematical model; $nICP_{FVd}$ (mmHg), estimator based on the diastolic cerebral blood flow velocity; $nICP_{CrCP}$ (mmHg), estimator based on the concept of critical closing pressure; $nICP_{PI}$ (mmHg), estimator based on the pulsatility index; $nICP_{Av}$ (mmHg), averaged estimator based on $nICP_{BB}$, $nICP_{FVd}$ and $nICP_{CrCP}$; R, Pearson correlation coefficient; CI: confidence interval; AUC: area under ROC curve; SD, standard deviation.

*Correlation is significant at the 0.05 level. +At the level of 0.05 the population mean is significantly different from the test mean (0).

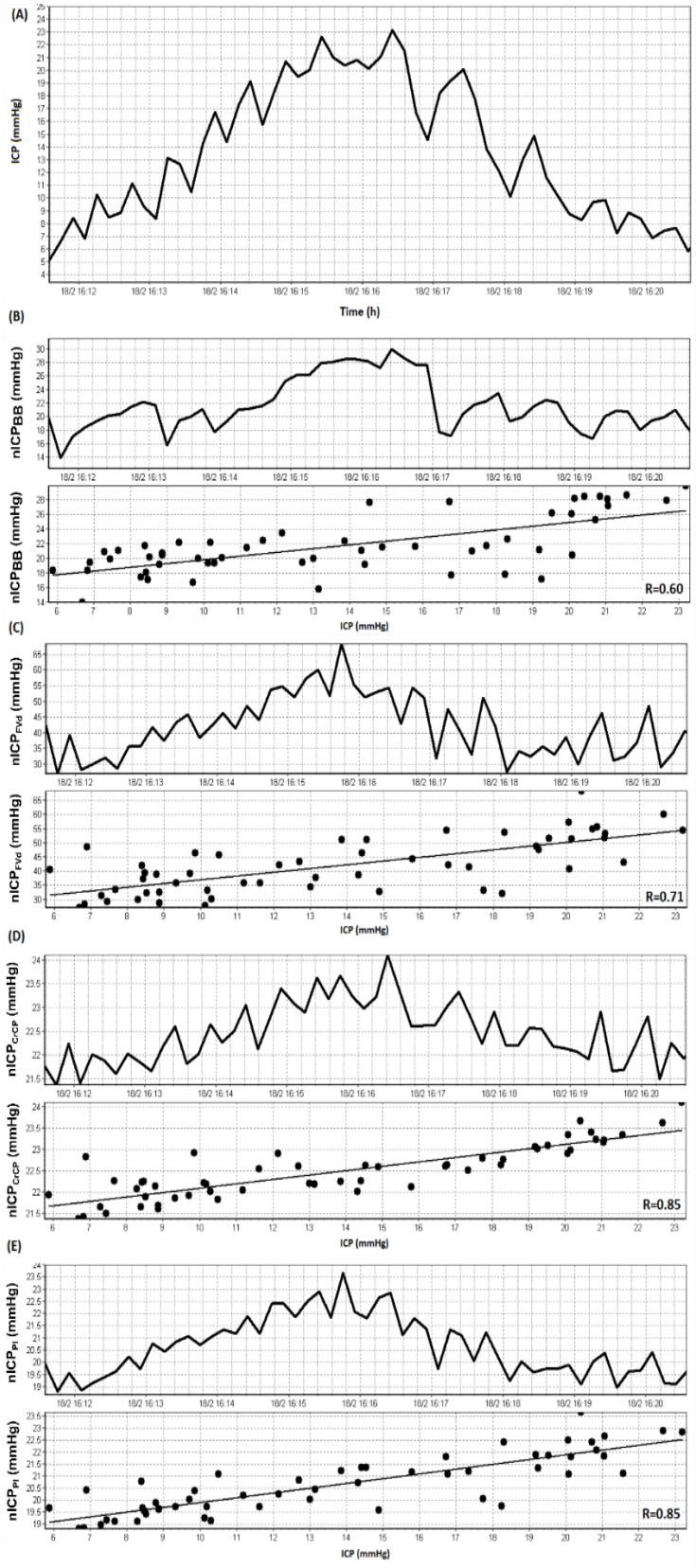

Figure 5.1. Example of recording of nICP with four investigated methods in a case when ICP changed considerably. (A) ICP; (B) $nICP_{BB}$; (C) $nICP_{FVd}$; (D) $nICP_{CrCP}$; (E) $nICP_{PI}$. In this case, all nICP estimators could replicate changes in ICP in time reliably (R>0.60).

ICP (mmHg), intracranial pressure; $nICP_{BB}$ (mmHg), estimator based on a black-box mathematical model; $nICP_{FVd}$ (mmHg), estimator based on the diastolic cerebral blood flow velocity; $nICP_{CrCP}$ (mmHg), estimator based on the concept of critical closing pressure; $nICP_{PI}$ (mmHg), estimator based on the pulsatility index; R, correlation coefficient in the time domain.

Figure 5.2. Linear regressions and Pearson correlation plots between ICP and nICP estimators for (A) $nICP_{BB}$, (B) $nICP_{FVd}$, (C) $nICP_{CrCP}$ and (D) $nICP_{PI}$. $nICP_{BB}$, $nICP_{FVd}$, $nICP_{CrCP}$ presented moderate correlations with ICP.

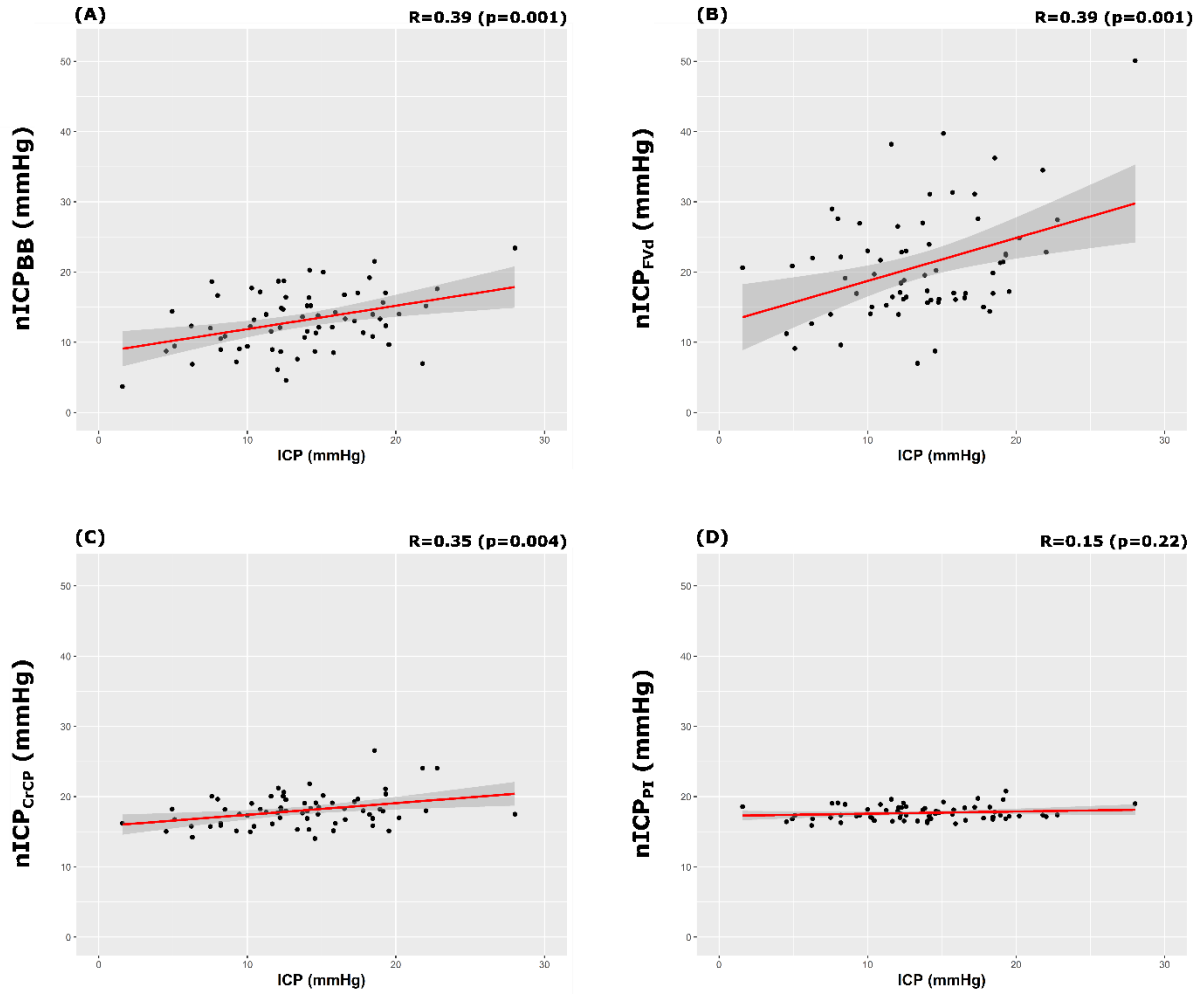

Grey shaded areas on the plots represent the 95% confidence intervals for the linear regressions between ICP and nICP.

ICP (mmHg), intracranial pressure; $nICP_{BB}$ (mmHg), estimator based on a black-box mathematical model; $nICP_{FVd}$ (mmHg), estimator based on the diastolic cerebral blood flow velocity; $nICP_{CrCP}$ (mmHg), estimator based on the concept of critical closing pressure; $nICP_{PI}$ (mmHg), estimator based on the pulsatility index; R, Pearson correlation coefficient.

Figure 5.3. Bland-Altman and error histograms plots showing bias and 95% CI for prediction of ICP for (A) $nICP_{BB}$, (B) $nICP_{FVd}$ (B), (C) $nICP_{CrCP}$ and (D) $nICP_{PI}$. The overall 95% CI ranged around 10 mmHg.

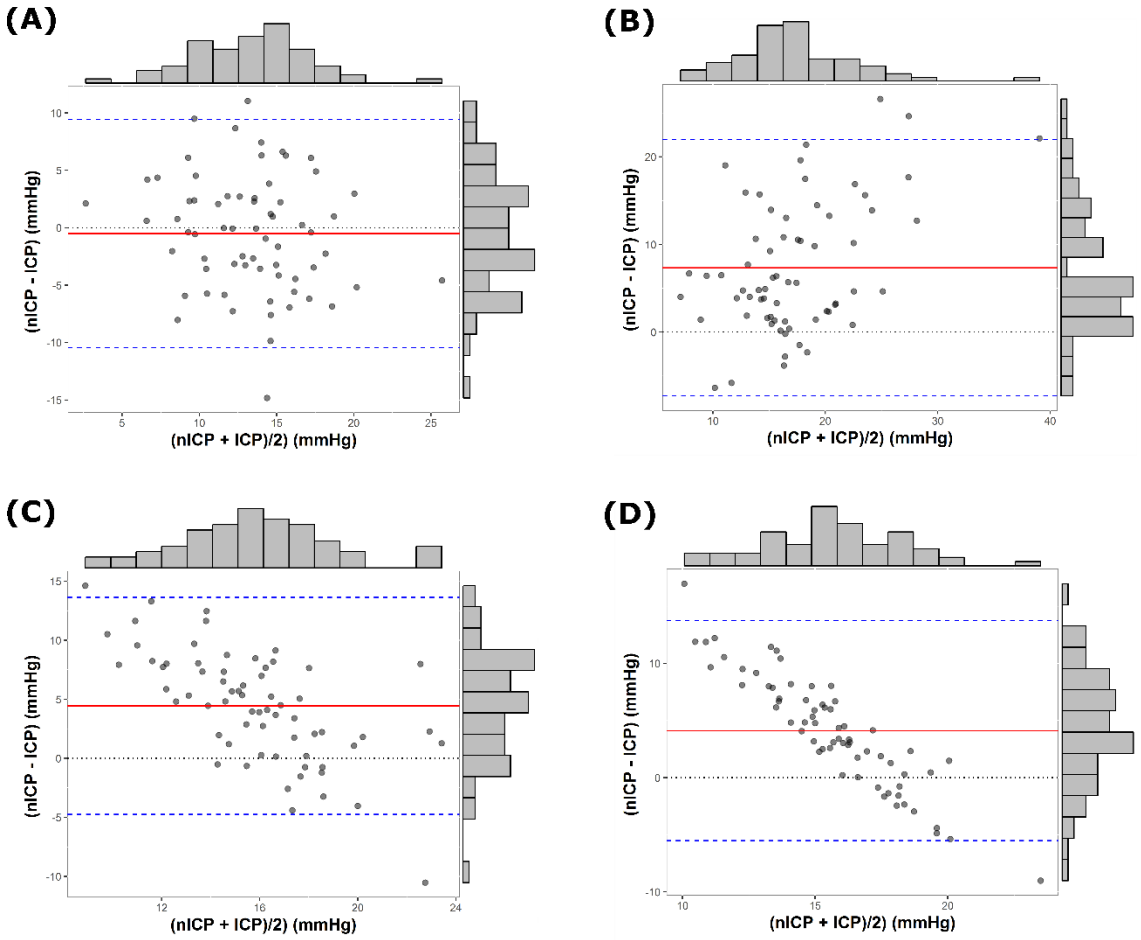

Red lines represent the bias between nICP and ICP; blue dashed lines represent the upper and lower 95% confidence intervals for ICP prediction.

ICP (mmHg), intracranial pressure; $nICP_{BB}$ (mmHg), estimator based on a black-box mathematical model; $nICP_{FVd}$ (mmHg), estimator based on the diastolic cerebral blood flow velocity; $nICP_{CrCP}$ (mmHg), estimator based on the concept of critical closing pressure; $nICP_{PI}$ (mmHg), estimator based on the pulsatility index.

Figure 5.4. Receiver operating characteristic analysis showing the area under the curve (AUC) for the averaged nICP estimator ($nICP_{Av}$, AUC = 0.73).

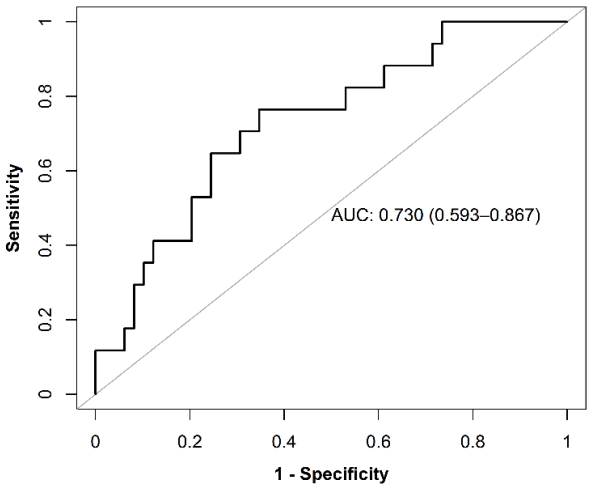

Discussion

Many pathological events occurring during intracranial hypertension, such as critically reduced CPP and episodic rises in ICP caused by hyperaemia, can be identified by remarkable changes in cerebral blood flow velocity assessed using TCD [116]. For instance, as ICP increases and CPP correspondingly decreases, a characteristic highly pulsatile FV pattern can be observed. Ongoing increases in ICP may result in reduction followed by loss of diastolic flow, progressing to isolated systolic spikes in the FV waveform. This culminates in an oscillating flow pattern which has been associated with the onset of intracranial circulatory arrest [103,117].

In this study, although mean nICP did not demonstrate a strong correlation with direct ICP, the cerebral circulation dynamics could be observed with TCD-based methods as nICP changes in the time domain.

The best performance for monitoring of ICP dynamics was presented by $nICP_{PI}$, which showed the strongest averaged correlation coefficient in the time domain across 8 patients (R=0.61), followed by $nICP_{BB}$ (R=0.48). Although none of the methods presented a satisfactory correlation between ΔnICP and ΔICP, $nICP_{BB}$ was the best considering variations of ICP ≥7 mmHg (R=0.68, p=0.06), demonstrating the ability of this method to detect differences in the magnitude of ICP changes recorded in time.

Considering the mean absolute changes in ICP, $nICP_{BB}$ had the best performance, as it presented the most consistent indicators for ICP prediction. For $nICP_{BB}$, the bias was not significantly different from zero, indicating that both methods were not different in rendering mean ICP values. Its 95% CI for prediction was even smaller as previously reported by Schmidt et al. (12.8 mmHg) [25] or for $nICP_{Heldt}$ (15 mmHg (SDE of 7.6 mm Hg) [36]. Furthermore, AUC for $nICP_{BB}$ was close to reasonable values (0.7) denoting the method's ability to distinguish elevated ICP.

In contrast, $nICP_{FVd}$ and $nICP_{CrCP}$ biases were significantly different from zero (Table 5.3). However, for $nICP_{FVd}$, moderate correlation coefficients and reasonable AUC were observed. $nICP_{CrCP}$, on the other hand, did not present a reasonable AUC. $nICP_{FVd}$ had the greatest 95% CI for ICP prediction and $nICP_{CrCP}$ the smallest. The low range of ICP encountered (Table 5.1) can be a potential limitation, as it prevented a thorough prediction analysis in conditions of elevated intracranial pressure. This characteristic can be attributed to the therapeutic protocol applied in TBI patients.

Despite the best ability to detect changes in ICP across time domain, $nICP_{PI}$ did not show any consistent statistical parameters for ICP estimation; hence, it can be considered the weakest estimator. These findings contradict the results published by Bellner et al., in which PI strongly correlated with ICP [27] (Section 3.3.1). However, such results agree with findings from Figaji et al., whose work shows that PI is not a reliable non-invasive estimator of ICP in children with severe TBI [28]. These results related to the non-specificity of PI to changes in ICP as discussed in Section 3.4 and demonstrated in Figure 3.4.

To find a more reliable method using an approach capable of approximating the different features of each estimator considered in this assessment, those methods presenting the best estimation for ICP 'as a number' (absolute ICP changes), i.e., $nICP_{BB}$, $nICP_{FVd}$ and $nICP_{CrCP}$, were averaged to form a new method, named $nICP_{Av}$. The inclusion of $nICP_{PI}$ in this calculation did not yield any improvement in estimation. In comparison to the best estimator $nICP_{BB}$, $nICP_{Av}$ only presented inferior values for bias, which was significantly different from zero. Thus, in this context, $nICP_{Av}$ represents a more reliable way to predict ICP non-invasively, possibly because it includes a broader set of inputs (ABP, mean FV, FV_d and CrCP).

Under these circumstances, the variability in accuracy observed for nICP may be explained by specific characteristics of the methods. $nICP_{BB}$, for instance, reflects ABP waveform being constantly modified by TCD characteristics; hence, it is susceptible to changes in vascular

components (such as CVR, C_a) and consequently CBF. $nICP_{FVd}$ responds to the ratio FV_d/FV_m, which is subject to decreases during hypoventilation due to vasodilation [71]. It also replicates changes in ICP provoked by varying ABP, as mean ABP is a multiplier in the formula. $nICP_{CrCP}$, as previously described, is also modulated by changes in CVR and C_a. For $nICP_{PI}$, it is known that decreasing CPP produces specific changes in FV with stable systolic and falling diastolic values [117,118]. These changes may be observed in PI, since this index is inversely proportional to CPP, among other factors [52]. These interactions illustrate that nICP methods essentially reflect changes in cerebrovascular parameters, particularly modulating cerebral blood flow velocity acquired using TCD. However, different methods might respond to specific factors.

An essential aspect of every monitoring method is the degree of accuracy required for clinical application. According to the Association for Advancement of Medical Instrumentation and the Brain Trauma Foundation guidelines [9,10,119], ICP monitoring devices should have continuous output in the 0-100 mmHg range, with an accuracy of ±2 mmHg in the 0-20 mmHg range, and maximum prediction error of 10% for ICP >20 mmHg. In this study, the estimation performance represented by the 95% CI ranged around 10 mmHg, with all methods above the specified limits.

Another aspect worthy of consideration in the assessment of non-invasive methods is the accuracy of the current invasive ICP methods and their agreement. In the clinical practice, intraventricular and intraparenchymal pressure methods represent the gold standard for ICP monitoring. However, epidural probes are also often used. Simultaneous measurement of ICP using intraparenchymal and intraventricular probes showed a bias of −1.2 and a 95% CI of 6.8 mmHg (SDE of 3.4 mmHg) [120]. In another study, simultaneous measurements of ICP using an intraparenchymal and epidural probes presented a bias of 4.3 mmHg, with 95% CI of 17 mmHg (SDE of 8.5 mmHg) [121].

Ideally, invasive and TCD-based nICP methods should present similar measures of accuracy. However, it is important to highlight that non-invasive techniques are subjected to certain interferences (signal attenuation and movement artefacts, for TCD), which certainly influence their degrees of accuracy.

Nevertheless, the nICP methods evaluated in this study, showing biases ranging from -0.5 to 7.34 mmHg and 95% CI from 9.19 to 14.68 mmHg (Table 5.3), in general, performed better than the invasive epidural method available for the clinical management of patients.

5.2 Non-invasive assessment of intracranial pressure during infusion test

The results presented in this section have been published in *Acta Neurochirurgica* [122]:

Cardim, D., Czosnyka, M., Donnelly, J., Robba, C., Cabella, B.C.T., Liu, X., Cabeleira, M.T., Smielewski, P., Haubrich, C., Garnett, M.R., Pickard, J.D., and Czosnyka, Z. (2016). Assessment of non-invasive ICP during CSF infusion test: an approach with transcranial Doppler. Acta Neurochir. (Wien). 158, 279–87.

Introduction

Infusion test is a diagnostic modality that enables the assessment of the CSF dynamics and the compensatory ability of the cranial-spinal fluid system in patients diagnosed with hydrocephalus [123]. The principle of this test is based on a constant infusion rate of artificial CSF into any accessible compartment, which produces a gradual and uncompensated increase in ICP [124].

Proceeding with the assessment of the nICP accuracy, this study compared the estimation performances of the four previously presented nICP methods in a prospective cohort of patients with hydrocephalus whose CSF dynamics were investigated using infusion tests with controllable rise of ICP.

Material and Methods

Patient population

This study included data from a retrospective database of patients with CSF disturbances described in Section 4.1.2. This material consisted of 53 patients who undertook infusion tests. The median age of the patients was 55 years (IQR: 66-38 years; 31 males (58.5%), 22 females (41.5%)). Most of the data collection took place in the first period of 1994-1996 (N=39, 73.6%). Nevertheless, the experimental protocol and materials used did not differ for data collected in 2006.

Infusion test

An infusion test is a computerised method involving the cerebrospinal infusion of artificial CSF (normal saline or Hartman's solution) into the subarachnoid space, based on the traditional constant rate infusion test described by Katzman and Hussey [124]. For this purpose, one spinal needle (18 G, 3.50 in) is inserted between the lumbar L3/L4 or L4/L5 vertebrae, and it is used for both pressure measurements and fluid infusion. This needle is connected to a pressure transducer via a stiff saline-filled tube and to an infusion device (Alaris® GH Plus Syringe Pump, Carefusion) with a 50 ml syringe (BD Plastic™), mounted on a trolley containing a pressure monitor (Simonsen & Will, Sidcup, England) connected to a computer [125]. The threshold of the opening pressure is 13 mmHg, and the infusion rate is 1 ml/min when the pressure is higher than the threshold. If the pressure is lower than the threshold, the infusion rate is 1.5 ml/min when. The start of the infusion is initiated after baseline recording (10 minutes), whereas the end of the infusion is signalled by the achievement of a steady-state ICP plateau phase. After termination of the infusion, ICP is continuously recorded until it reaches a steady baseline level [125] as depicted in Figure 5.5.

Clinical monitoring and data collection

The implemented clinical monitoring included ABP, ICP and FV (Figure 5.5) as described in Section 4.2.1, in a total of 53 recordings. In this case, ABP was monitored non-invasively using a Finapres® finger cuff device (Ohmeda Finapres® 2300, Englewood, Colorado, USA), calibrated at the level of the heart. This device supports applications in which waveform-dependent indices are extracted [126]; however, its absolute ABP measurements presented inter-individual variability [127].

$nICP_{BB}$, $nICP_{FVd}$, $nICP_{CrCP}$ and $nICP_{PI}$ were evaluated. nICP methods and derived physiological parameters were calculated as described in Section 4.2.3.

Figure 5.5. Example of recording demonstrating the baseline and plateau phases of the infusion test and the parameters assessed (ABP, ICP, FV).

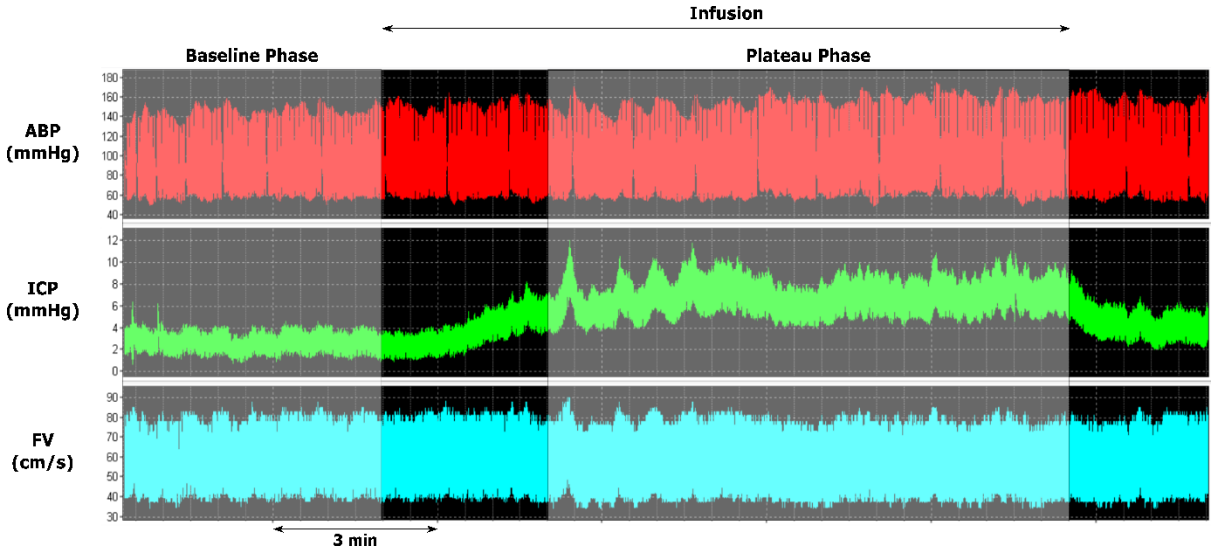

ABP (mmHg), arterial blood pressure; ICP (mmHg), intracranial pressure; FV (cm/s), cerebral blood flow velocity.

Statistical analysis

The data were tested for normal distribution using the Shapiro-Wilk test and distributions were non-parametric. The analysis included Spearman correlations (R) between mean ΔICP and ΔnICP and averaged correlations for variations of nICP in the time during ICP increase. The magnitude of ICP changes (Δ) was calculated as the difference between mean values of plateau and baseline phases in each recording during the test. Median values of ICP and nICP are presented with their respective interquartile range (IQR) in mmHg. The Bland-Altman method was used to determine the agreement between measured ICP and the various nICP methods, with their respective 95% CI for prediction of ICP and bias for baseline and plateau phases. Also, the Mann-Whitney test was used to assess whether nICP samples differed significantly from ICP for both baseline and plateau phases. Wilcoxon test was applied to determine whether the population medians differed between baseline and plateau phases for each nICP estimator and other physiological parameters.

Results

Table 5.4 presents comparisons among non-invasive methods adopted in this study. Table 5.5 presents the assessed physiological parameters applied for nICP estimations, at baseline and plateau phases, and their Δ correlations with ΔICP and ΔABP.

Regarding confidence intervals (bias±95% CI), $nICP_{BB}$ showed 4.46±15.33 mmHg; $nICP_{FVd}$ showed 11.90±25.19 mmHg; $nICP_{CrCP}$ showed 11.12±15.09 mmHg and $nICP_{PI}$ showed 8.91±10.58 mmHg. During plateau phase, every method presented increased 95% CI: -7.35±19.21 mmHg for $nICP_{BB}$; 1.66±29.97 mmHg for $nICP_{FVd}$; -2.53±17.80 mmHg for $nICP_{CrCP}$ and -6.18±19.07 mmHg for $nICP_{PI}$ (Table 5.4).

Correlations between ΔICP and ΔnICP were better represented by $nICP_{PI}$ and $nICP_{BB}$, R= 0.45 (p=0.0007) and R=0.30 (p=0.03), respectively. $nICP_{FVd}$ and $nICP_{CrCP}$ presented lower and non-significant correlations: R=0.20 (p=0.15), R=0.21 (p=0.13), respectively (Figure 5.6, Table 5.5).

For nICP changes in time domain during ICP increase, $nICP_{PI}$, $nICP_{BB}$ and $nICP_{FVd}$ presented similar averaged correlations, 0.39±0.40, 0.39±0.43 and 0.35±0.41, respectively. $nICP_{CrCP}$ presented a smaller correlation (R=0.29±0.24). Figure 5.7 demonstrates the variability in the correlations in the time domain between nICP and ICP, with examples of a good and a poor recording of nICP with the four investigated methods when ICP changed considerably during the infusion test.

Figure 5.6. Linear regressions and correlation plots considering the differences (Δ) between plateau and baseline phases during infusion tests. (A) $\Delta nICP_{BB}$, (B) $\Delta nICP_{FVd}$, (C) $\Delta nICP_{CrCP}$ and (D) $\Delta nICP_{PI}$. Only $nICP_{BB}$ and $nICP_{PI}$ presented moderate significant correlations with direct ICP.

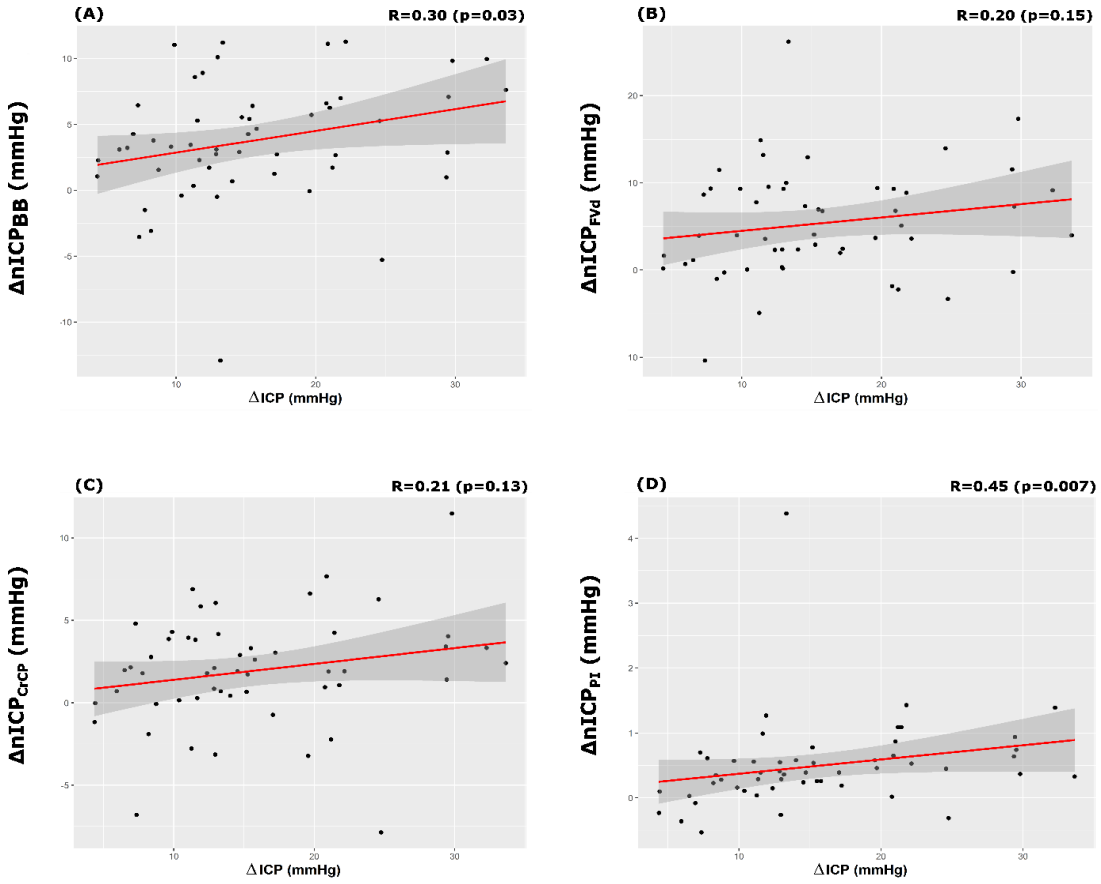

Grey shaded areas on the plots represent the 95% confidence intervals for the linear regressions between ΔnICP and ΔICP.

Δ, magnitude of changes between baseline and plateau phases during infusion test; ICP (mmHg), intracranial pressure; $nICP_{BB}$ (mmHg), estimator based on a black-box mathematical model; $nICP_{FVd}$ (mmHg), estimator based on the diastolic cerebral blood flow velocity; $nICP_{CrCP}$ (mmHg), estimator based on the concept of critical closing pressure; $nICP_{PI}$ (mmHg), estimator based on the pulsatility index; R, Spearman correlation coefficient.

Figure 5.7. Examples of good (A) and poor (B) recordings of nICP with the four investigated methods when ICP changed considerably during the infusion test. Correlation coefficients in the time domain (R) are depicted for each nICP method in each situation.

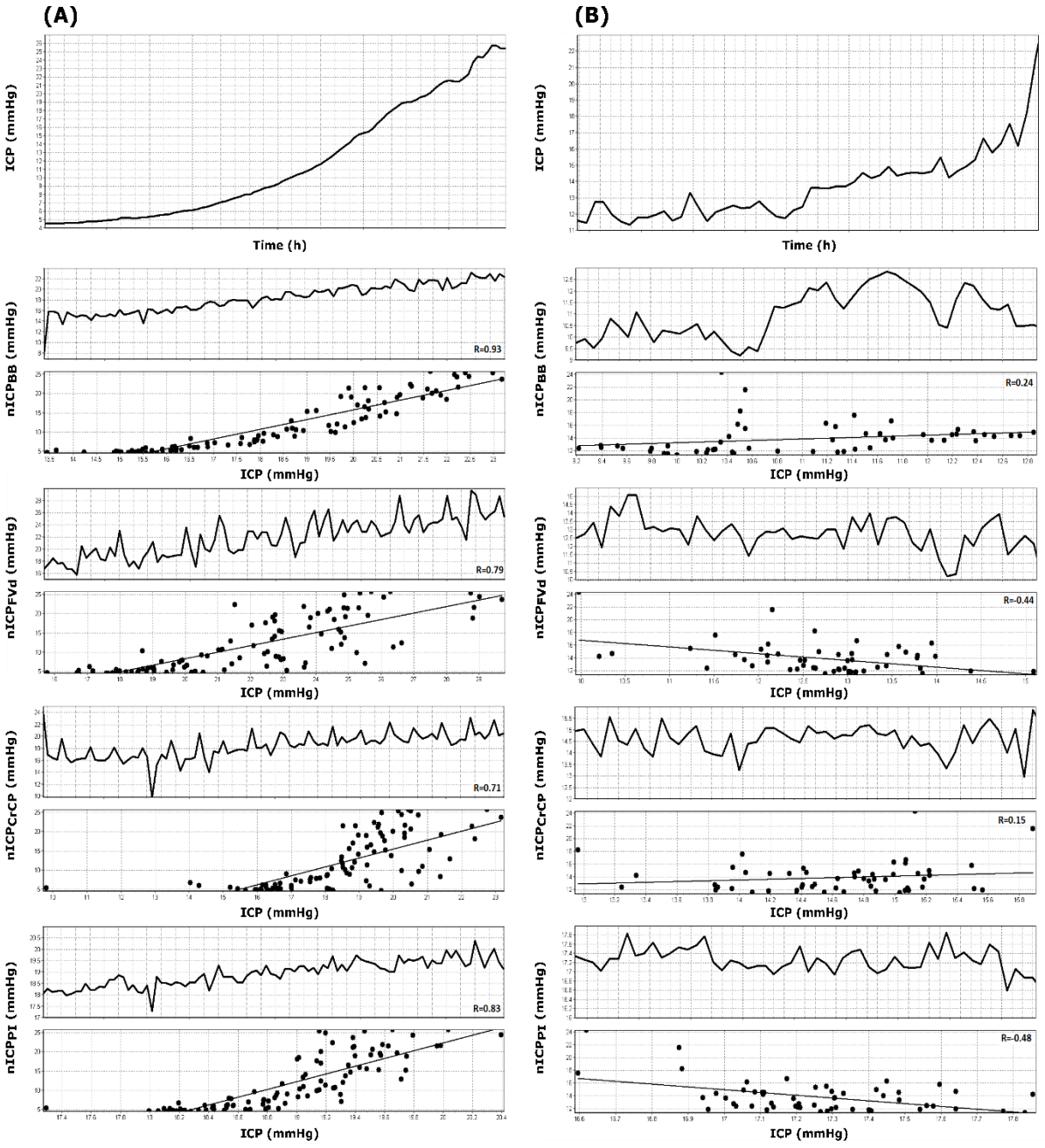

ICP (mmHg), intracranial pressure; $nICP_{BB}$ (mmHg), estimator based on a black-box mathematical model; $nICP_{FVd}$ (mmHg), estimator based on the diastolic cerebral blood flow velocity; $nICP_{CrCP}$ (mmHg), estimator based on the concept of critical closing pressure; $nICP_{PI}$ (mmHg), estimator based on the pulsatility index; R, correlation coefficient in the time domain.

Table 5.4. Median values (IQR), bias (±SD) and 95% CI for ICP prediction are described for baseline and plateau phases. Spearman correlation between ΔICP and ΔnICP and averaged correlation across time during ICP increase are described (N=53). At the 0.05 level, baseline and plateau distributions of nICP and ICP were significantly different.

Method	Baseline Phase			Plateau Phase			R	R
	Median (IQR)	Bias	95% CI	Median (IQR)	Bias	95% CI	(ΔICP vs ΔnICP)	(time domain)
$nICP_{BB}$	10.76 (15.08-7.30)*	4.46±7.82†	15.33	14.86 (20.1-11.26)*	-7.35±9.80†	19.21	0.30+	0.39±0.43
$nICP_{FVd}$	16.97 (22.56-11.64)*	11.90±12.85†	25.19	21.74 (32.85-14.15)	1.66±15.29	29.97	0.20	0.35±0.41
$nICP_{CrCP}$	18.34 (20.38-14.89)*	11.12±7.07†	15.09	19.65 (23.80-16.92)	-2.53±9.08†	17.80	0.21	0.29±0.24
$nICP_{PI}$	16.57 (17.46-16.06)*	8.91±5.40†	10.58	17.12 (17.73-16.40)*	-6.18±9.73†	19.07	0.45+	0.39±0.40
ICP	7.74 (11.06-2.95)	-	-	22.13 (29.77-16.41)	-	-	-	-

ICP (mmHg), intracranial pressure; $nICP_{BB}$ (mmHg), estimator based on a black-box mathematical model; $nICP_{FVd}$ (mmHg), estimator based on the diastolic cerebral blood flow velocity; $nICP_{CrCP}$ (mmHg), estimator based on the concept of critical closing pressure; $nICP_{PI}$ (mmHg), estimator based on the pulsatility index; CI, confidence interval; Δ, magnitude of changes between baseline and plateau phases during infusion test; R, Spearman correlation coefficient; SD, standard deviation.

*At the 0.05 level, distributions between nICP and ICP are significantly different.

†The population mean is significantly different with the test mean (zero).

+Spearman correlation coefficient is significant at the 0.05 level.

Table 5.5. Median (IQR) values for all physiological variables estimated during baseline and plateau phases, with their corresponding Δ correlations with ΔICP and ΔABP.

Variable	Baseline	Plateau	p value	R (ΔICP)	R (ΔABP)
ICP	7.77 (11.06-2.95)	22.13 (29.77-16.41)*	<0.001	-	0.1
ABP	89.68 (101.5-78.23)	96.08 (121-87.07)*	<0.001	0.11	-
HR	67.86 (77.96-61.98)	70.12 (79-60.83)	0.39	0.15	0.28+
CPP	82 (98.67-73.27)	79.40 (96.53-67.14)*	<0.001	-0.38+	0.82+
FV_m	54.2 (66.27-42.47)	49.76 (61.92-39.07)*	<0.001	0.14	-0.20
FV_s	81.61 (101.6-66.76)	79.97 (98.65-63.35)	0.07	-0.03	-0.21
FV_d	33.17 (43.86-27.32)	31.93 (40.61-23.57)*	<0.001	-0.22	0.21
PI	0.84 (1.05-0.76)	0.99 (1.13-0.83)*	<0.001	0.45+	-0.04
CVR	1.64 (1.95-1.22)	1.55 (2.05-1.13)	0.56	-0.21	0.62+

ICP (mmHg), intracranial pressure; ABP (mmHg), arterial blood pressure; HR (beats/min), heart rate; CPP (mmHg), cerebral perfusion pressure; FV (cm/s), cerebral blood flow velocity (m, mean; s, systolic; d, diastolic); PI, pulsatility index; CVR (mmHg · s/cm); R, Spearman correlation coefficient; Δ, magnitude of changes between baseline and plateau phases during infusion test.

*At the 0.05 level, distributions between baseline and plateau are significantly different.

+ Spearman correlation coefficient is significant at the 0.05 level.

Discussion

The assessment of TCD-based nICP estimators during infusion tests revealed a limited accuracy of non-invasive ICP and a discrepancy in the ICP estimation. Among the estimators evaluated, relative changes in mean ICP were better associated with $nICP_{PI}$ and $nICP_{BB}$. Considering trends of measured ICP in the time domain, all nICP methods presented better performance and the overall correlations were comparatively more balanced.

The mean absolute values estimated by all nICP methods were significantly different from ICP during baseline phase, whereas during plateau phase $nICP_{FVd}$ and $nICP_{CrCP}$ had the same distributions as ICP. This indicates the inaccuracy of the nICP methods to predict the absolute measure of ICP in the context of infusion tests. Nevertheless, all paired comparisons between estimators for baseline and plateau showed significant differences, demonstrating that infusion test produced a significant increase in nICP for every estimator. Although significant within the same method, these differences were disproportional in the comparison between direct ICP and nICP estimations. Such disproportionality was reflected in the 95% CI for ICP prediction found for baseline and plateau phases.

$nICP_{PI}$ and $nICP_{BB}$ were the only estimators presenting significant correlations between ΔICP and ΔnICP and demonstrated a moderate ability to detect the magnitude of changes in direct ICP (Table 5.4). $nICP_{PI}$, $nICP_{BB}$ and $nICP_{FVd}$ displayed moderate averaged correlations for detection of ICP trends in the time domain. Generally, nICP estimation differed mostly regarding prediction of ICP absolute values during infusion tests, and in a lesser extent, for detection of dynamic changes.

The relative accuracy of TCD-based nICP methods may vary between different types of intracranial hypertension: vasogenic, CSF circulatory or secondary to brain volumetric changes. The nature of ICP elevation during infusion test is attributed to increasing CSF circulation due to the addition of an increasing volume into the CSF space. TCD ultrasonography, however, is a technique mainly capable of detecting arterial cerebrovascular changes [128]. Hence, it would be expected that TCD-based nICP methods would present better accuracy to detect ICP changes of vasogenic origin, rather than changes related CSF circulation. This can be exemplified by the fact that for cases in which ICP changes related to vasogenic fluctuations (plateau waves, B waves) overlapped the rise related to increasing CSF

circulation, the correlation in the time domain between ICP and nICP appeared remarkably better (Figure 5.8). In these cases, the vasogenic waves patterns were reliably replicated.

ICP changes originating from increased CSF circulation have direct and indirect influences on cerebral haemodynamics. The direct impact is represented by changes in CPP, altered directly by ICP. On the other hand, ICP has a secondary effect on cerebral haemodynamics, via changes in systemic haemodynamics. The changes in ABP observed during infusion tests are associated with an early Cushing response [129], in which rising ICP produces an increase in ABP. Therefore, the transmission of fluctuations in CSF circulation to the cerebral arterial bed is primarily a result of CPP decrease and secondarily an ABP increase.

In respect to hemodynamic and TCD-derived cerebrovascular parameters used for the methods' estimations (Table 5.5), only HR, FV_s and CVR did not differ between baseline and plateau phases. Within the variables presenting significant difference, only changes in CPP and PI (ΔCPP and ΔPI) were significantly correlated with changes in ICP. Contrary to more optimistic studies on the relationship between ICP and PI [27], in this case, PI presented a moderate correlation with ICP. This was mainly associated with changes in FV_d since FV_s did not differ significantly between baseline and plateau phases.

The changes in ABP were found to be significantly correlated to changes in CVR. Although CVR was not significantly different between baseline and plateau phases, the subsequent increase in ABP produced by an early Cushing response caused minor vasogenic changes in cerebral haemodynamics [129]. This could have contributed to the better accuracy in cases presenting changes in ICP of vasogenic origin.

In this scenario, the low accuracy of ICP prediction observed for TCD based-methods can be attributed to the nature of ICP elevation during infusion tests. Although increased CSF circulation can produce secondary changes on cerebral haemodynamics, the specificity of TCD for cerebrovascular changes, like ICP changes of vasogenic origin, may preclude the reliable application of TCD-based nICP methods in conditions which ICP changes are related to CSF circulation. However, it is also important to consider that the nICP methods evaluated were derived from cohorts of TBI patients. Therefore, different physiological mechanisms leading to ICP fluctuations in TBI and hydrocephalus might have interfered in the way ICP was estimated.

Figure 5.8. Modified from Cardim et al. [122]. Examples of vasogenic waves during infusion test. (A) Shadowed area represents a plateau wave of ICP. (B) Shadowed area represents B waves of ICP. A noticeable positive correspondence between ICP and nICP methods are observed during the occurrence of vasogenic waves.

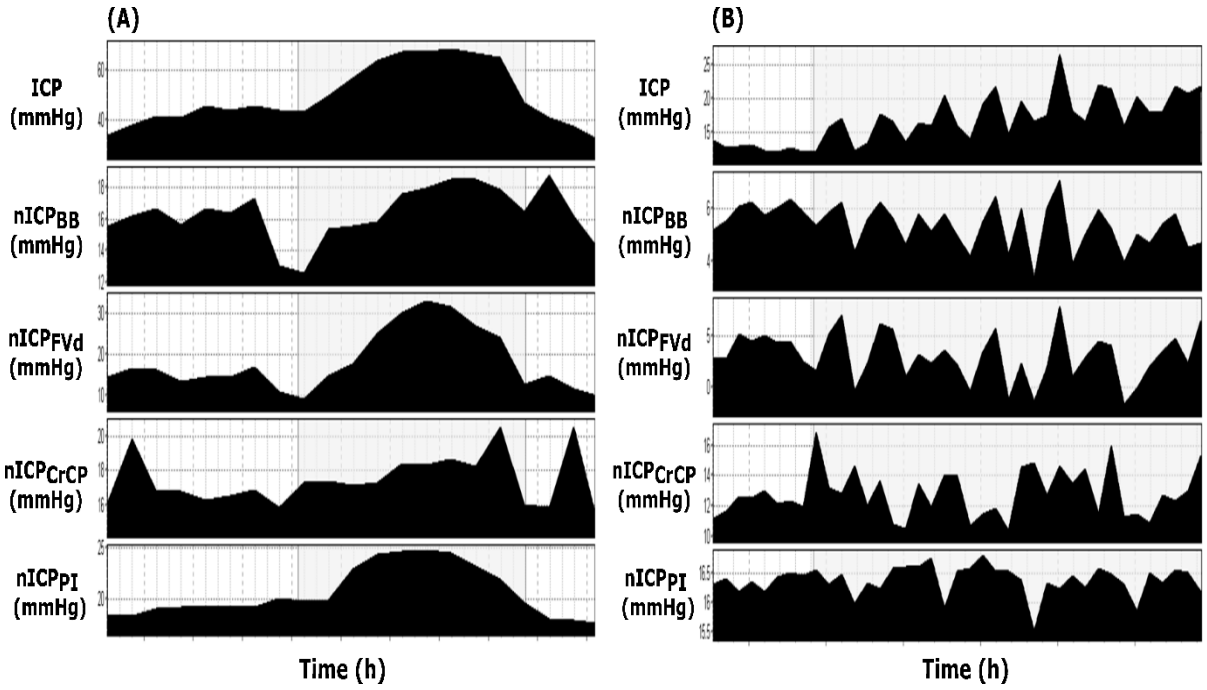

ICP (mmHg), intracranial pressure; $nICP_{BB}$ (mmHg), estimator based on a black-box mathematical model; $nICP_{FVd}$ (mmHg), estimator based on the diastolic cerebral blood flow velocity; $nICP_{CrCP}$ (mmHg), estimator based on the concept of critical closing pressure; $nICP_{PI}$ (mmHg), estimator based on the pulsatility index.

5.3 Non-invasive assessment of intracranial pressure during plateau waves

The results presented in this section have been published in *Neurocritical Care* [130]:

Cardim, D., Schmidt, B., Robba, C., Donnelly, J., Puppo, C., Czosnyka, M., and Smielewski, P. (2016). Transcranial Doppler Monitoring of Intracranial Pressure Plateau Waves. Neurocrit. Care, 1–9.

Introduction

Plateau waves of ICP (or Lundberg A waves) [131,132] are frequent phenomena leading to acute intracranial hypertension in patients requiring neurocritical care. They are characterised by acute and relevant increases in ICP (generally up to 40 mmHg [87]), related to increased volume of arterial blood in response to an arterial vasodilation stimulus. Such phenomena may develop in patients with intact cerebral autoregulation [87] and low cerebrospinal compensatory reserve [133], suffering from many cerebral pathological conditions including TBI [87], idiopathic intracranial hypertension [134], SAH [135], brain tumours, hydrocephalus [136], and craniosynostosis [137].

During the occurrence of plateau waves, ICP rises from normal or slightly elevated to uncompensated levels, with relatively stable ABP [138]. The mechanism driving plateau waves can be described as a 'vasodilatory cascade', initiated by vasodilatory stimuli like ABP decrease [87]. Following this, a rapid increase in cerebral arterial blood volume (C_aBV) leads to a cyclic rise in ICP, decrease in CPP, further vasodilation and a further rise in ICP. This cycle is maintained until the cerebral vasculature reaches a state of maximum vasodilation, biologically fixed by the rigid collagen fibres in the tunica adventitia [138]. The reverse of this positive feedback loop occurs when a vasoconstrictive stimulus initiates a vasoconstrictive cascade, decreasing C_aBV with a consequent drop in ICP towards normal levels [138,139].

The previous sections of this chapter have shown that TCD-based nICP estimators present with different measures of accuracy [39], with potential indications that their accuracy is better when changes of ICP are related to vasogenic phenomena [122,140]. Considering these assumptions, this study aimed to assess the four previously described TCD-based nICP methods in a cohort of patients presenting changes in ICP purely of vasogenic origin (specifically plateau wave increases of ICP), to verify whether they predict ICP under such conditions reliably.

Materials and methods

Patient population

From the previously described database of 446 adult TBI patients (Section 4.1.2) (median age of patients: 30 years (IQR: 18–78, with 75% being male), 27 patients were identified, in whom at least one plateau wave occurred during the monitoring period. One of these patients (with one recording of plateau wave) was recruited at the Universidad de la República School of Medicine Hospital, Montevideo, Uruguay (with the approval of the local ethical committee). Plateau waves were identified as sudden and spontaneous increases in ICP and pulse amplitude of ICP during which CPP and FV_m dropped while ABP remained relatively stable (Figure 5.9).

Clinical monitoring and data collection

The implemented clinical monitoring included ABP, ICP and FV as described in Section 4.2.1. $nICP_{BB}$, $nICP_{FVd}$, $nICP_{CrCP}$ and $nICP_{PI}$ were evaluated. nICP methods and derived physiological parameters were calculated as described in Section 4.2.3.

Figure 5.9. Example of the algorithm used for identification of plateau waves: sudden and spontaneous increases in ICP and pulse amplitude of ICP during which CPP and FV dropped while ABP remained relatively stable.

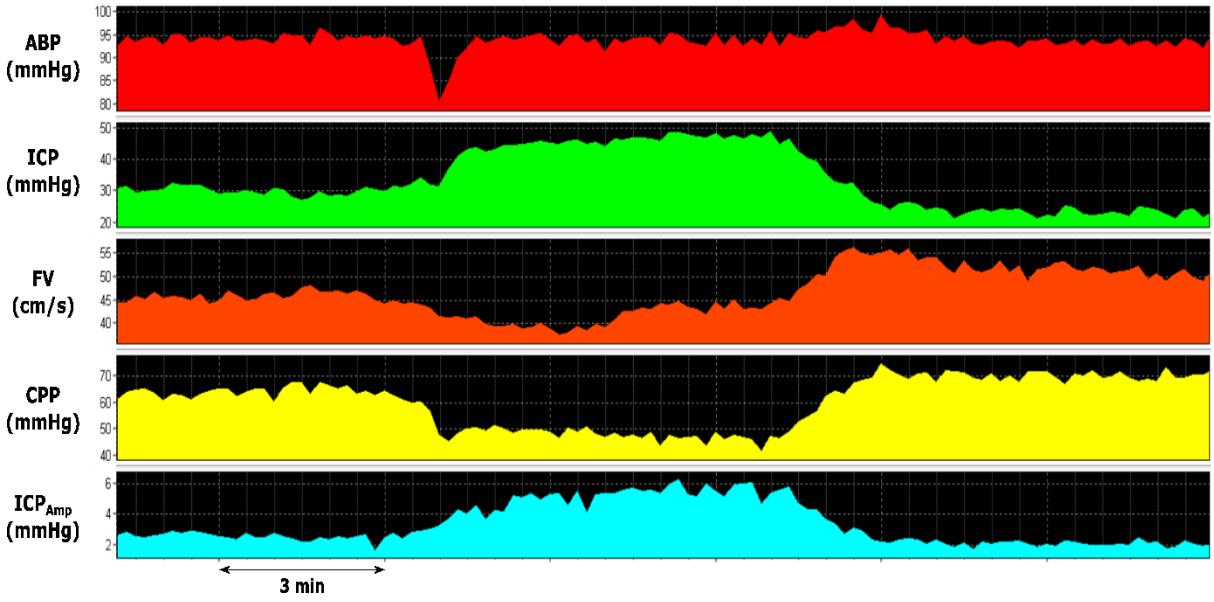

ABP (mmHg), arterial blood pressure; ICP (mmHg), intracranial pressure; FV (cm/s), cerebral blood flow velocity; CPP (mmHg), cerebral perfusion pressure; ICP_{Amp} (mmHg), pulse amplitude of ICP.

Statistical analysis

All plateau waves were treated as independent phenomena. The data were tested for normal distribution using the Shapiro-Wilk test and found to be non-parametric. The analysis included Spearman correlations between ΔICP and ΔnICP, and averaged correlations for variations of nICP in the time domain during plateau waves. "Δ" (magnitude) represents the difference between plateau phase (at the top of plateau waves), and baseline phase (before the onset of plateau waves) mean values in each recording. R symbolises the Spearman correlation coefficient, with the level of significance set at 0.05. Median values of ICP and nICP are presented with their respective IQR in mmHg.

A ROC analysis was performed to determine the ability of the non-invasive methods to detect raised ICP during plateau waves, using a threshold of 35 mmHg. This threshold was chosen considering the high values of ICP observed during both phases of plateau waves. In this case, 35 mmHg represents mathematically half way between baseline and plateau phases ICP values. Also, considering the spontaneous nature of plateau waves, a ROC analysis was also performed to determine the ability of the methods to distinguish relative changes in ICP between baseline and plateau phases.

Results

In 27 patients, 36 plateau waves were identified during the TCD monitoring sessions. 7 patients presented two plateau waves, and one patient presented 3 consecutive plateau waves. The mean length of plateau waves was 13 min, ranging from 2–30 min. Table 5.6 presents correlations (ΔR) between ΔICP and ΔnICP, averaged correlations in the time domain and prediction values for each nICP method.

The correlations in the time domain were reasonably good, with R>0.60 for all methods. $nICP_{PI}$, $nICP_{BB}$ and $nICP_{CrCP}$ presented similar averaged correlations ($R \geq 0.78$). Examples of good and poor correlations between ICP and nICP during plateau waves are shown in Figure 5.10.

Correlations between ΔICP and ΔnICP were better represented by $nICP_{CrCP}$ and $nICP_{BB}$, whereas the other methods presented inferior and non-significant correlations (Figure 5.11). All ΔnICP mean values were significantly underestimated in comparison to ΔICP.

Table 5.6. Median values (IQR) of the differences between plateau and baseline phase (Δ, in mmHg), Δ correlations with ICP and correlations in the time domain for all nICP methods evaluated. ΔICP and ΔnICP distributions were significantly different in all cases. AUC for each nICP method is presented considering the threshold of 35 mmHg.

Method	Δ	R (ΔICP vs ΔnICP)	R (time domain)	AUC (95% CI)
$nICP_{BB}$	9.00 (13.18-5.05)	0.44*	0.78±0.15	0.82 (0.71-0.93)
$nICP_{FVd}$	10.10 (17.74-4.56)	0.19	0.62±0.46	0.77 (0.65-0.88)
$nICP_{CrCP}$	2.89 (4.12-2.11)	0.48*	0.78±0.30	0.79 (0.67-0.91)
$nICP_{PI}$	2.82 (5.20-1.92)	0.30	0.80±0.24	0.81 (0.70-0.91)
ICP	24.49 (26.72-21.19)	-	-	-

ICP (mmHg), intracranial pressure; $nICP_{BB}$ (mmHg), estimator based on a black-box mathematical model; $nICP_{FVd}$ (mmHg), estimator based on the diastolic cerebral blood flow velocity; $nICP_{CrCP}$ (mmHg), estimator based on the concept of critical closing pressure; $nICP_{PI}$ (mmHg), estimator based on the pulsatility index; Δ magnitude of changes between baseline and plateau phases during plateau waves.

*Spearman correlation coefficient is significant at the 0.05 level.

$nICP_{PI}$ presented the best AUC value for predicting intracranial hypertension (at the threshold of ICP ≥35 mmHg). Nevertheless, all methods presented AUC above 0.7, an indication of reasonable prediction abilities for detecting ICH. The DeLong's test for two correlated ROC curves did not reveal any statistically significant difference between nICP methods. The ICP thresholds yielding the best sensitivity and specificity were 27.41 mmHg (AUC = 0.86), 28.42 mmHg (AUC = 0.79), 23.08 mmHg (AUC = 0.75), 20.28 mmHg (AUC = 0.84), respectively for $nICP_{BB}$, $nICP_{FVd}$, $nICP_{CrCP}$ and $nICP_{PI}$, respectively.

Figure 5.10. Modified from Cardim et al. [130]. Example of recordings showing reliable and unreliable replications of ICP plateau waves by different TCD-based nICP methods (panels A and B, respectively). On Y axis, mean absolute values of ICP and nICPs are presented; and on X axis, relative changes of ICP and nICP in the time domain.

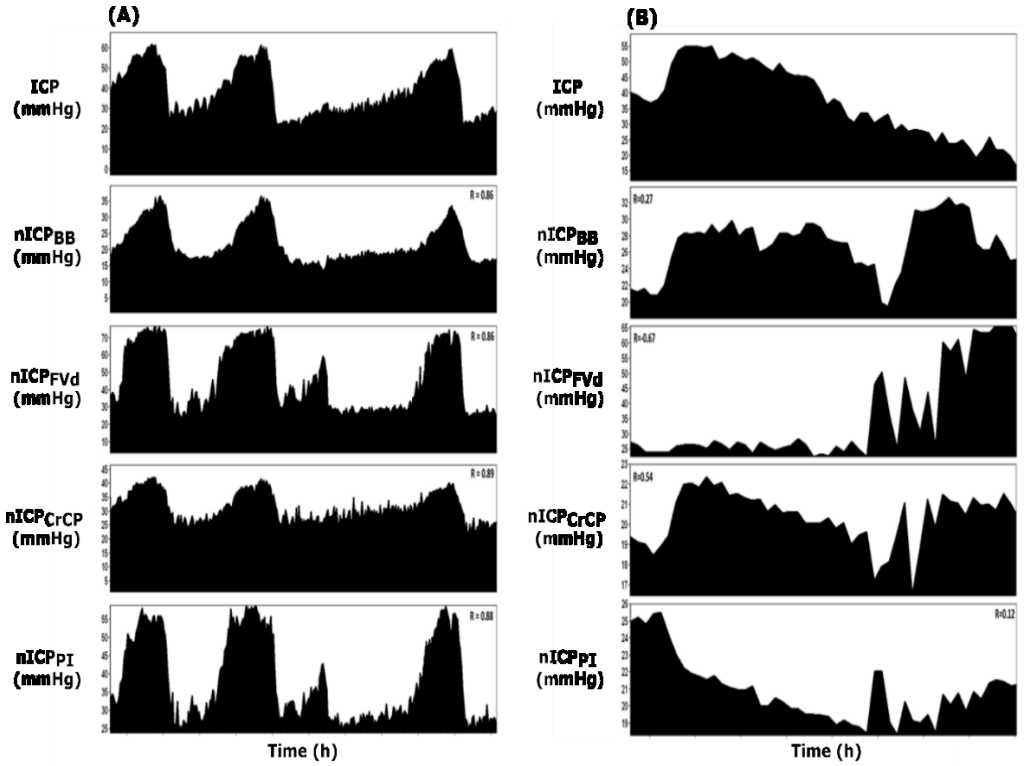

ICP (mmHg), intracranial pressure; $nICP_{BB}$ (mmHg), estimator based on a black-box mathematical model; $nICP_{FVd}$ (mmHg), estimator based on the diastolic cerebral blood flow velocity; $nICP_{CrCP}$ (mmHg), estimator based on the concept of critical closing pressure; $nICP_{PI}$ (mmHg), estimator based on the pulsatility index.

$nICP_{CrCP}$ and $nICP_{PI}$ presented null values for specificity and negative predictive value, indicating that values of these two estimators during plateau waves were always below 35 mmHg (although they reacted to rise in ICP, a notable underestimation of direct ICP was observed). Nevertheless, all methods presented good positive predictive values (65%, 69%, 58%, 58% for $nICP_{BB}$, $nICP_{FVd}$, $nICP_{CrCP}$ and $nICP_{PI}$, respectively), which otherwise would indicate that many of the positive results were false positives.

Figure 5.11. Linear regressions and Spearman correlation plots between ΔICP and ΔnICP for (A) $nICP_{BB}$, (B) $nICP_{FVd}$, (C) $nICP_{CrCP}$ and (D) $nICP_{PI}$. Only $nICP_{BB}$ and $nICP_{CrCP}$ presented statistically significant correlations with ICP.

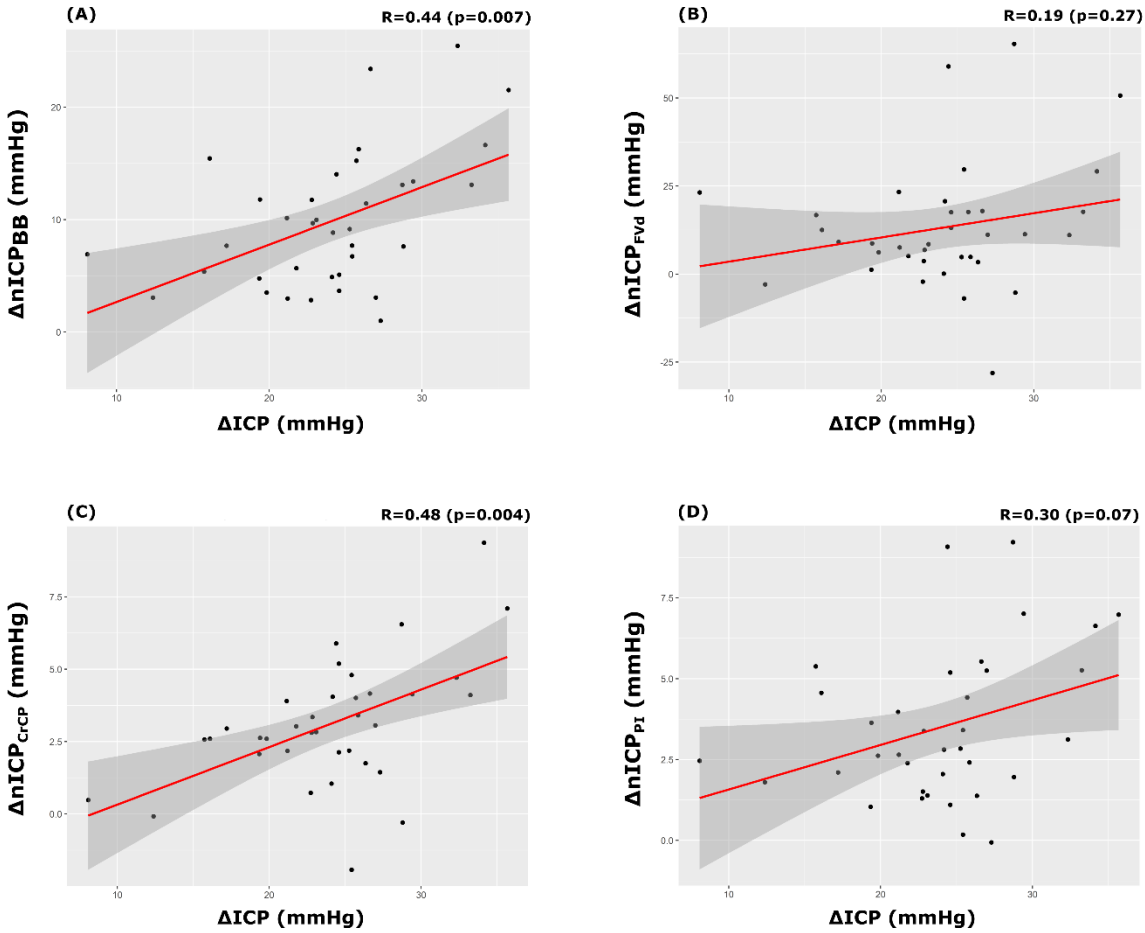

Grey shaded areas on the plots represent the 95% confidence intervals for the linear regressions between ΔnICP and ΔICP.

Δ, magnitude of changes between baseline and plateau phases during plateau waves; ICP (mmHg), intracranial pressure; $nICP_{BB}$ (mmHg), estimator based on a black-box mathematical model; $nICP_{FVd}$ (mmHg), estimator based on the diastolic cerebral blood flow velocity; $nICP_{CrCP}$ (mmHg), estimator based on the concept of critical closing pressure; $nICP_{PI}$ (mmHg), estimator based on the pulsatility index; R, Spearman correlation coefficient.

To distinguish relative changes in ICP between baseline and plateau phases, $nICP_{PI}$ and $nICP_{BB}$ presented the best prediction abilities (AUC = 0.84 (95% CI: 0.74-0.93) and AUC = 0.80 (95% CI: 0.70-0.91), respectively). The DeLong's test did not reveal a significant difference in AUC between these methods (p=0.51). $nICP_{FVd}$ and $nICP_{PI}$ presented lower prediction abilities, with AUC = 0.75 (95% CI: 0.63-0.86) and AUC = 0.74 (95% CI: 0.62-0.85), respectively.

Table 5.7 presents the median values (IQR) for the physiological parameters evaluated during baseline and plateau phases. During plateau waves, ICP and pulse amplitude of ICP (ICP_{Amp}) increased and CPP decreased significantly, whereas ABP remained unchanged. FV_m and FV_d presented significant decreases, whereas FV_s increased significantly. This resulted in significant increase in PI and decrease in CVR.

Table 5.7. Median (IQR) values for all physiological parameters estimated during baseline and plateau phases.

Variable	Baseline	Plateau
ICP	22.81 (28.49-19.91)	46.45 (55.22-40.64)*
ABP	93.34 (98.30-86.14)	93.55 (97.44-85.28)
HR	75.72 (84.91-65.42)	74.73 (80.45-66.14)*
CPP	70.89 (78.22-60.38)	45.91 (52.87-37.17)*
FV_m	57.31 (71.87-43.16)	45.52 (63.96-33.15)*
FV_s	109.35 (132.35-92.78)	113.55 (141.72-99.44)*
FV_d	31.04 (40.24-23.26)	22.99 (36.60-10.97)*
PI	1.39 (1.68-1.21)	2.00 (2.83-1.68)*
CVR	1.23 (1.47-1.00)	0.99 (1.25-0.68)*
C_aBV_{Amp}	2.38 (3.73-1.82)	3.36 (4.77-2.42)*
CrCP	51.37 (56.88-41.89)	65.33 (70.67-52.07)*
ICP_{Amp}	2.21 (2.58-1.70)	6.16 (7.88-4.90)*
$nICP_{BB\ Amp}$	1.97 (2.70-1.61)	3.44 (4.07-2.67)*

ABP (mmHg), arterial blood pressure; C_aBV_{Amp} (mmHg), cerebral arterial blood volume amplitude; CPP (mmHg), cerebral perfusion pressure; CrCP (mmHg), critical closing pressure; CVR (mmHg · s/cm), cerebral vascular resistance; FV (cm/s), cerebral blood flow velocity (m, mean; s, systolic; d, diastolic); HR (beats/min), heart rate; ICP (mmHg), intracranial pressure; ICP_{Amp} (mmHg), pulse amplitude of ICP; $nICP_{BB\ Amp}$ (mmHg), pulse amplitude of non-invasive ICP based on the black-box model; PI, pulsatility index;

*At the 0.05 level, distributions between baseline and plateau are significantly different.

As the only nICP method providing waveform, $nICP_{BB}$ also presented increased pulse amplitude ($nICP_{BB\ Amp}$), even with replication of the characteristic triangular waveform shape observed during plateau waves [141] (Figure 5.12). The correlation between ΔICP_{Amp} and $\Delta nICP_{BB\ Amp}$ was significant ($R=0.50$, $p<0.05$), however, $nICP_{BB\ Amp}$ was significantly underestimated in comparison to ICP_{Amp} during plateau phase (bias=-2.88 mmHg, $p<0.05$).

Figure 5.12. Modified from Cardim et al.[130]. Example of plateau wave recording with direct ICP and $nICP_{BB}$. In comparison to baseline phase, at the top of plateau waves, ICP and $nICP_{BB}$ presented an increased pulse amplitude. The characteristic triangular shape of ICP waveform observed during plateau waves was replicated by $nICP_{BB}$.

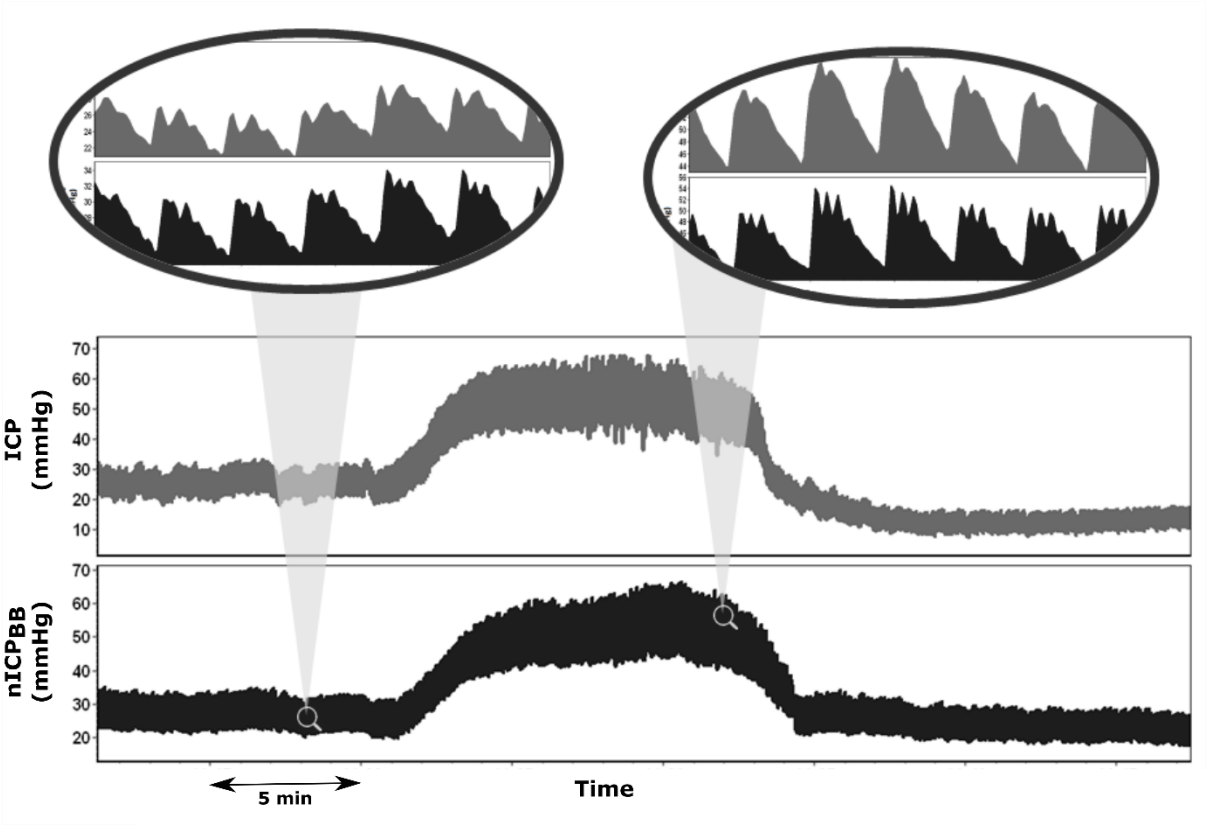

ICP (mmHg), intracranial pressure; $nICP_{BB\ Amp}$ (mmHg), pulse amplitude of non-invasive ICP based on the black-box model.

Discussion

Among the methods evaluated, only $nICP_{BB}$ and $nICP_{CrCP}$ presented significant correlations with ΔICP in patients with changes in ICP purely of vasogenic origin. On the other hand, relative changes in ICP across time were confidently replicated by all methods. Moreover, they presented reasonable prediction ability to detect intracranial hypertension and relative changes in ICP associated with plateau waves.

Given the findings presented in Section 5.2, it appears that ICP changes in the time domain are better estimated by TCD-based nICP methods when changes in ICP are related to vasogenic phenomena. For instance, during CSF infusion tests, a controlled and artificial increase in CSF circulation causes an elevation in ICP similar to the pattern observed during plateau waves. Nevertheless, the correlations in the time domain obtained were considerably weaker in comparison to those observed for plateau waves, in which ICP changes were specifically related to increases in cerebral arterial blood volume. Furthermore, such findings were not better replicated in the analysis considering the prospective TBI cohort presented in Section 5.1, in which changes in ICP across time were not always related to vasogenic waves.

In retrospect, the accuracy measures of the nICP methods evaluated in different clinical conditions can be summarised as presented in Table 5.8. The average 95% confidence interval for nICP estimation has been around 20-25 mmHg during plateau waves and 17 mmHg for infusion test, whereas generally in TBI it has shown a smaller value, around 10 mmHg. $nICP_{BB}$ has been the best method in the clinical conditions evaluated. The correlation in the time domain between direct and estimated ICP has been strongest during plateau waves (around 0.8, except for $nICP_{FVd}$, R=0.63). For infusion test, this correlation has been much lower (between 0.3 and 0.4 for $nICP_{BB}$, $nICP_{FVd}$ and $nICP_{CrCP}$). In TBI, it has been between 0.5 to 0.6, but only for $nICP_{BB}$ and $nICP_{PI}$.

Table 5.8. Summary of the accuracy measures for TCD-based nICP methods in different clinical conditions.

Accuracy measure	Plateau Waves				CSF infusion test[39]				TBI[8]			
	$nICP_{BB}$	$nICP_{FVd}$	$nICP_{CrCP}$	$nICP_{PI}$	$nICP_{BB}$	$nICP_{FVd}$	$nICP_{CrCP}$	$nICP_{PI}$	$nICP_{BB}$	$nICP_{FVd}$	$nICP_{CrCP}$	$nICP_{PI}$
Bias $_{baseline}$	-2.74	3.60	-2.93	-3.99	4.46	11.90	11.12	8.91	-	-	-	-
Bias $_{plateau}$	17.12	-7.22	-23.86	-24.46	-7.35	1.66	-2.53	-6.18	-	-	-	-
95% CI $_{baseline}$	18.02	23.85	18.85	17.58	15.33	25.19	15.09	10.58	-	-	-	-
95% CI $_{plateau}$	21.54	35.54	19.83	20.53	19.21	29.97	17.80	19.07	-	-	-	-
Bias $_{whole\ recording}$	-9.93	-1.81	-13.39	-14.22	-	-	-	-	-0.50	7.34	4.44	4.11
95% $_{whole\ recording}$	24.46	31.97	28.51	28.02	-	-	-	-	9.94	14.62	9.19	9.62
R in time	0.77±0.15	0.63±0.45	0.77±0.30	0.80±0.24	0.39±0.40	0.39±0.43	0.35±0.41	0.29±0.24	0.48±0.40	-0.28±0.69	0.18±0.56	0.61±0.35
ΔR	0.41*	0.19	0.45*	0.32	0.30*	-0.17	0.21	0.45*	-	-	-	-

$nICP_{BB}$ (mmHg), estimator based on a black-box mathematical model; $nICP_{FVd}$ (mmHg), estimator based on the diastolic cerebral blood flow velocity; $nICP_{CrCP}$ (mmHg), estimator based on the concept of critical closing pressure; $nICP_{PI}$ (mmHg), estimator based on the pulsatility index. CI (mmHg), confidence interval for ICP prediction; R, correlation coefficient; **Δ,** magnitude of changes in ICP.

*Spearman correlation coefficient is significant at the 0.05 level.

All nICP methods assessed in this chapter are not patient-specific, therefore requiring formation datasets for their generation. Their calibration factors were derived from extensive TBI datasets, in which, for most cases, ICP variations were smaller than during plateau wave genesis. The cerebrovascular model for estimation of ICP ($nICP_{Heldt,}$ Section 3.3.3) [36], for example, is a nICP method that produces patient-specific ICP estimates not relying on formation datasets or training procedures. $nICP_{Heldt}$ has been tested in two cases presenting plateau waves and showed a 95% CI of 6.4 mmHg (in a situation of a single plateau wave) and 18.8 mmHg (in a situation of two consecutive plateau waves).

The results of a previous assessment of $nICP_{BB}$ during plateau waves have been described in Section 3.3.3. In that study, clinical material from 17 TBI patients was used to construct the nICP simulation model, which resulted in better accuracy and the stronger correlation between ΔICP and $\Delta nICP_{BB}$ in comparison to this current assessment (see Table 3.3) [140]. The formation dataset, in that case, was more specific for plateau waves, in which 7 patients (41% of the dataset) presented such phenomena. In contrast, the model of $nICP_{BB}$ used in this thesis considered a large general TBI cohort (N=140 patients) (described in Sections 3.3.3 and 4.2.3). Consequently, the way $nICP_{BB}$ was generated in both studies might have contributed to such discrepancy in results.

Under these circumstances, it is possible to infer that nICP methods derived from formation datasets specific for certain conditions may present better accuracy than those based on general datasets. Some findings supporting this inference were discussed in Section 5.1, which demonstrated that the nICP methods presented smaller 95% CI in the analysis of a TBI cohort convergent to the methods' formation datasets, i.e., general regarding different sources of ICP changes. However, one obvious disadvantage of specific formation datasets is the restriction of applicability of the nICP method in differing clinical conditions.

This effect can also be exemplified with the results from Section 5.2, in which the assessment of nICP methods derived from TBI datasets in patients with hydrocephalus resulted in a bad accuracy.

Despite the lack of individual calibration, the nICP methods presented reliable accuracy to track changes in ICP across time during plateau waves and identify these events associated with ICH thresholds. Since plateau waves are recurrent phenomena in TBI patients, affecting approximately 25% of cases [138] and a predictor of poor outcome [138], the identification of these ICP surges non-invasively could represent a major application of TCD-based nICP methods.

In the clinical practice, it could provide a better understanding of the clinical state of the patient and guide oriented treatments in situations of sustained plateau waves.

5.4 General limitation factors

The quality of TCD and ABP recordings are essential requirements for ICP estimation using TCD-based methods. Aspects such as depleted signal resolution and noise, for instance, may prevent a meaningful nICP estimation.

The use of radial artery ABP calibrated at the level of the heart instead of actual blood pressure at head level could also limit nICP estimation. This condition approximate peripheral ABP to intracranial ABP non-accurately, and might affect the accuracy of methods that rely on ABP waveform analysis.

6 RESULTS & DISCUSSIONS II: FEASIBILITY OF TCD-BASED nICP MONITORING

This chapter presents the results of studies on the feasibility of nICP monitoring in three clinical conditions. There are various situations inside and outside the neurocritical care settings in which the impracticality or invasiveness of the current methods for ICP monitoring impedes the assessment of this parameter, therefore precluding more oriented treatment protocols in cases of disturbed cerebral haemodynamics.

The presented studies aim to assess the feasibility of TCD-based nICP monitoring in clinical conditions in which invasive monitoring was impractical or unachievable. The nICP estimator used in these studies was the black box model ($nICP_{BB}$), based on its comparative best performance to other TCD-based methods as presented in Chapter 5.

6.1 Feasibility of nICP to detect interhemispheric pressure gradients in closed traumatic brain injury

Introduction

The central nervous system presents a compartmentalised structure with rigid subdivisions. In the cranium, such components consist of the left and right hemisphere divided by the falx, the ventricles, the posterior fossa separated by the tentorium, and the extracranial space below the foramen magnum [142]. In pathological conditions such as TBI, sustained and significant intercompartmental pressure gradients between these structures can cause brain midline shift [143] and herniations [142] (Figure 6.1).

Figure 6.1. Head CT scan illustrating a brain midline shift. In this example, the shift occurs from the right to the left brain hemisphere.

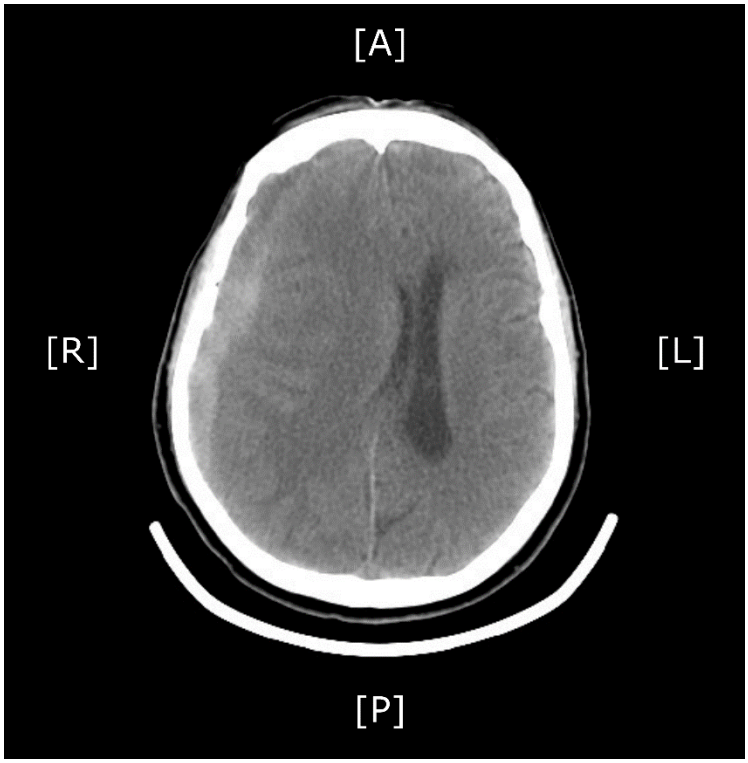

CT, computed tomography; A, anterior; L, left; P, posterior; R, right.

If CSF circulates freely, it cancels possible pressure gradients in the brain, as per Pascal law, the pressure is uniformly distributed in the fluid. Following TBI, local or global brain swelling may acutely disturb the CSF circulation. Therefore, the concept that the intracranial compartment is a space in which ICP is uniformly distributed has been challenged [144–146]. Although there is a consensus on the existence of craniospinal and suprainfratentorial pressure gradients, the existence of interhemispheric gradients is still debatable [144]. Intracranial pressure gradients have been reported in adult and paediatric TBI populations [147,148] in the presence [144,149,150] and absence [143,144,151,152] of unilateral mass lesions, and also in patients with non-traumatic unilateral mass lesions [143].

Assuming the existence of interhemispheric pressure gradients, there is a concern in cases of unilateral mass lesions related to ICP at the ipsilateral and contralateral sides of contusion. Most studies comparing ICP in such conditions suggested a greater pressure ipsilateral to the contusion [144,153]; however, this is still a matter of debate since other findings suggested a greater

pressure at the contralateral side [145,146]. Potential explanations for this controversy lay on the issue that different types of lesions may produce different patterns of pressure gradients [144]. Nevertheless, one should consider that pressure asymmetry could also be associated with derangements in the cerebral vasculature as a secondary injury following TBI.

Considering that bilateral ICP monitoring can be impractical and unavailable in many centres, these questions have remained unanswered. In this scenario, techniques that can provide a non-invasive global assessment of the cerebral haemodynamics and nICP monitoring could help elucidate this controversy.

This study aims to evaluate the presence of interhemispheric pressure gradients in patients managed for closed head injury with brain midline shift, using bilateral TCD ultrasonography as means for nICP monitoring.

Material and methods

Patient population

A group of 97 patients from the retrospective TBI cohort described in Section 4.1.2 was analysed in this study. The patient's median age was 34 years (range 13-76 years; 78% males). The median initial GCS score was 6 (range 3–15).

All patients were sedated, paralysed, ventilated, and treated with a CPP-oriented strategy, targeted at least 70 mmHg [154]. The patients were kept normothermic (body temperature at 35-37˚C), an ICP higher than 25 mmHg was treated with mannitol (2 mg/kg), and ABP was maintained by volume expansion and administration of dopamine and/or epinephrine.

All significant intracranial mass lesions that were observed on initial CT scans were promptly removed by the consultant neurosurgeon. For methodological purposes, all patients in whom a craniectomy was performed before the assessments were excluded from the study, as this could artificially disturb the symmetry of cerebral blood flow. The inclusion criteria were the presence of a unilateral lesion, the presence of midline shift and absence of craniectomy at the moment of monitoring.

In the current clinical practice, patients with midline shift not treated actively (including the early evacuation of compression, decompressive craniectomy) are rarely seen. This is the reason the study was based on a retrospective cohort with midline shift without evacuation of any mass lesion.

Analysis of CT Scans

Brain CT scans were analysed and graded using a simplified system based on the classification of Marshall et al. [155], focussing on brain swelling, dominant side of lesion and midline shift. Only CT scans that had been obtained close to the time of the TCD recording were selected and analysed. For those patients who underwent early neurosurgical interventions, the postoperative CT scan rather than the scan that was obtained initially was chosen.

Brain swelling was scored according to the following radiographic features: the disappearance of sulci, effacement of ventricles, basal cistern compression, and reduction in the difference between white and grey matter (i.e., the disappearance of the white-grey matter difference in more than 50% of the slices). The sum of these factors produced a score from 0 to 4, with 0 indicating no swelling and 4 indicating severe swelling.

The side of the brain containing the primary lesion was noted, but the type and specific location of intraparenchymal lesions were not considered. Three groups were identified: patients with parenchymal lesions on the right or left side and patients without any noticeable parenchymal lesion but presenting midline shift.

The midline shift was measured in millimetres according to the scale on the CT scan. A positive value was assigned to displacement of the midline from the right to the left side, and a negative value to the displacement of the midline from the left to the right side. No midline shift was graded as a zero value.

Clinical monitoring and data collection

The implemented clinical monitoring included ABP, ICP and FV as described in Section 4.2.1. The ICP probe was inserted intraparenchymally into the right frontal region. FV was obtained from the left and right middle cerebral arteries for a period of 20 minutes to 2 hours.

The nICP assessment was performed using the black-box model ($nICP_{BB}$). Derived physiological parameters and $nICP_{BB}$ were calculated as described in Section 4.2.3. nCPP was derived from $nICP_{BB}$.

All recordings were performed on separate days, and the measured parameters from each recording were averaged over the whole monitoring period so that every recording was represented by one set of averaged data including left and right FV, nICP, nCPP and CT findings. The nCPP was calculated as the difference between mean ABP and $nICP_{BB}$.

Analysis considered the calculations of the left–right mean value of the nICP ($nICP_m = [nICP_L + nICP_R]/2$), the left–right difference in nICP ($nICP_{Diff} = nICP_L - nICP_R$), and its absolute left–right difference ($nICP_{Abs\ Diff} = |nICP_L - nICP_R|$). The same calculations were performed for nCPP and FV.

Statistical analysis

Multiple measurements were treated as independent events. The data were tested for normal distribution using the Shapiro-Wilk test and are presented as median (IQR). Data distributions were non-parametric. Correlations between the different variables were performed using the Spearman correlation coefficient (R), with statistical significance set at 0.05. Statistical measurements were performed with the Wilcoxon rank sum test with continuity correction, and the Wilcoxon signed rank test.

Results

Interhemispheric difference in non-invasive ICP and CPP

From 97 patients, 73 did not meet the inclusion criteria: 64 patients did not present midline shift at any moment; 9 patients had either unilateral or bilateral craniectomy - two of these patients presented midline shift before having a craniectomy, and their recordings were considered for analysis.

From the 24 patients presenting midline shift, the total number of recordings was 63; 34 presenting midline shifts from left to right (-), and 29 from right to left (+). For these patients, only CT scans obtained before craniectomy were used for midline shift assessment. Midline shift varied from 1.0 to 14 mm (median 3 (5-2)). The location of the head injury lesions in these patients was predominant on the left side (N=14 (58%)). The degree of swelling was moderate (median score of 2 (3-2), range 0-4; swelling score 0: N=1; score 1: N=9; score 2: N=29; score 3: N=23; score 4: N=1). The values of midline shift and brain swelling were correlated (R=0.30, $p<0.01$).

Table 6.1 lists the median (IQR) of pressure and flow for patients. Figure 6.2 shows an example of a patient recording presenting a noticeable nICP asymmetry.

$nICP_L$ and $nICP_R$ were correlated with each other (R=0.79, $p<0.001$), and with invasive ICP (Figure 6.3, R=0.50 and 0.51 ($p<0.001$), respectively for left and right sides). $nICP_m$ was also correlated with ICP (R=0.53, $p<0.001$). $nICP_{Diff}$, $nICP_{Abs\ Diff}$ and invasive ICP were not significantly correlated with brain swelling (R=-0.16, R=0.24 and R=0.07, respectively).

There was a significant correlation between $nICP_{Diff}$ and the extent of midline shift (R=0.34, $p<0.01$). This relationship indicates that nICP on the side of brain expansion was smaller than in the compressed side when there was a midline shift (Figure 6.4). nICP at the side of expansion was significantly different in comparison to the compressed side (18.86±5.71 mmHg (mean ± SD) versus 20.30±6.78 mmHg for expansion and compressed sides, respectively; with a mean difference of -1.44±3.61 mmHg, $p<0.01$).

Table 6.1. Median (IQR) of the assessed variables.

Variable	Median (IQR)
ABP	103.40 (109.20-94.00)
ICP	21.27 (26.48-16.60)
CPP	80.58 (86.17-72.64)
FV_m	55.21 (65.76-43.89)
FV_L	56.18 (64.53-40.45)
FV_R	56.68 (70.37-41.07)
$FV_{Abs\ Diff}$	10.88 (18.06-6.09)
$nICP_m$	19.95 (24.16-16.88)*
$nICP_L$	19.42 (23.65-15.70)*
$nICP_R$	20.93 (25.82-17.21)*
$nICP_{Abs\ Diff}$	2.37 (5.00-1.11)
$nCPP_m$	82.42 (87.06-75.69)**
$nCPP_L$	82.95 (88.13-76.43)**
$nCPP_R$	81.24 (86.71-74.31)**
$nCPP_{Abs\ Diff}$	2.37 (5.00-1.11)

*nICP (left, right and mean) is not significantly different from ICP ($p>0.05$).

**nCPP (left, right and mean) is not significantly different from CPP ($p>0.05$).

Abs = absolute; diff = difference; m, mean; L, left; R, right.

ABP (mmHg), arterial blood pressure; CPP (mmHg), cerebral perfusion pressure; FV (cm/s), cerebral blood flow velocity; ICP (mmHg), intracranial pressure; nICP (mmHg), non-invasive intracranial pressure; nCPP (mmHg), non-invasive cerebral perfusion pressure.

Similarly to nICP, $nCPP_L$ and $nCPP_R$ were correlated with each other (R=0.89, p<0.001), as well as with invasive CPP (R=0.71 and 0.67 (p<0.001), respectively for left and right sides). $nCPP_m$ was also correlated with CPP (R=0.71 (p<0.001)). CPP and $nCPP_m$ presented an inverse relationship with brain swelling (R=-0.29 (p=0.02), R=-0.27 (p=0.04), respectively). There was a trend between $nCPP_{Abs\ Diff}$ and brain swelling (R=0.24 (p=0.06)).

$nCPP_{Diff}$ was inversely correlated with midline shift (R=-0.34 (p<0.01)), indicating that nCPP was greater on the side of brain expansion (Figure 6.5). nCPP at the side of expansion was significantly different in comparison to the compressed side (79.48±7.84 mmHg versus 78.03±8.93 mmHg for expansion and compressed sides, respectively; with a mean difference of 1.45±3.61 mmHg (p<0.01)).

Cerebral haemodynamics in patients with midline shift

FV_L and FV_R presented a strong correlation with each other (R=0.79 (p<0.001)), but not with $nICP_m$ or ICP. FV_{Diff} did not significantly correlate with midline shift (R=-0.19). There was no significant difference between FV at the sides of expansion and compression (difference of 3.27±13.73 cm/s). $FV_{Abs\ Diff}$ did not correlate with brain swelling (R=-0.02).

Figure 6.2. An example of continuous recording of mean ABP, FV and nICP of a patient presenting a midline shift of -3.0 mm. It is possible to observe the asymmetry of nICP in this patient, in whom the mean left-right difference throughout the monitoring period was 11.67 mmHg.

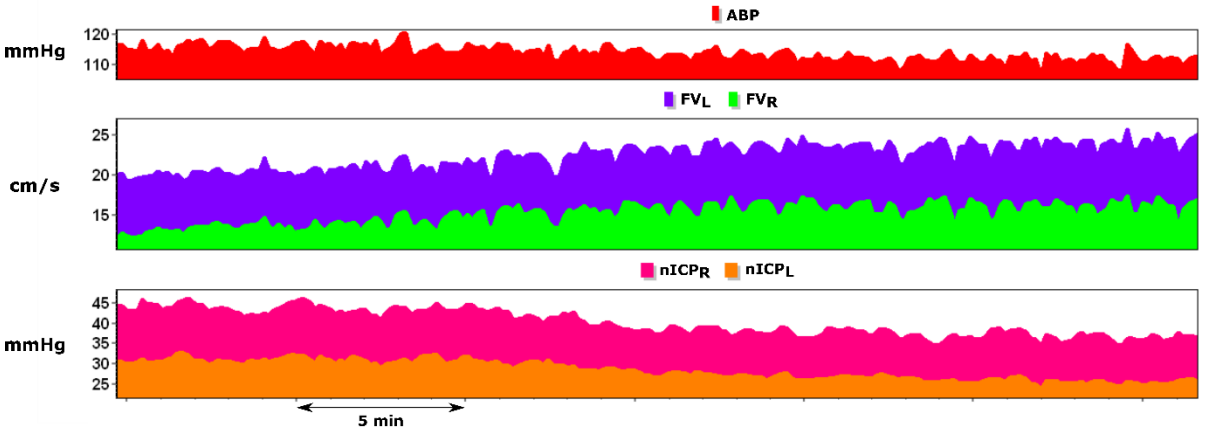

ABP (mmHg), arterial blood pressure; FV (cm/s), cerebral blood flow velocity; nICP (mmHg), non-invasive intracranial pressure.

Figure 6.3. Correlation scatterplots between ICP and nICP. (A) Left nICP vs ICP (R=0.50, p<0.001); (B) Right nICP vs ICP (R=0.51, p<0.001).

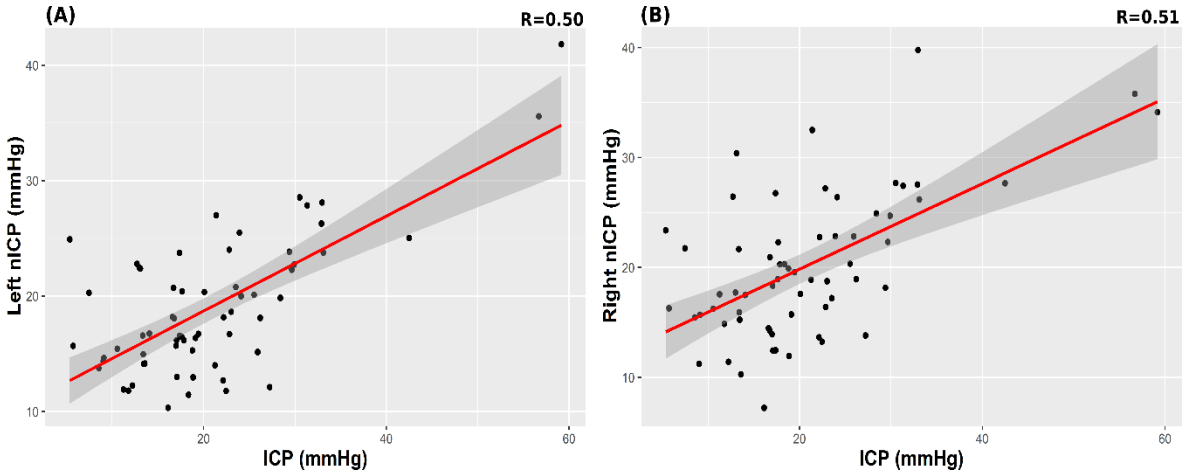

Grey shaded areas on the plots represent the 95% confidence intervals for the linear regressions between ICP and nICP.

ICP (mmHg), intracranial pressure; nICP (mmHg), non-invasive intracranial pressure.

Figure 6.4. Correlation scatterplot of the relationship between brain midline shift and the interhemispheric difference in nICP (R=0.34, p<0.01). Negative values for midline shift represent a brain expansion from the left to the right side; for positive values, an expansion from the right to the left side. When there is a midline shift, it is suggested that nICP was smaller on the side of brain expansion; therefore, nICP cannot be considered the driving force of the brain asymmetry demonstrated by a noticeable midline shift.

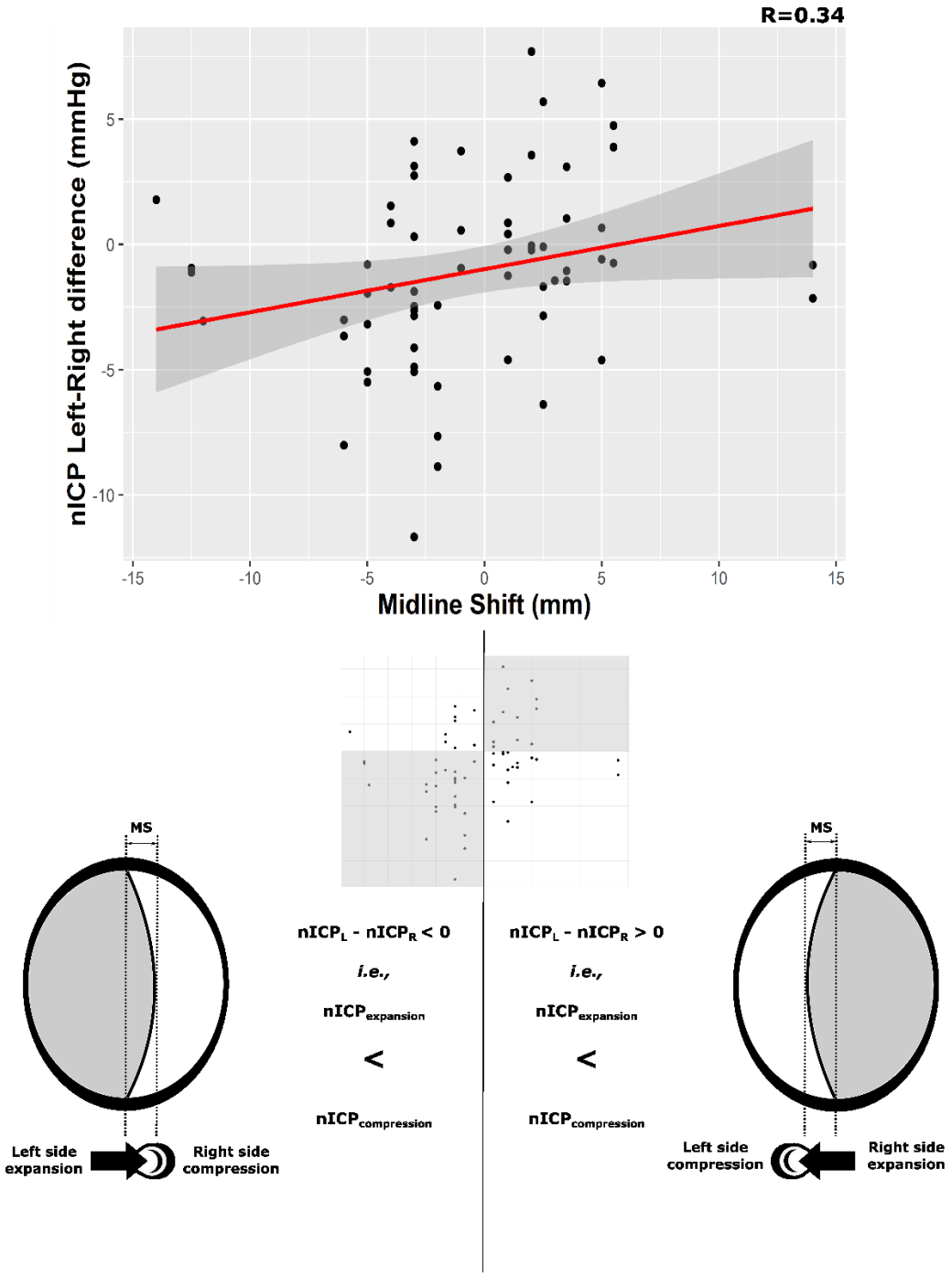

Grey shaded area on the upper panel represents 95% confidence intervals for the linear regressions between nICP and midline shift.

MS, midline shift (mm); nICP, non-invasive intracranial pressure (mmHg).

Figure 6.5. Scatterplot of the relationship between brain midline shift and the left-right difference in nCPP (R=-0.34, p<0.01). Similarly to Figure 6.4 negative values for midline shift represent a brain expansion from the left to the right side; for positive values, an expansion from the right to the left side. When there is a midline shift, it is suggested that nCPP is greater on the side of brain expansion.

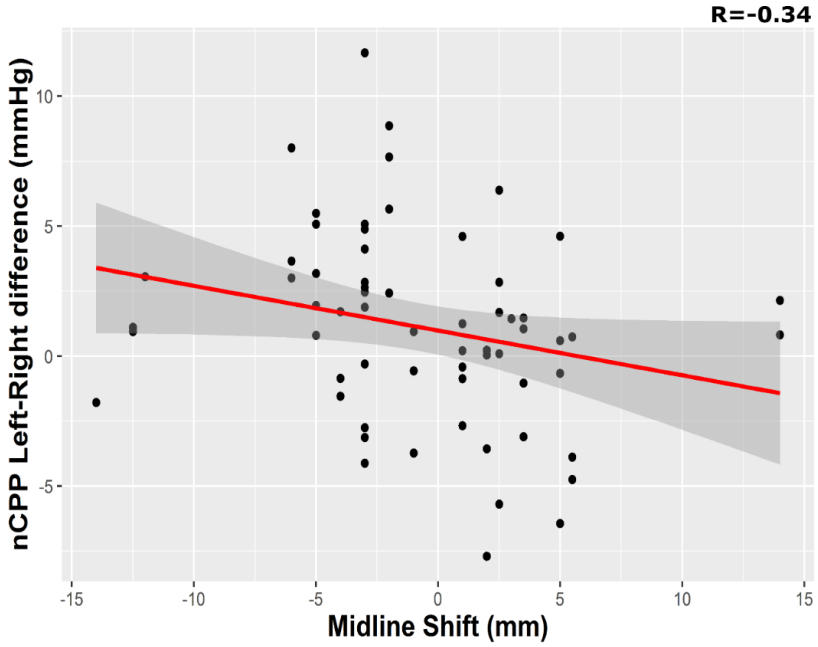

nCPP (mmHg), non-invasive cerebral perfusion pressure.

Discussion

Pressure gradients have been observed between a variety of intracranial compartments previously [142], and the specific vulnerability of the brain to it seems to have been neglected so far. Clinically, ICP transducers are usually only placed unilaterally in the brain parenchyma or intraventricularly. Nevertheless, in conditions which an interhemispheric pressure gradient is present, elevated ICP in the contralateral hemisphere may be treated insufficiently or even disregarded. Particularly, the absence of bilateral monitoring gains importance if one takes into consideration that intracranial hypertension [7] and brain midline shift [156] are related to poor outcome after TBI. In such cases, an early identification of interhemispheric pressure gradients without the risks associated with invasive monitoring would be useful.

There has been a controversy in the literature concerning interhemispheric pressure gradients in cases with focal lesions. Sahuquillo et al. [144] affirmed that patients after TBI presented ICP higher in the hemisphere with the mass lesion. Such results are in agreement with the majority of findings in experimental models, in which ICP was always higher ipsilateral to the mass lesion [157]. Nevertheless, Wolfla et al. [145,146], verified in a swine model of extradural temporal lesions that ICP was always highest on the contralateral side to the mass. These contradicting results may be because intradural and extradural lesions produce different patterns of pressure gradients, or due to anatomical differences between the intracranial compartment of humans and swine [145]. Another potential explanation lays on the fact that different mechanisms could generate interhemispheric pressure gradients. For example, a complete or partial blockage of the subarachnoid space between brain hemispheres impairing the free circulation of CSF, or even derived from differences in CPP [145].

Asymmetry of ICP and CPP assessed non-invasively

The common conceptual thinking about interhemispheric pressure gradients dictates that ICP will be higher on the side of brain expansion in response to trauma and consequent local tissue pressure gradients leading to mass shifts [158]. Contrarily to what is mostly reported in the literature, in our study, intracranial pressure estimation was smaller on the side of brain expansion, and therefore not the plausible driving force of the observed brain asymmetry as evidenced by a measurable midline shift. However, uneven CPP distributions across hemispheres were the plausible cause of the midline shift.

A greater CPP on the side of brain expansion could originate from derangements in the cerebral vasculature as a secondary consequence of head trauma. It has been reported that TBI patients may present with a heterogeneous pattern of cerebrovascular dysfunction [159,160]. For example, a dysfunction of the cerebrovascular endothelial wall may initiate an uncontrolled ion and protein transfer from the intravascular to the extracellular brain compartments. Anatomically, this process increases the volume of the extracellular space by water accumulation, causing brain swelling [161]. However, other scenarios, like unilateral vasoparalysis, leading to purely cerebral blood volume increase, are also possible.

A previous study on the same group of TBI patients with midline shift [162], showed that cerebral autoregulation assessed using TCD was impaired on the side of brain expansion. Another study [163] exploring the effects of brain asymmetry on cerebral haemodynamics, found that the critical

closing pressure of the vessels [164] was lower on the side of brain expansion. This could be related to damaged and dilated vessels, resulting in a lower vascular resistance in comparison to vessels in the uninjured contralateral hemisphere.

In the present assessment, it appears that an impaired cerebrovascular bed was associated with a greater blood perfusion to the side of brain expansion. In addition, the absolute interhemispheric difference in nCPP presented a positive trend with brain swelling, suggesting that the more asymmetrical nCPP is, the greater the brain swelling. This is in agreement with the hypothesis of an impaired cerebrovascular bed in this patient cohort, as brain swelling might originate following endothelial dysfunction in TBI [161].

These findings jointly with our results suggest that interhemispheric pressure gradients might not be a direct pressure gradient-controlled phenomenon, in which mass lesions are the only source of pressure gradients and brain asymmetry. Instead, considering the observed patterns of cerebral haemodynamics displayed by nCPP, it appears to be a phenomenon that presents components of vascular and vasogenic origins.

Clinical relevance of interhemispheric gradients and the significance of nICP monitoring

For patients with mass lesions and vulnerable to interhemispheric pressure gradients, a bilateral ICP monitoring would be essential as it could guide a more oriented management. Moreover, unilateral ICP monitoring can be imprecise, and sometimes the presence of interhemispheric pressure gradient can lead to delayed cerebral ischaemia. Nevertheless, the invasiveness of the ICP monitoring techniques has prevented their widespread use.

TCD-based nICP monitoring would potentially eliminate these complications, but despite its ability to detect dynamic changes in ICP, the accuracy of ICP estimation in comparison with invasive methods is not ideal. In the present study, the 95% CI for ICP prediction considering nICP estimated at the right hemisphere (where invasive ICP was measured) was ±14.7 mmHg. However, if only applied to measure the relative left-right difference in nICP, the accuracy of this method does not play a crucial role in the interpretation of the findings.

The use of TCD-based nICP monitoring would be useful in anticipating the identification of pressure gradients that would only be detected by a head CT. In practical terms, for instance, had an increasing pressure gradient been detected, it would be useful to repeat imaging, as it

could confirm potential haemorrhage or increasing midline shift. Although there are no standard protocols on how to treat pressure gradients in the brain, a possible management would be targeting CPP to standard thresholds [9] and treating ICP based on the highest value. This management should also consider that ICP is not solely a number, but a trend containing relevant information about cerebral haemodynamics [165].

Limitations

This retrospective cohort analysis reaches for old material, as according to changes in practice, patients with midline shift rarely are managed without surgery, such as evacuation of lesion or decompression. Although such cases are currently less common, this study could demonstrate the applicability of TCD as an alternative for bilateral ICP monitoring.

The data are not homogeneous, particularly concerning age, GCS and number of recordings per patient. However, stratification of the data was not applied as each measurement was considered an independent event in the analysis if patients presented persistent midline shift and managed for traumatic brain injury.

It is presumed that there was an interhemispheric cerebral arterial pressure gradient. Therefore, differences in bilateral nICP may be directly translated to differences in nCPP. In regards to the CPP-oriented management protocol applied (CPP ≥70 mmHg), this is no longer used in clinical practice [9]. However, driving CPP to 70 mmHg could have contributed to further shifts in the absence of adequate cerebral autoregulation.

6.2 Feasibility of nICP associated with a TCD multiparameter assessment of cerebral haemodynamics during orthotopic liver transplant

Introduction

The pathophysiology of hepatic encephalopathy is not completely understood, but the development of cerebral oedema resulting in ICH and neurologic deterioration is a well-known phenomenon of acute liver failure (ALF) [166,167].

ICH development may be linked to both the systemic inflammatory state and effects of neurotoxins in ALF. Cerebral hyperammonaemia due to compromised detoxification in the failing liver results in its enzymatic conversion to osmotically active glutamine, with subsequent astrocyte swelling and brain oedema [168]. Although the prevalence and mortality caused by these complications have decreased in the past years due to advancements in treatment, the onset of oedema and ICH in ALF patients represent a leading cause of death (mortality >50%) [169] and permanent neurological damage [170,171].

Patients with ALF are vulnerable to sudden relevant changes of ABP, causing changes in CBF in conditions of functional loss of cerebral blood flow autoregulation. For the same reason, they may be considered less suitable for major surgery with significant blood losses and fluid shifts, such as orthotopic liver transplantation (OLT). Arterial hypertensive or hypotensive episodes during OLT may provoke cerebral hypoperfusion or hyperperfusion leading to either ischemia or aggravation of cerebral oedema and even cerebral haemorrhage. Failure to regain consciousness despite satisfactory graft function has also been reported after OLT [172–175], which may originate from episodes of ICH during transplantation.

In patients with ALF, the benefits of ICP monitoring include the precise and early detection of ICH; a correct evaluation of response to therapies; the knowledge of cerebral perfusion pressure, which guides vasopressors administration in the setting of loss of cerebral autoregulation characteristic of ALF[176]; the procurement of prognostic information, especially for deciding candidacy for transplant; the lengthening of survival time, increasing the chances for organ allocation[177]; and the improvement of anaesthetic management during OLT, in which ICH is common[178].

On the other hand, in patients with hepatic failure, due to the risk of coagulopathy, the standard invasive ICP monitoring may cause some complications, like haemorrhage (approximately 49% [179]). Taking these implications into account, this study aims to test the feasibility of nICP monitoring in association with a TCD multiparameter approach for cerebral haemodynamics assessment in patients with ALF undergoing OLT.

Materials and methods

Patient population

Six patients from the retrospective OLT material described in Section 4.1.2 were analysed in this study. The median age was 56 years (range 51-65 years; 67% males). On arrival to the surgical suite, a standard monitoring was applied, including pulse-oximetry, electrocardiography and invasive arterial blood pressure monitoring. Patients were not pre-medicated. After preoxygenation, general anaesthesia was induced with intravenous with propofol alfentanil (0.25 – 1.0 mg) and paralysis achieved with atracurium (0.6 mg/kg). A continuous infusion of remifentanil was started after induction (20 mg at a rate of 4-6 ml/h). Muscle relaxation was maintained with a continuous infusion of atracurium (40 – 60 mg/h, 10 mg/ml). A mixture of air/oxygen/isoflurane at sub-minimal alveolar concentrations (0.5 – 1.5%) was the volatile agent of choice. Ventilation was controlled to an end-tidal carbon dioxide ($ETCO_2$) of 4-4.5 kPa during surgery.

Clinical monitoring and data collection

The implemented clinical monitoring included ABP and FV as described in Section 4.2.1. FV was obtained from the left and right middle cerebral arteries throughout the surgery. During every surgery, three time periods were defined: the dissection phase (T0), from surgical start till portal vein has been clamped; the anhepatic phase (T1), when the portal vein is clamped; and at last the reperfusion phase (T2), when the portal vein is released until the completion of the surgery. The mean recording time was 6 hours.

The analysis considered the calculations of the left and right sides mean values of each TCD-derived parameter, which included $nICP_{BB}$, nCPP (derived from $nICP_{BB}$), cerebral autoregulation (Mxa), pulsatility index, critical closing pressure, diastolic closing margin and optimal ABP as described in Section 4.2.3.

Statistical analysis

Data were tested for normal distribution using the Shapiro-Wilk test and are presented as median (IQR). Data distributions were non-parametric. Statistical measurements were performed with the Kruskal-Wallis rank sum test followed by pairwise comparisons using Wilcoxon rank sum test across the different phases of OLT. The statistical significance level was set at $p<0.05$.

Results

Table 6.2 summarises patient demographics and clinical information. Table 6.3 shows the different parameters assessed at each phase during OLT averaged by patient. Table 6.4 shows the same parameters for individual patients evaluated at each phase during OLT.

The variable presenting statistically significant changes between surgery phases was nCPP (T0-T2, mean decrease of 8.17 mmHg ($p=0.03$)). ABP and DCM presented a reduction trend throughout OLT, as well as FV and CrCP from T0 to T1. PI presented an increasing trend, whereas nICP remained constant (Table 6.3).

Table 6.2. Patients demographics and acute liver failure aetiology.

Patient	Age	Sex	ALF aetiology
1	51	M	ArLD/HCV
2	60	M	ArLD
3	51	M	Cryptogenic cirrhosis (likely NASH)
4	65	F	HCV/HCC
5	53	F	PSC
6	57	M	PSC

ALF, acute liver failure; ArLD, alcohol-related liver disease; HCV, hepatitis C virus; NASH, non-alcoholic steatohepatitis; HCC, hepatocellular carcinoma; PSC, primary sclerosing cholangitis; M, male; F, female.

Considering reference values for TCD parameters in a healthy population [55], patients presented low FV in all phases during OLT (FV <60 cm/s). In an individualised analysis, patients 2, 3, 5 and 6 presented low flow velocity patterns in all phases; patient 4 presented low flow only during T2. PI values deviated from normal ranges in all patients throughout OLT (PI >0.8 [55]) (Table 6.4).

Table 6.3. Variables assessed at each phase during OLT averaged by patient. Only nCPP presented statistically significant changes between surgery phases (T0-T2, mean decrease of 8.17 mmHg (p=0.03)).

	T0	T1	T2
ABP	72.22 (77.92-69.93)	69.86 (74.19-66.34)	63.36 (66.58-59.17)
ABP_s	111.2 (117.00-109.60)	108.08 (112.94-105.35)	101.65 (108.46-97.45)
ABP_d	52.82 (56.18-50.04)	52.32 (56.25-46.09)	44.48 (47.64-41.22)
FV	53.90 (58.65-33.65)	44.04 (51.29-38.57)	52.87 (65.72-40.03)
PI	1.15 (1.42-1.06)	1.17 (1.24-1.14)	1.28 (1.41-1.18)
nICP	12.50 (14.22-10.89)	12.09 (12.79-11.45)	12.12 (13.25-8.70)
nCPP	58.25 (63.35-58.00)	57.73 (60.92-55.71)	51.14 (51.62-50.47)
Mxa	0.50 (0.60-0.48)	0.64 (0.69-0.54)	0.61 (0.76-0.51)
CrCP	23.00 (21.91-19.77)	26.02 (28.60-24.10)	23.12 (23.22-21.28)
DCM	30.00 (33.73-26.52)	23.63 (28.25-21.50)	21.82 (26.07-19.89)

ABP (mmHg) (s, systolic; d, diastolic), arterial blood pressure; FV (cm/s), cerebral blood flow velocity; PI, pulsatility index; nICP (mmHg), non-invasive intracranial pressure; nCPP (mmHg), non-invasive cerebral perfusion pressure; Mxa, autoregulation index; CrCP (mmHg), critical closing pressure; DCM (mmHg), diastolic closing margin.

Overall, nCPP presented low values in all phases (<60 mmHg [180]). Individually, patients 2, 3 and 6 presented low nCPP in all phases; patient 4 only during T0 and T1; patient 1 during T1 and T2 and patient 5 only during T0. nICP was below the clinical threshold of 20 mmHg for intracranial hypertension throughout OLT for all patients (Table 6.4).

Mxa index showed impaired cerebral autoregulation throughout OLT. Furthermore, Mxa showed a gradual worsening in autoregulation from T0-T1. CrCP was never close to ABP in any phases. Consequently, DCM did not reach critical values (≤0 mmHg) throughout OLT, remaining above a median of 23 mmHg (Table 6.3).Figure **6.6** shows an example of monitored ABP, FV, nICP, nCPP, CrCP and Mxa throughout OLT phases for a single patient. Figure 6.7 depicts individual and mean changes for ABP, nICP and nCPP; Figure 6.8 for FV and PI; Figure 6.9 for the autoregulation index; and Figure 6.10 for CrCP and DCM.

Figure 6.11 and Figure 6.12 show examples of optimal curves for ABP obtained from individual patients, in which nPRx below levels associated with impairment of cerebral autoregulation (<0.25) revealed optimal values for ABP in certain cases (U-shaped curves).

Figure 6.6. Representation of multiparameter monitoring performed with transcranial Doppler during orthotopic liver transplant. This figure depicts "patient 5", in which is possible to observe the overall changes in cerebral haemodynamics among different surgical phases.

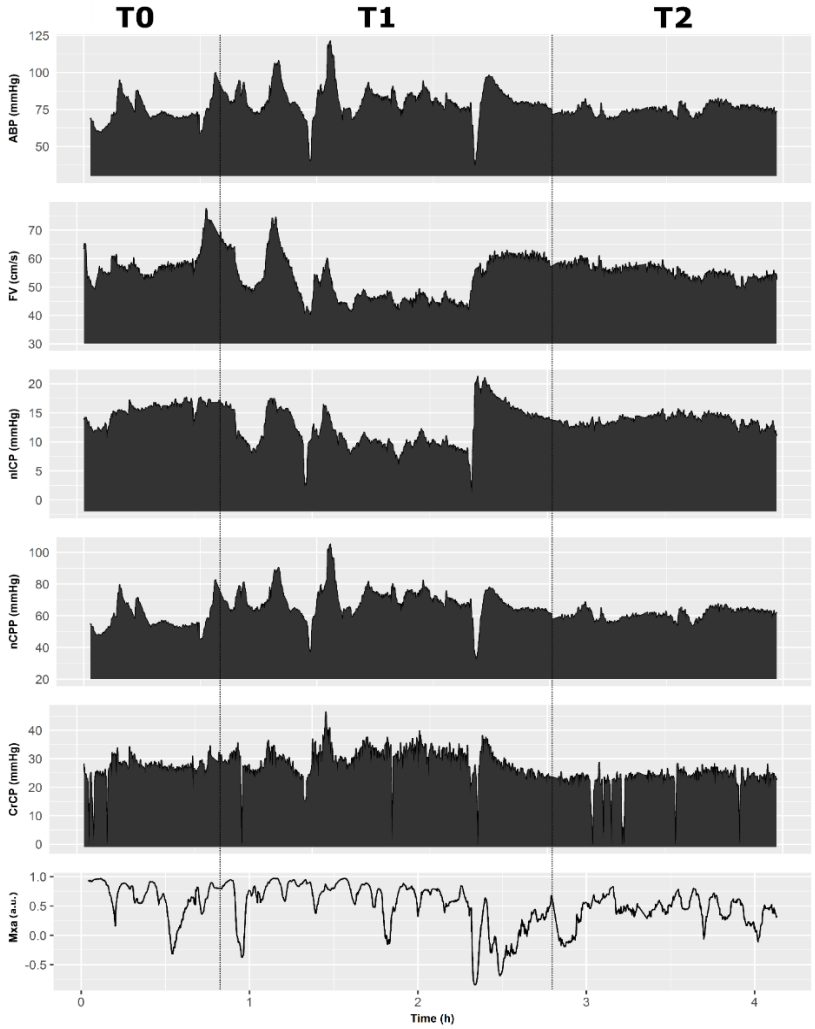

ABP (mmHg), arterial blood pressure; FV (cm/s), cerebral blood flow velocity; nICP (mmHg), non-invasive intracranial pressure; nCPP (mmHg), non-invasive cerebral perfusion pressure; CrCP (mmHg), critical closing pressure; Mxa (a.u.), autoregulation index; T0, dissection phase; T1, anhepatic phase; T2, reperfusion phase.

Table 6.4. Variables assessed at each phase during OLT considering individual cases.

	T0						T1						T2					
	1	**2**	**3**	**4**	**5**	**6**	**1**	**2**	**3**	**4**	**5**	**6**	**1**	**2**	**3**	**4**	**5**	**6**
ABP	81.96	69.07	62.63	79.50	73.15	71.29	64.77	66.08	67.12	74.72	81.24	72.60	58.06	54.13	64.20	62.52	74.39	67.38
ABP_s	118.91	110.92	111.46	120.73	106.35	109.18	104.57	99.53	117.84	107.68	114.42	108.47	96.86	99.23	109.92	92.75	116.25	104.07
ABP_d	59.23	49.30	40.70	57.11	52.25	53.39	44.78	50.00	40.66	56.78	63.30	54.64	40.81	36.02	42.44	46.53	54.29	48.01
FV	63.47	49.61	23.44	58.80	58.18	28.32	73.53	40.58	37.89	47.50	52.55	32.29	69.20	50.44	33.45	74.49	55.29	36.55
PI	0.91	1.21	1.88	1.08	1.06	1.49	1.18	1.17	1.55	1.13	0.94	1.26	1.36	1.43	1.54	1.19	1.17	1.18
nICP	9.65	10.63	11.68	14.52	15.09	13.31	9.12	12.16	11.26	13.36	12.02	13.00	7.70	5.65	12.54	11.71	13.48	15.90
nCPP	72.31	58.44	50.95	64.98	58.06	57.97	55.66	53.92	55.86	61.66	69.22	59.60	50.35	48.47	51.66	50.81	60.91	51.48
Mxa	0.48	0.49	0.45	0.67	0.63	0.5	0.44	0.7	0.68	0.69	0.52	0.60	0.49	0.56	0.66	0.82	0.42	0.8
CrCP	23.97	18.94	15.82	22.26	26.78	23.75	23.79	26.99	20.10	32.55	29.14	25.04	23.22	13.72	23.04	25.19	23.20	20.69
DCM	35.26	30.36	24.88	34.85	25.47	29.64	20.99	23.02	20.56	24.23	34.17	29.59	17.59	22.30	19.40	21.33	31.09	27.33

ABP (mmHg) (s, systolic; d, diastolic), arterial blood pressure; FV (cm/s), cerebral blood flow velocity; PI (a.u.), pulsatility index; nICP (mmHg), non-invasive intracranial pressure; nCPP (mmHg), non-invasive cerebral perfusion pressure; Mxa (a.u.), autoregulation index; CrCP (mmHg), critical closing pressure; DCM (mmHg), diastolic closing margin.

Figure 6.7. Longitudinal plots for (A) arterial blood pressure, (B) non-invasive intracranial pressure and (C) non-invasive cerebral perfusion pressure throughout OLT. Although all three parameters had a decreasing trend, only nCPP presented significant changes between phases (T0-T2 ($p<0.03$)).

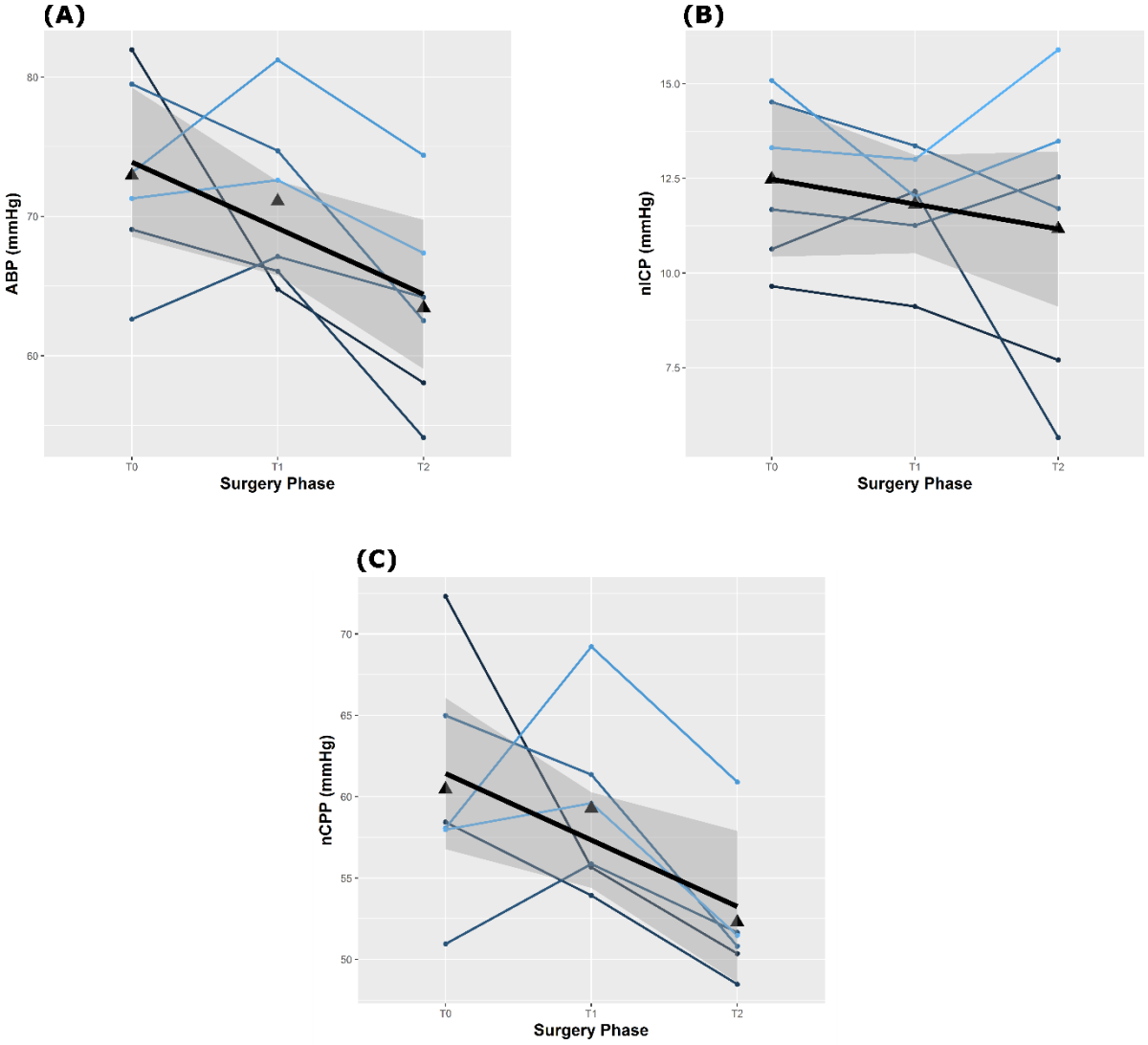

Triangles on the plots represent the mean values for each variable at a specific surgery phase. Thick black lines represent the linear fit of the data; grey shadowed areas represent the 95% confidence interval of the linear model representative of the data.

ABP (mmHg), arterial blood pressure; nICP (mmHg), non-invasive intracranial pressure; nCPP (mmHg), non-invasive cerebral perfusion pressure; OLT, orthotopic liver transplant.

Figure 6.8. Longitudinal plots for (A) cerebral blood flow velocity and (B) pulsatility index throughout OLT. The patients presented low FV (<60 cm/s) and augmented PI (>0.8) in all phases during OLT.

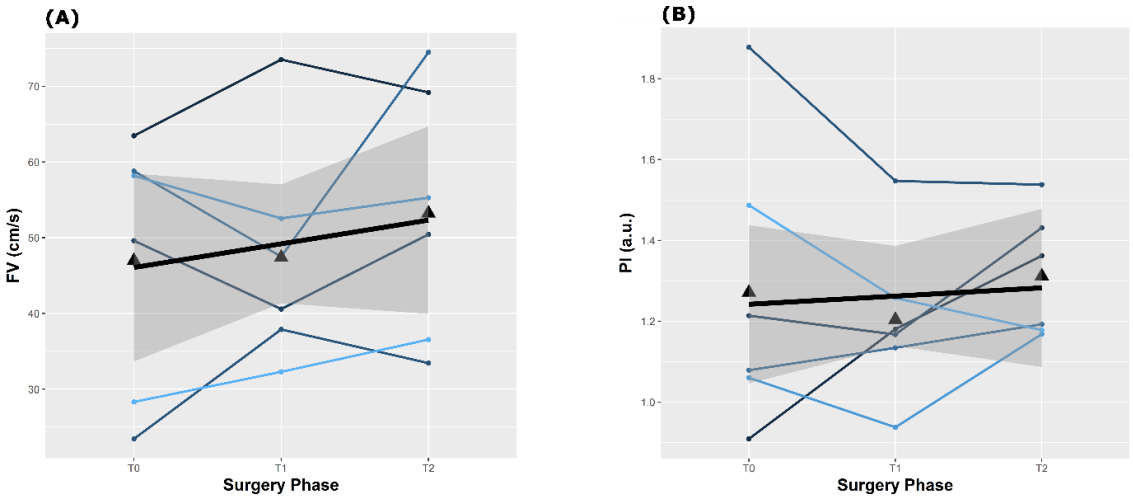

Triangles on the plots represent the mean values for each variable at a specific surgery phase. Thick black lines represent the linear fit of the data; grey shadowed areas represent the 95% confidence interval of the linear model representative of the data.

FV (cm/s), cerebral blood flow velocity; PI (a.u.), pulsatility index; OLT, orthotopic liver transplant.

Figure 6.9. Longitudinal plot for autoregulation index throughout OLT. Mean Mxa demonstrates impaired cerebral autoregulation throughout OLT, with gradual worsening from T0-T1.

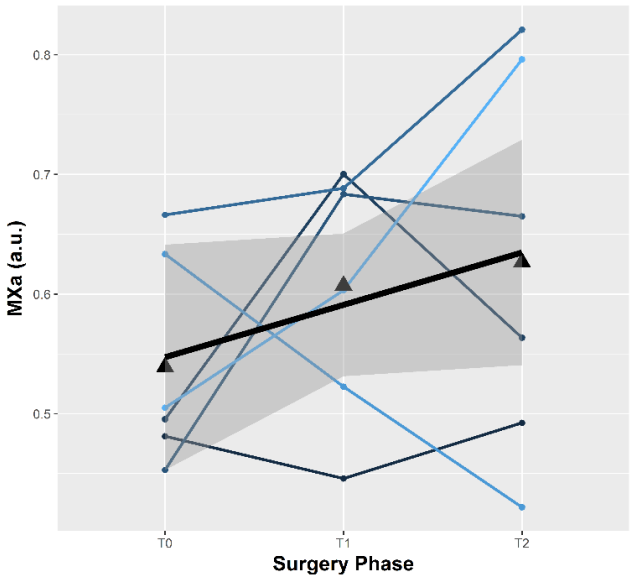

Triangles on the plots represent the mean values for each variable at a specific surgery phase. The thick black line represents the linear fit of the data; grey shadowed areas represent the 95% confidence interval of the linear model representative of the data.

Mxa, autoregulation index; OLT, orthotopic liver transplant.

Figure 6.10. Longitudinal plots for (A) CrCP and (B) DCM throughout OLT. CrCP was never close to ABP in any phases. Therefore, DCM did not reach critical values (≤0 mmHg).

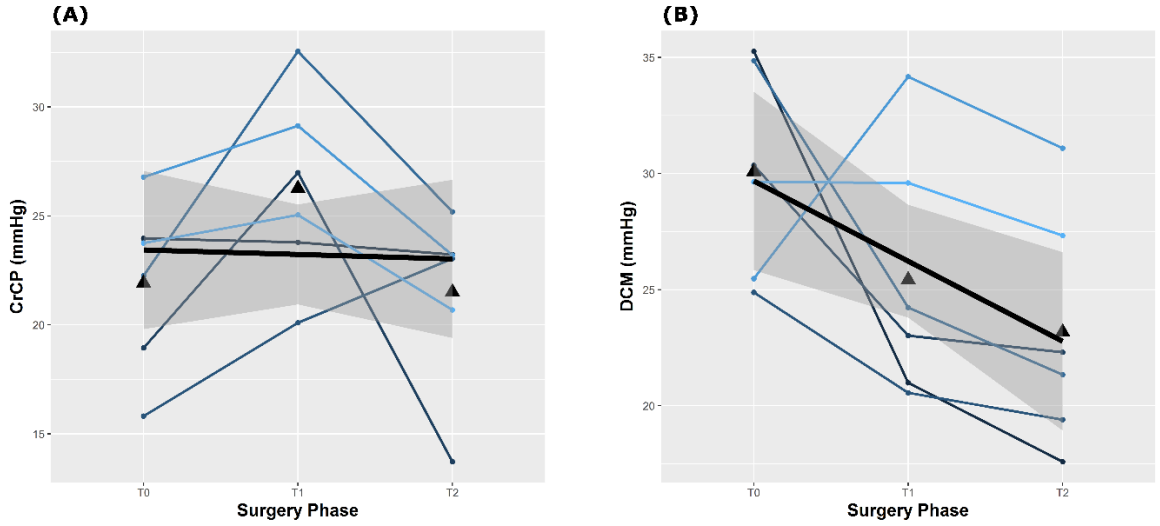

Triangles on the plots represent the mean values for each variable at a specific surgery phase. The thick black lines represent the linear fit of the data; grey shadowed areas represent the 95% confidence interval of the linear model representative of the data.

CrCP (mmHg), critical closing pressure; DCM (mmHg), diastolic closing margin; OLT, orthotopic liver transplant.

Figure 6.11. An example of an optimal curve for arterial blood pressure with corresponding recordings of ABP, ICP and nCPP throughout OLT.

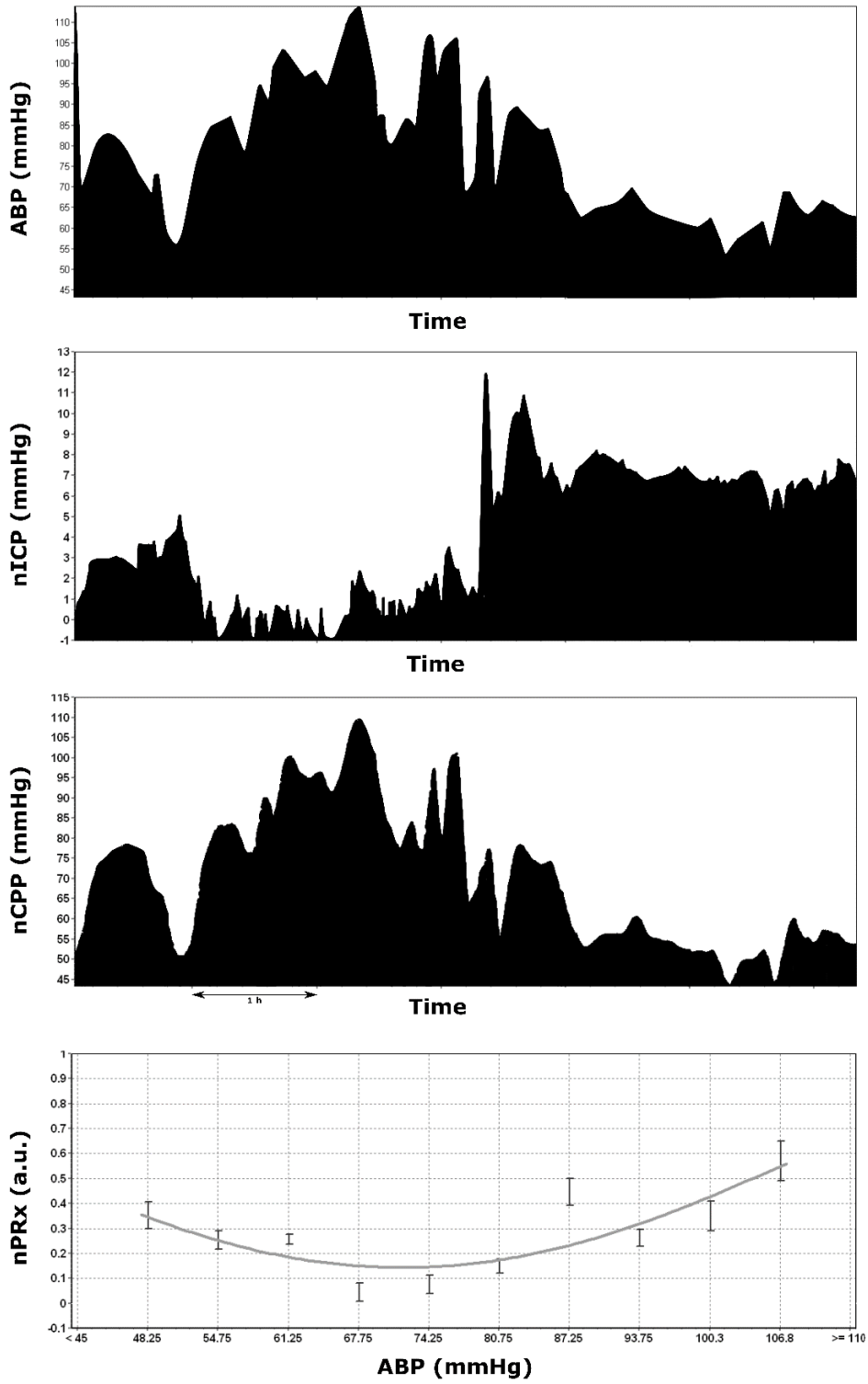

The lowest point on the "U-shaped" curve represents the optimal values for ABP, which, in this case, was close to 70 mmHg.

ABP (mmHg), arterial blood pressure; nICP (mmHg), non-invasive intracranial pressure; nCPP (mmHg), non-invasive cerebral perfusion pressure; nPRx (a.u.), autoregulation index; OLT, orthotopic liver transplant.

Figure 6.12. Optimal curves for arterial blood pressure obtained in different patients.

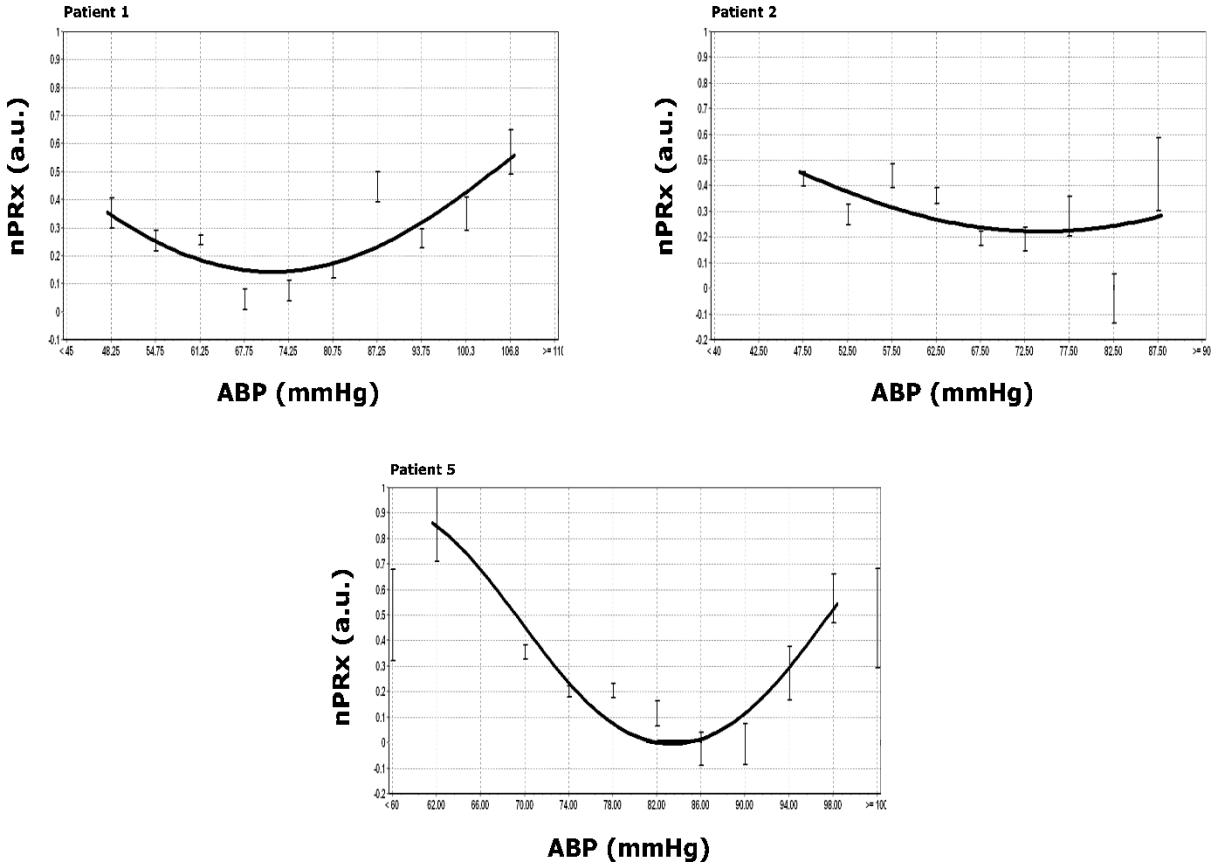

The lowest points on the "U-shaped" curves represent the optimal values for ABP.

ABP (mmHg), arterial blood pressure; nPRx (a.u.), autoregulation index.

Discussion

In a variety of clinical settings, multimodal applications of TCD may provide an early detection of the onset of cerebrovascular derangements and facilitate their clinical management. In previous studies on ALF, TCD provided a repeatable and reliable non-invasive, bedside assessment of CBF changes, allowing the evaluation of the OLT feasibility [181] and the identification of predominant haemodynamic patterns [182]. In the present study, different patterns of cerebral haemodynamics could be identified non-invasively during OLT using a

TCD-derived multimodal approach englobing nICP, nCPP, cerebral autoregulation, CrCP and DCM.

The assessment of cerebral autoregulation with TCD during OLT has been investigated previously. In a study of Ardizzone et al. [183], this parameter was evaluated by investigating parallel changes in ABP and FV during a slow phenylephrine infusion at the beginning and end of OLT for 1 hour at each period compared with a baseline. Before OLT, autoregulation was impaired in all patients (N=6). However, it markedly improved at the end of surgery. In another study from the same author using a larger patient cohort (N=23) [184], autoregulation and cerebrovascular resistance significantly increased from anhepatic to postreperfusion phases (within the first hour), decreasing from postreperfusion to recovery in the neohepatic phase (end of surgery). Such results agree with findings of this study, as cerebral autoregulation assessed through changes of either ABP and FV (Mxa, Figure 6.9) demonstrated values indicative of a non-reactive cerebrovascular bed throughout OLT.

The scenario of impaired cerebral autoregulation may explain the low cerebral blood flow velocity pattern presented by patients. In addition, the estimated cerebral perfusion pressure below 60 mmHg may indicate that patients were on the verge of the lower limit of autoregulation. In this condition, FV decreases passively with decreasing CPP [105].

PI, as an index describing changes in TCD waveform resulting from changes in CPP, deviated from normal range under these conditions. However, it did not show increased values as demonstrated by Abdo et al. [182] in previous works assessing cerebral haemodynamics in patients with ALF (PI=2.4 or PI=1.71 [185]).

Although ICP monitoring is not an uncommon practice in patients with ALF developing severe hepatic encephalopathy [186,187], ICP behaviour during OLT has been reported only in few studies. In a study of six cases from Keays et al. [188], the mean ICP level was higher during the "preclamp phase" and the "graft reperfusion" phase than the "anhepatic phase". Lidofsky et al. [178] have shown that ICP tended to vary significantly intraoperatively. It initially increased during the dissection phase, then declined over the anhepatic phase, and again increased during the reperfusion phase. Lastly, Detry et al.'s study [189] suggested that in ALF patients, particularly in those who developed intracranial hypertension before OLT, the dissection and reperfusion phases were associated with a risk of brain injury secondary to elevated ICP and low CPP. The anhepatic phase, as similarly to the previous studies, seemed to be linked to a decrease in ICP. ICP increase occurring during liver dissection and reperfusion phases suggest

a possible role of toxic substances released from necrotic hepatocytes during liver handling and products of ischemia/reperfusion injury released during reperfusion phase [189].

The overall nICP behaviour was kept relatively constant throughout OLT. An exception was patient 5 (Figure 6.6), who presented a similar pattern of ICP decrease during anhepatic phase and increase during reperfusion as previously described [178,188,189]. However, changes in nICP between phases were not significantly different, and nICP mean values were not associated with intracranial hypertension.

nCPP presented a stronger decrease tendency, particularly from anhepatic to reperfusion phases, in which all patients presented nCPP decrease. As nICP remained relatively constant during this period, the observed changes can be attributed to decreases in ABP (Figure 6.7).

Considering that cerebral autoregulation in pathological conditions is subject to haemodynamic changes such as in ABP, ICP and CPP, the determination of optimal thresholds for these parameters could provide a reasonable, individualised management of cerebral haemodynamics in critical situations, such as ICP surges. Based on these assumptions, a previous study could identify a narrow CPP target (optimal CPP (CPP_{opt})) by defining the level of best cerebrovascular reactivity, using PRx [112]. The authors showed that the deviation from CPP_{opt} was associated with worse outcome in TBI patients [112]. In the present study, optimal ABP could be obtained in certain patients, demonstrating the feasibility of identifying these targets during OLT using TCD-based non-invasive monitoring. (Figure 6.11, Figure 6.12).

Critical closing pressure is another useful TCD-derived parameter related to critical thresholds for ABP. By monitoring CrCP, the DCM can also be trended and may represent a significant clinical threshold in patients with arterial hypotension, ICH, or with pathologically increased vascular wall tension [100]. In the six cases evaluated, although DCM decreased significantly throughout OLT (Figure 6.10), it was not exhausted (≤0 mmHg), indicating that cerebral blood flow circulation was not completely compromised.

Although this is a retrospective observational study with a limited sample size, TCD appears to be a feasible tool for assessment of cerebral haemodynamics in the OLT setting and could provide clinically relevant information for patient management in such conditions with high risk of neurological impairment.

6.3 Feasibility of nICP associated with a TCD multiparameter assessment of cerebral haemodynamics during shoulder surgery in the beach chair position

Introduction

The beach chair position (BCP) offers several advantages for shoulder surgery, such as a better intra-articular visualisation and less risk of neurovascular trauma in comparison to surgery performed in the lateral decubitus position [190]. However, BCP may provoke hypotension in the presence of general anaesthesia, which alters cardiovascular reflex responses [191,192].

There are published reports of rare but devastating neurologic injuries occurring in healthy patients in the beach chair position. These included stroke, spinal cord ischemia, and transient visual loss [193–200]. The incidence of neurologic complications after shoulder surgery in the beach chair position remains unknown, but a survey of the American Shoulder and Elbow Surgeons indicated that the incidence of major stroke in this clinical setting is 0.0004% [196].

Because of the gravitational effects of positioning the head above the level of the heart and ABP hypotension, such neurologic complications reported after shoulder surgery in BCP may be the result of impaired cerebral autoregulation, inadequate cerebral perfusion and cerebral ischaemia. By assessing cerebral haemodynamics in patients undergoing surgery in the beach chair position, this study aims to provide possible answers to the questions listed above.

There are few published reports on the use of TCD for the assessment of cerebral haemodynamics of patients in BCP, however, most simply used mean FV as the main parameter [201,202]. Therefore, the objective of this study is to assess cerebral haemodynamics using a multiparameter TCD-derived approach in patients undergoing shoulder surgery who were positioned from supine to beach chair position.

Material and methods

Patient population

This study included prospectively collected data described in Section 4.1.1. This material consisted of 33 patients undergoing shoulder surgery in the beach chair position. The study considered a group of 23 patients: 4 patients could not be included due to the absence of an insonation window for TCD; 6 patients due to poor recordings of either ABP or FV. The median age was 55 (N=23; IQR: 66.50-37; 18 males (78%)).

On arrival to the surgical suite, a standard monitoring was applied, including pulse-oximetry, electrocardiography, and non-invasive arterial blood pressure in the arm. Patients were not pre-medicated. After preoxygenation, general anaesthesia was induced with intravenous propofol (2 mg/kg). To facilitate endotracheal intubation, cisatracurium besilate (0.15 mg/kg) was administered intravenously, and then lungs were ventilated with a mixture of oxygen/air and sevoflurane (mean alveolar concentration of 0.8 to 1.0) to maintain an $ETCO_2$ of 4.5 to 5.5 kPa during surgery.

Ultrasound guided interscalene block using an in-plane approach was performed to provide intra and post-operative analgesia. Initially, the probe was placed at the level of the cricoid cartilage and scanned laterally to identify the carotid artery and internal jugular vein. The sternocleidomastoid muscle overlies these structures. The anterior scalene muscle is seen below the lateral edge of the sternocleidomastoid by moving the probe laterally. The brachial plexus was identified as a groove containing the hypo-echoic nerve structures between the anterior and the middle scalene muscle. Then, the needle was brought in the same plane as the probe so that the whole length of the needle could be visualised. A small amount of local anaesthetic was injected to hydro-dissect and open the fascial plane. This allowed clearer visualisation of the nerve structures; then, 15 to 20 ml of bupivacaine 0.25-0.5% were injected around superior and middle trunks of brachial plexus, between anterior and middle scalene muscles.

Clinical monitoring and data collection

The implemented clinical monitoring included ABP and FV as described in Section 4.2.1. Arterial blood pressure was non-invasively measured for clinical purposes with a cuff via an

oscillometric method from the arm (ABP_{ARM}). For the study, ABP was monitored non-invasively using a finger-cuff (Finometer Pro®, Finapres Medical Systems, Amsterdam, The Netherlands) calibrated at the auditory meatus level (ABP_{FINGER})). Cerebral haemodynamics parameters were calculated using ABP_{FINGER}. FV was assessed ipsilateral to the surgery side. Only ABP_{FINGER} and FV signals were recorded simultaneously.

ABP_{FINGER} and FV monitoring were performed in two different periods: in the supine position, immediately after induction of anaesthesia (phase A); and before the commencement of surgery with the patient in beach chair position (phase B). Beach chair position was achieved by tilting the table to an angle range of 45-90 degrees adjusted for surgical exposure on an individual basis. The mean monitoring time was 5.40±1.60 minutes for phase A and 5.30±1.50 minutes for phase B. ABP_{ARM} was collected retrospectively from the hospital's electronic records system during the study's analysis phase. Preoperative (in the anaesthetic room, before anaesthesia induction) and operative values (in the operation room, with the patient in beach chair position) for ABP_{ARM} were collected. All parameters were calculated and averaged for both phases.

The analysis considered the calculations of the mean values of each TCD-derived parameter evaluated, which included $nICP_{BB}$, nCPP (derived from $nICP_{BB}$), cerebral autoregulation (ARI), pulsatility index, critical closing pressure and diastolic closing margin as described in Section 4.2.3. In this case, given the short monitoring periods, ARI provides a better measure of cerebral autoregulation owing to its shorter calculation window.

Statistical analysis

The data were tested for normal distribution using the Shapiro-Wilk test and are presented as median (IQR). All parameters assessed were non-parametric. Statistical measurements were performed with the Wilcoxon rank sum test with continuity correction, and the Wilcoxon signed rank test for paired comparisons. Also, a Spearman correlation coefficient matrix analysis was employed to assess correlations between the various parameters considering differences from supine to beach chair position (delta correlations (Δ)). Delta differences between parameters are presented as mean and percentage of change. The statistical significance level for all tests was set at $p<0.05$.

Results

Table 6.5 presents demographics, medical and surgical characteristics of patients undergoing shoulder surgery. Table 6.6 presents results for all physiological and cerebral haemodynamics parameters assessed on phase A (supine), phase B (beach chair position) and their respective mean delta changes expressed in percentage. Table 6.7 presents the correlation coefficients of changes in FV and ABP with changes in other parameters evaluated.

Table 6.5. Patient's demographic characteristics, medical history and type of surgical procedures performed (N=23).

Characteristics	
Age (years)	55 (66.50-37.00)
Sex, male/female, n (%)	18 (78%) / 5 (22%)
BMI (kg/m^2)	27.70 (34.35-25.70)
Medical history	
Hypertension	30%
Diabetes mellitus	13%
Hypercholesterolemia	9%
Myocardial infarction	4%
Obesity	4%
Depression	22%
Asthma	13%
Sleep apnoea	4%
Thyroid lump	4%
Adrenal mass	4%
Factor XI haemophilia	4%
Gastroesophageal reflux disease	4%
Procedure	
Arthroscopic subacromial decompression	26%
Arthroscopic cuff repair	22%
Shoulder replacement	17%
Arthroscopic acromioclavicular joint	17%
Shoulder stabilization	13%
Arthroscopic shoulder capsular release	4%

BMI, body-mass index.

Table 6.6. Physiological and cerebral haemodynamics parameters assessed on phases A and B. Significant differences occurred in DCM (mean decrease of 6.43 mmHg (-34%) (p=0.009)) and PI (mean increase of 0.11 (+11%) (p=0.05)).

	A	B	p-value
ABP_{FINGER}	61.71 (69.30-52.41)	48.53 (66.35-37.64)	0.21
$ABP_{s\ FINGER}$	83.52 (95.40-67.72)	76.22 (90.71-58.29)	0.39
$ABP_{d\ FINGER}$	48.83 (56.38-41.67)	34.58 (55.47-25.34)	0.17
FV	40.86 (50.77-33.72)	43.01 (51.66-32.06)	0.27
nICP	4.52 (9.57-2.07)	2.14 (9.14-(-0.18))	0.66
nCPP	57.66 (63.92-49.54)	43.79 (57.66-37.46)	0.14
ARI	1.53 (2.59-0.68)	1.41 (2.21-0.91)	0.96
PI	1.00 (0.85-1.14)	1.03 (0.90-1.34)	0.048
CrCP	31.65 (37.94-22.18)	25.33 (41.95-13.15)	0.60
DCM	18.08 (23.88-11.23)	10.44 (15.71-7.78)	0.01
$ETCO_2$	5.30 (5.40-4.90)	5.20 (5.35-4.80)	0.17

ABP_{FINGER} (mmHg) (s, systolic; d, diastolic), arterial blood pressure monitored at the auditory meatus level; FV (cm/s), cerebral blood flow velocity; nICP (mmHg), non-invasive intracranial pressure; nCPP (mmHg), non-invasive cerebral perfusion pressure; ARI, cerebral autoregulation index; PI, pulsatility index; CrCP (mmHg), critical closing pressure; DCM (mmHg), diastolic closing margin; $ETCO_2$ (kPa), end-tidal carbon dioxide concentration.

Table 6.7. Mean delta (magnitude) changes and correlation coefficients between FV and ABP.

	Δ (%)	R with ΔABP	p-value	R with ΔFV	p-value
ABP_{FINGER}	-14	-	-	0.48	0.02
$ABP_{s\ FINGER}$	-7.8	-	-	0.57	0.005
$ABP_{d\ FINGER}$	-18.4	-	-	0.46	0.03
FV	-6%	0.48	0.02	-	-
nICP	-29%	0.61	0.002	0.33	0.12
nCPP	-12%	0.95	0	0.42	0.05
ARI	+7%	-0.14	0.52	0.12	0.58
PI	+11%	-0.1	0.64	-0.23	0.29
CrCP	-9%	0.8	0	0.17	0.43
DCM	-34%	0.61	0.01	0.36	0.09
$ETCO_2$	-3%	0.04	0.84	-0.01	0.95

ABP_{FINGER} (mmHg) (s, systolic; d, diastolic), arterial blood pressure monitored at the auditory meatus level; FV (cm/s), cerebral blood flow velocity; nICP (mmHg), non-invasive intracranial pressure; nCPP (mmHg), non-invasive cerebral perfusion pressure; ARI, cerebral autoregulation index; PI, pulsatility index; CrCP (mmHg), critical closing pressure; DCM (mmHg), diastolic closing margin; $ETCO_2$ (kPa), end-tidal carbon dioxide concentration; Δ (delta), variation between phases A and B in percentage; R, Spearman correlation coefficient.

There was a significant difference between preoperative and operative ABP_{ARM} (86.67 (80.83-95.67) and 76.00 (69.83-80.83), respectively; mean decrease of 9.68 mmHg (-12%) ($p<0.001$)). Between supine and BCP (Table 6.6), significant differences occurred in DCM (mean decrease of 6.43 mmHg (-34%) ($p=0.009$)) and PI (mean increase of 0.11 (+11%) ($p=0.05$)). Mean ABP_{FINGER} exhibited a decreasing trend from phase A to B, as well as nICP, nCPP and CrCP. $ETCO_2$ did not change significantly between the two phases.

When compared to TCD parameters in a healthy population [55], patients in this study had low FV (<60 cm/s). PI values also deviated from normal ranges in both measurement points (PI >0.8 [55]). nCPP values were lower than previously reported in healthy volunteers (<60 mmHg [180]) and decreased further from supine to BCP. nICP presented a decreasing trend between phases; however, the observed changes in nCPP were better correlated with changes in ABP_{FINGER} than nICP (Table 2, $\Delta R=0.95$ ($p<0.001$) and $\Delta R=0.44$ ($p=0.04$), respectively).

ARI showed lower levels indicating impaired cerebral autoregulation (ARI <3 [107,109,110]) in phases A and B. CrCP did not approach diastolic ABP_{FINGER} from phase A to B. Consequently, DCM did not reach critical values (≤0 mmHg), remaining above a mean of 12 mmHg during BCP. Changes in CrCP were strongly correlated with changes in estimated diastolic ABP ($\Delta R=0.82$, $p<0.001$). Nevertheless, considering individual cases, two patients during phase B (one with a history of arterial hypertension) and one patient during phase A presented alarming values for DCM below 5 mmHg. Changes in DCM and diastolic FV were correlated ($\Delta R=0.40$ ($p=0.05$)).

No patient presented any symptoms or signs suggestive of neurological damage after shoulder surgery in our cohort. Individual and mean changes across phases from supine (A) to beach chair position (B) are shown in Figure 6.13 for ABP_{FINGER}, FV, nICP and nCPP; Figure 6.14 for autoregulation index; and Figure 6.15 for CrCP and DCM.

Figure 6.13. Longitudinal plots showing changes between supine (phase A) and beach chair position (phase B) for (A) ABP_{FINGER}, (B) FV, (C) nICP and (D) nCPP. Mean ABP exhibited a decreasing trend, which was reflected in the other parameters.

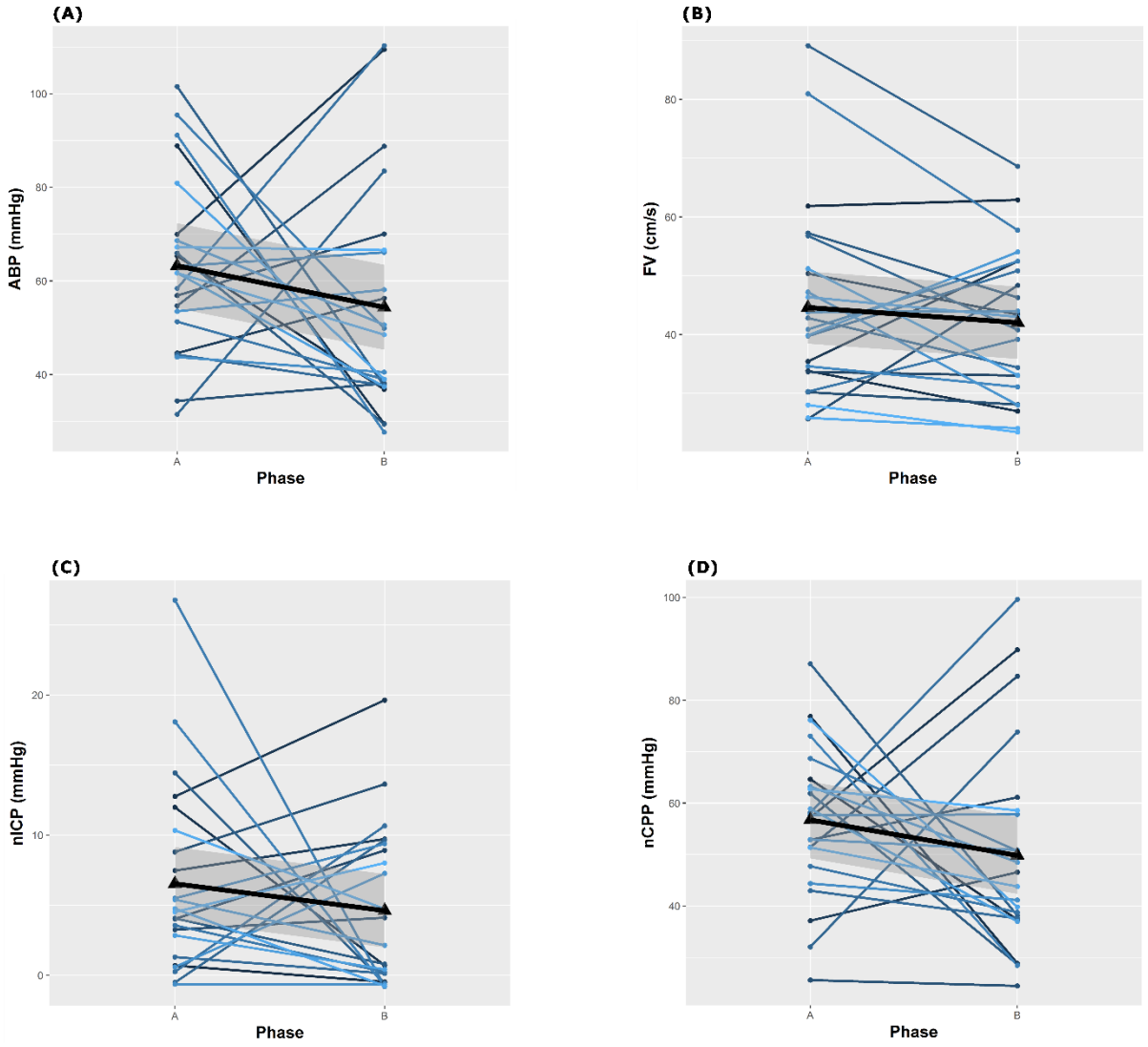

Triangles on the plots represent the mean values for each variable at a specific surgery phase. Thick black lines represent the linear fit of the data; grey shadowed areas represent the 95% confidence interval of the linear model representative of the data.

ABP (mmHg), non-invasive arterial blood pressure calibrated at the auditory meatus; FV (cm/s), cerebral blood flow velocity; nICP (mmHg), non-invasive intracranial pressure; nCPP (mmHg), non-invasive cerebral perfusion pressure.

Figure 6.14. Longitudinal plot showing changes between supine (phase A) and beach chair position (phase B) for cerebral autoregulation index (ARI). Mean ARI showed lower levels indicating impaired cerebral autoregulation (ARI <3).

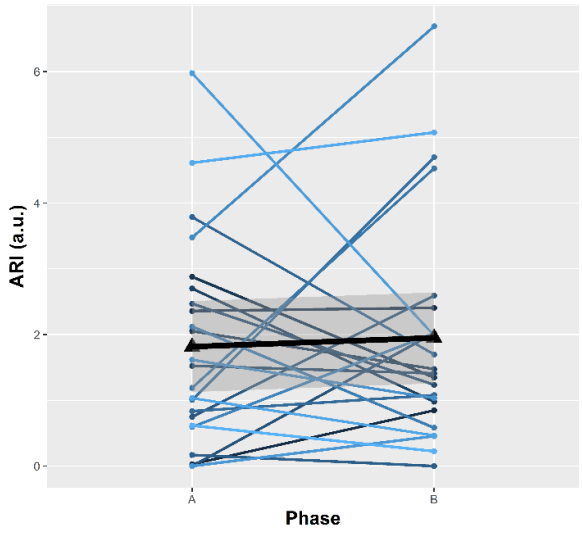

Triangles on the plots represent the mean values for each variable at a specific surgery phase. The thick black line represents the linear fit of the data; grey shadowed areas represent the 95% confidence interval of the linear model representative of the data.

ARI (a.u.), autoregulation index.

Figure 6.15. Longitudinal plots showing changes between supine (phase A) and beach chair position (phase B) for critical closing pressure (A) and diastolic closing margin (B). CrCP did not approach diastolic ABP. Consequently, DCM did not reach critical values (≤0 mmHg).

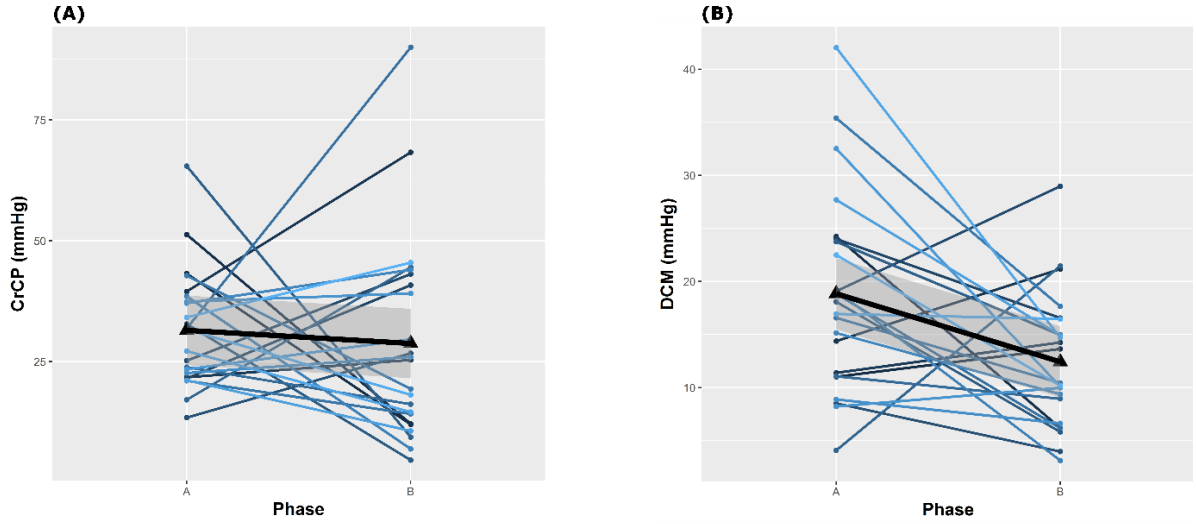

Triangles on the plots represent the mean values for each variable at a specific surgery phase. The thick black lines represent the linear fit of the data; grey shadowed areas represent the 95% confidence interval of the linear model representative of the data.

CrCP (mmHg), critical closing pressure; DCM (mmHg), diastolic closing margin.

Discussion

This study demonstrates that changing from the supine to beach chair position adversely affects cerebral haemodynamics with a significant decrease in DCM and increase in pulsatility index; and impairment in all cerebral haemodynamics parameters. Overall, all patients studied had impaired cerebral autoregulation in both positions.

In previous studies reporting catastrophic perioperative central nervous system infarction associated with shoulder surgery in the sitting position, the patients did not present any risk factors for perioperative stroke [195]. Despite its low incidence, intraoperative stroke associated with shoulder surgery remains a significant problem. Shoulder surgery in the beach chair position presents a unique risk for intraoperative stroke among orthopaedic procedures, which can be attributed to postural hypotension as well as head and neck manipulation leading to cerebral hypoperfusion. Another key factor that may compromise CBF is mechanical obstruction due to embolic events, such as atherosclerotic plaques, thromboemboli (platelet aggregation), air, or fat [195]. Nevertheless, the contribution of thromboembolic mechanisms for neurologic events during shoulder surgery remains unclear. For instance, in Pohl and Cullen's report [195], out of 4 cases presenting complications, one was diagnosed with a left hemisphere watershed stroke.

A pattern of cerebral hypoperfusion observed in the study can be represented by the low cerebral blood flow velocity pattern, and it may be explained by the absence of optimal cerebral autoregulation (Figure 6.14). Moreover, estimated cerebral perfusion pressure below 60 mmHg in both phases may indicate that patients were on the verge of the lower limit of autoregulation, pointing out that FV decreases passively with CPP [105]. Pulsatility index, as a parameter describing changes in TCD waveform resulting from changes in CPP, deviated from normal range under these conditions. However, PI did not show high values as indicated in previous studies assessing cerebral haemodynamics in patients with traumatic brain injury, for instance (PI>2) [52].

Cerebral autoregulation has been reported as diminished in patients undergoing shoulder surgery in the beach chair position previously. A study from Laflam et al. [203], applying near-infrared spectroscopy (NIRS) for autoregulation assessment using COx (a correlation index between ABP and regional cerebral oxygen saturation ($rSCO_2$)), indicated that these patients were more likely to have impaired autoregulation and lower $rSCO_2$ in comparison to patients

undergoing surgery in the lateral decubitus position. Although other authors have applied TCD as a tool for cerebral haemodynamics assessment during BCP [203], this is the first study reporting the impairment of TCD-based cerebral autoregulation in this surgery setting.

The cerebral autoregulation was impaired in both positions. Considering that the patients studied did not present any previous indications of neurological impairment, disturbed autoregulation during supine position could be attributed to the effects of anaesthetic agents on cerebral circulation. Propofol has been reported to preserve autoregulation either at high or low doses in healthy individuals [204]. However, high doses of this drug have been shown to impair autoregulation in TBI patients [205]. Sevoflurane in standard doses has not been reported to alter global CBF and autoregulation [206,207]; however, alterations on regional CBF have been reported with inhalational anaesthetic agents [208]. Although the anaesthetic agents used in the study have not been reported to alter cerebral autoregulation, an early hypotensive effect and decrease in systemic vascular resistance [209] after administration of propofol could have been the cause for the disturbed autoregulation during the supine phase, as monitoring was performed immediately after anaesthesia induction. An example of how ABP and CBF velocity generally behaved in both surgery phases is depicted in Figure 6.16.

Figure 6.16. Example demonstrating the behaviour of ABP and FV during phases A (supine position) and B (beach chair position). Changes in ABP with correspondent changes in FV indicate disturbed cerebral autoregulation.

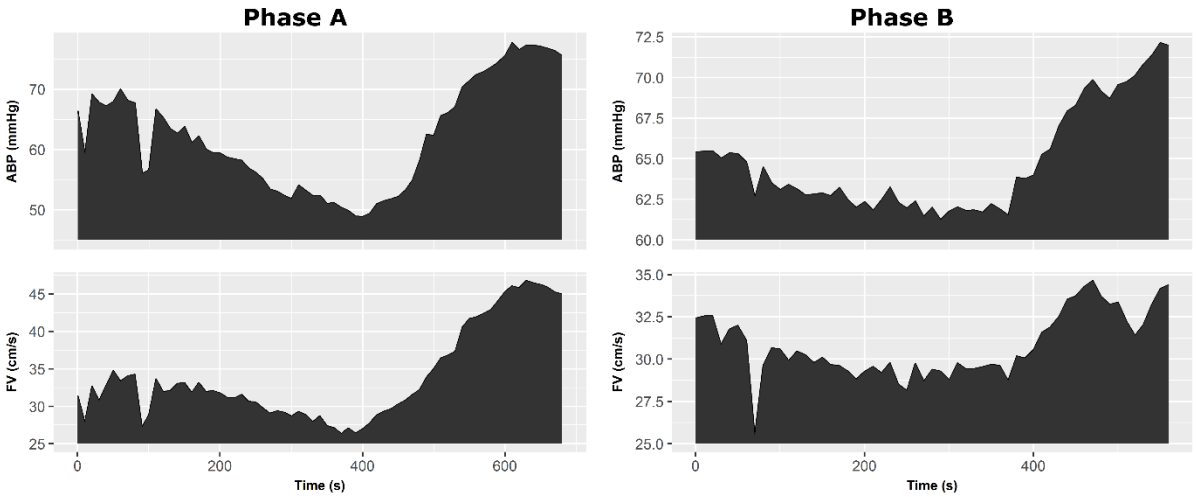

ABP (mmHg), non-invasive arterial blood pressure calibrated at the auditory meatus; FV (cm/s), cerebral blood flow velocity.

The changes in estimated cerebral perfusion pressure were strongly correlated with changes in ABP monitored at the auditory meatus level (Table 6.7, $\Delta R = 0.82$ ($p<0.001$)). It is believed that the gravitational effects of BCP contribute to the observed arterial hypotension and consequent CPP decrease, as in anaesthetised patients an altered baroreflex compromises haemodynamic control in the sitting position [210]. Arterial hypotension is commonly reported in procedures performed in this surgery setting, which has been reported to produce ABP decreases of 20% in an extensive study including 5177 patients undergoing neurosurgery and orthopaedic surgeries. 50% of these patients experienced a severe hypotension defined as an ABP decrease ≥40% relative to preoperative values [211]. In another study including 4169 shoulder surgery procedures, 47% of patients presented hypotension defined as an ABP <66 mmHg or a decrease >30% from pre-anaesthesia values. 37% of these patients experienced severe hypotension [198]. Other studies from McCulloch et al. [201], Hanouz et al. [202] and Buget et al. [212] also reported decreases in ABP after supine to BCP positioning.

Although the decrease in ABP_{FINGER} reached an average of 14% (also observed for ABP_{ARM} – 12% decrease), besides cerebral hypoperfusion, the changes from supine to BCP were also reflected in DCM (Table 6.7, Δ of -34%, delta correlation with ABP, $R=0.8$ ($p<0.001$)).

Cases with DCM ≤0 mmHg could not be identified in the cohort, although DCM decreased significantly between phases (Figure 6.10). Nevertheless, in 3 isolated cases, DCM approached alarming values (~5 mmHg), which could have been the ideal scenario for fluid and vasopressor administration to increase ABP towards safe levels concerning cerebral perfusion. In addition, overall changes in DCM and diastolic FV were correlated, indicating a decrease in FV during diastole and consequent increase in pressure passivity to cerebral circulation [100].

For instance, in a study of Hanouz et al. [202], the authors reported that beach chair position induced ABP decrease requiring vasopressors and fluid challenge in 44 patients (83% of the study's cohort). In this study, the authors only relied on ABP decrease of 20% from pre-induction values to guide the vasopressors intervention, only considering mean FV for the assessment of cerebral haemodynamics.

Given these findings, continuous multiparameter TCD monitoring could provide a more comprehensive interpretation of the haemodynamic changes and guide individualised management of ABP and cerebral haemodynamics in the BCP operative setting. A special scenario would be combining ABP and multiparameter TCD monitoring for cases at imminent risk of cerebrovascular derangements such as patients with idiopathic intracranial

hypertension, hydrocephalus, diabetes, arterial hypertension and patients with a history of stroke. In these cases, special attention should be given to managing ABP within normal ranges with vasopressors or fluids before and throughout beach chair position to maintain an adequate cerebral perfusion pressure.

Limitations

This study has several potential limitations. First, simultaneous measurements of baseline FV and ABP were not monitored before anaesthesia induction. It was hypothesized that supine position after induction should be the baseline phase, as the effects of anaesthesia on cerebral haemodynamics should be considered. Moreover, due to surgical configurations, an extended monitoring of the parameters throughout surgery could not be performed. However, according to Hanouz et al. [202], significant changes in cerebral haemodynamics occurred only from baseline (after anaesthesia induction in supine position) to BCP. Because of technical reasons, FV was assessed only ipsilateral to the side of surgery, therefore not accounting for differences in flow that may exist between left and right MCAs. ABP_{ARM} and ABP_{FINGER} could not be compared effectively in any stages of the experimental protocol since simultaneous recordings of these parameters were technically unfeasible.

7 RESULTS & DISCUSSIONS III: ASSESSMENT OF nCPP USING A SPECTRAL VOLUME ACCOUNTING METHOD

Introduction

Cerebral perfusion pressure is one of the primary modalities in neurocritical care [7]. It is defined as the difference between arterial blood pressure and intracranial pressure. CPP is interpreted as the main force maintaining CBF. Its accuracy in direct monitoring depends on the precision of two independent pressure transducers for each ABP and ICP.

ABP is usually measured with an external transducer, with input blood pressure transmitted via an indwelling arterial catheter. It is typically zeroed at the heart level, but for neurocritical care patients requiring monitoring of CPP, it should be zeroed at the level of the auditory meatus and re-zeroed following every change of body position. As most patients receiving neurocritical care are managed with head elevation (to ease brain venous return), zeroing the ABP transducer at the heart level may produce overestimation of CPP from 10 to 20 mmHg [213]. Since blood flows vertically from the heart, with head elevation, there is a reduction in ABP directly related to the water column between heart and brain (generally 1 mmHg for each 1.35 cm) [214].

Furthermore, contemporary ICP microtransducers are zeroed against atmospheric pressure only once during implantation. Their drift over time (usually not above 1 mmHg per day [215]) may accumulate over long monitoring period (usually 2-3 weeks), adding significant additional errors in CPP monitoring.

Therefore, direct invasive monitoring of mean CPP is more complex than it appears. As described Chapter 3, Section 3.3.2, various studies have been conducted to measure CPP non-invasively (nCPP) based on TCD monitoring of blood flow profiles in the MCA [71,73,76,78,216]. The relative accuracy of such estimation was reported to vary from 12-20 mmHg [71,73,76,78,216]. However, due to inappropriate zeroing of pressure transducers, these assessments could be inaccurate since direct CPP is uncertain.

In this study, a new TCD-based method for nCPP estimation (spectral nCPP or $nCPP_s$) is proposed. This method is based on accounting for changes in pulsatile cerebral arterial blood

volume (C_aBV) applied to the analysis of a simplified hydrodynamic model of CBF and CSF dynamics [89,139,217]. This study aims to test the performance of this method by comparing changes in $nCPP_s$ versus changes in direct CPP. Since their absolute comparison is limited due to problems secondary to ABP zeroing, this assessment is focused on cases in which CPP is changing in the time domain: I) rise during vasopressor-induced augmentation of ABP, and II) decrease during spontaneous changes in ICP (plateau waves).

Material and methods

Spectral non-invasive cerebral perfusion pressure estimation method

A common approach to model the cerebral vasculature is to compartmentalise the different regions of the brain and mechanistically capture their interactions through a mathematical model. A model of CBF and CSF dynamics has been proposed previously by Ursino and Lodi [89,139], which captures the dynamics in the arterial, capillary, venous and CSF circulation. This model has been modified later by Czosnyka et al. [217], by incorporating realistic values for known components including cerebrovascular resistance, intracranial and arterial compliance, and CSF outflow resistance. The electrical equivalence of this model is presented in Figure 7.1.

The input circuit of the model may be presented in a simplified way as a resistance-conductance circuit. A parallel switch of ohmic resistance (CVR) and conductive resistance ($1/j\omega \cdot C_a$) adds to a total impedance:

Equation 7.1

$$Z(j\omega) = \frac{\frac{CVR}{j\omega \cdot C_a}}{CVR + \frac{1}{j\omega \cdot C_a}} = \frac{CVR}{j\omega \cdot CVR \cdot C_a + 1} \quad (7.1)$$

Where ω symbolizes circular frequency ($\omega = 2\pi \cdot frequency$); CVR represents cerebrovascular resistance; C_a, compliance of cerebral arteries and arterioles. Units are given in mmHg/(cm^3/s).

Figure 7.1. The electrical model of cerebral blood flow (CBF) and cerebrospinal fluid (CSF) dynamics, extracted from Czosnyka et al. [217].

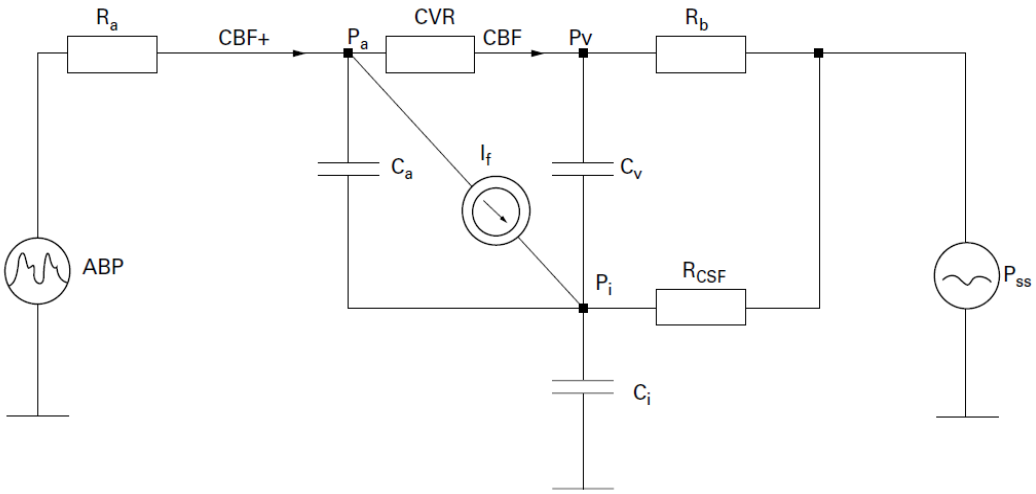

The CBF pathway starts with the arterial blood inflow to the brain through the resistance of large intracranial arteries (R_a), with arterial blood pressure (ABP) as the input pressure from the carotid and basilar arteries. From there, arterial blood passes at high pressure (P_a), through the small cerebral arteries. These vessels act as a storage system for pulsatile blood volume, which is modelled by the compliance C_a. Forward flow through the cerebrovascular resistance (CVR) vessels is modulated by the cerebral autoregulation. The capillary and venous blood flow and storage are lumped together and modelled by the compliance of C_v at pressure P_v. Finally, venous blood flows out through the bridging veins represented by the Starling resistor R_b to the sagittal sinus at pressure P_{ss}. The CSF pathway encompasses formation of CSF (with a rate of I_f), storage in the distensible fluid structures formed by the ventricles, basal cisterns and spinal sac (with compliance of C_i), and finally reabsorption through the arachnoid granulations to the sagittal sinus with the resistance to outflow being denoted as R_{CSF}. Both CBF and CSF pathways take place inside the rigid skull with an intracranial pressure being depicted here as P_i. The model was calibrated using realistic values for known components including cerebrovascular resistance, intracranial and arterial compliance, and CSF outflow resistance [217].

The modulus of impedance can be expressed as:

Equation 7.2

$$|Z(\omega)| = \frac{CVR}{\sqrt{CVR^2 \cdot C_a \cdot \omega^2 + 1}} \tag{7.2}$$

which depends on the frequency f of the flow ($\omega = 2\pi \cdot f$). Units are given in mmHg/(cm^3/s).

For a constant flow ($\omega=0$), the modulus of impedance becomes:

$$|\mathrm{Z}(0)| = CVR = \frac{CPP}{FV} \qquad (7.2a)$$

CPP denotes mean cerebral perfusion pressure; *FV*, mean blood flow velocity in the MCA.

Considering pulse waves (ω_{HR}=*heart rate* (HR)), the modulus equals the ratio *a1/f1:*

$$|\mathrm{Z}(\omega_{HR})| = \frac{a1}{f1} \qquad (7.2b)$$

Where *a1*, represents the pulse amplitude of the first harmonic of the ABP waveform; *f1*, the pulse amplitude of the first harmonic of the FV waveform. The pulse amplitude of first harmonics is determined with FFT.

Considering Equation 7.2 for heart rate ($\omega= 2\pi \cdot HR$), and substituting CVR and $\mathrm{Z}(\omega_{HR})$ by Equation 7.2a and Equation 7.2b, it results in:

Equation 7.3

$$CPP = \frac{a1}{sPI} \times \sqrt{(CVR \cdot C_a)^2 \cdot HR^2 \cdot (2\pi)^2 + 1} \ \ (mmHg) \qquad (7.3)$$

Where:

$$sPI = \frac{f1}{FV}$$

sPI denotes the spectral pulsatility index. *HR* is expressed in Hz.

Equation 7.3 presents the non-invasive estimator of CPP that can be evaluated on the heart beat-by-beat basis. *CVR* and C_a used in Equation 7.3 can be estimated using mathematical transformations of TCD and ABP pulse waveforms measurements based on a model of cerebral arterial blood volume changes presented below.

The amount of arterial blood supplied to the cerebral space by the vascular system during a cardiac cycle is partially compensated by the simultaneous outflow of blood through the venous system. Both the arterial inflow (CBF_a) and venous outflow (CBF_v) of cerebral blood have a pulsatile character, but their pulse waveform shapes are phase-shifted resulting in detectable cerebral blood volume *(CBV)* changes during a heartbeat. The interaction between pulsatile changes in CBF_a and CBF_v determines the transient, time dependent change in cerebral blood volume (ΔCBV) and can be described by the following equation [218]:

Equation 7.4

$$\Delta CBV(t) = \int_{t_0}^{t} \left(CBF_a(s) - CBF_v(s)\right) ds \tag{7.4}$$

where t_0 is the beginning of a single cardiac cycle and s is the variable of integration.

With TCD, venous outflow cannot be monitored continuously (contrary to phase-coded MRI [219], for instance), thus two models of approximation of ΔCBV are worth consideration:

1. **Continuous flow forward model (CFF):** it is presumed that venous outflow, being far less pulsatile [220] may be substituted by the mean value of arterial CBF. This leads to the formula:

Equation 7.5

$$\Delta C_a BV_{CFF}(t) = \int_{t_0}^{t} (CBF_a(s) - mean\ CBF_a)\, ds \tag{7.5}$$

where C_aBV represents cerebral arterial blood volume. Units are given in cm^3.

2. **Pulsatile flow forward model (PFF):** in this approach, the pulsatile arterial blood inflow inflating and deflating cerebral arteries during each heart cycle is modelled as the difference between *CBF(t)* and cerebral blood flow forward from large arteries to small resistive arterioles:

Equation 7.6

$$\Delta C_a BV_{PFF}(t) = \int_{t_0}^{t} \left(CBF_a(s) - \frac{ABP(s)}{CVR} \right) ds \tag{7.6}$$

Where CVR is defined as the ratio between mean ABP and FV (Equation 4.3). Units are given in cm^3.

Equation 7.5 and Equation 7.6 will yield values of CBV per unit of cross-sectional area of the insonated vessel. Assuming that the cross-sectional area remains constant, *FV* can substitute CBF_a in Equation 7.5 and Equation 7.6.

Obtained from the presented calculations, both virtual signals C_aBV_{CFF} and C_aBV_{PFF} have a pulsatile component. However, the shape of the C_aBV_{PFF} waveform is different, and its amplitude is lower than C_aBV_{CFF} (amplitudes of first harmonic of C_aBV_{CFF} and C_aBV_{PFF} for the heart frequency are denoted further as $C1_{CFF}$ and $C1_{PFF}$) – see Figure 7.2.

Then arterial compliances are defined, accordingly:

Equation 7.7

$$C_{aCFF} = {C1_{CFF}}/{a1} \tag{7.7}$$

Equation 7.8

$$C_{aPFF} = {C1_{PFF}}/{a1} \tag{7.8}$$

Both compliances have units (cm/mmHg), expressed as a value of arterial compliance per unit of cross sectional area of the insonated vessel.

CVR can be estimated in two ways:

Equation 7.9

$$CVR_1 = \frac{ABP}{FV} \tag{7.9}$$

Equation 7.10

$$CVR_2 = a1/f1 \tag{7.10}$$

CVR_2 is an equivalent of the so-called 'resistance area product' [221] and is usually lower than CVR_1, but its advantage is the immunity to inaccuracies related to not zeroing the blood pressure transducer for cerebral arterial circulation since it does not rely on mean values for ABP and FV.

Any combination of $CVR \cdot C_a$ (four combinations altogether): $CVR_1 \cdot C_{aPFF}$, $CVR_2 \cdot C_{aPFF}$, $CVR_1 \cdot C_{aCFF}$, $CVR_2 \cdot C_{aCFF}$ may result in four nCPP estimators. The average of these four estimators was called spectral nCPP ($nCPP_s$).

While estimators using CFF are not affected by time delays between any signals, estimators using PFF are: ABP is usually measured from the radial artery distant from the brain, and therefore is delayed in comparison to MCA flow velocity signal (Figure 7.2). The delay may range from a median ± interquartile range (IQR) of 10 ± 15 ms, according to unpublished material analysing 53 healthy volunteers. It may be different between individuals and may vary in time. To compensate for this delay, estimators of *C1* can be calculated in the spectral domain. This considers that the Fourier transform of the integral of the time function *f(t)* is equal to its Fourier transform divided by $j\omega$. For the frequency of heart rate, this will be $j\omega_{HR}$. Under the assumption that the phase shift between the first harmonic of *ABP(t)* and *FV(t)* signals is small (median ± IQR: 13.12 ± 3.59 degrees after adjustment for time delays resulting from the distance between the site of ABP measurement and the MCA – unpublished material analysing 53 healthy volunteers), the frequency domain estimators of *C1* can be expressed as:

Equation 7.11

$$C1_{CFF} = \frac{f1}{\omega_{HR}} \tag{7.11}$$

Equation 7.12

$$C1_{PFF} = \frac{(f1 - a1/CVR)}{\omega_{HR}} \tag{7.12}$$

Figure 7.2. Example of signals of ABP, ICP, FV and estimators of pulsatile arterial blood volume calculated using constant flow forward (C_aBV_{CFF}) and pulsatile flow forward (C_aBV_{PFF}) methods.

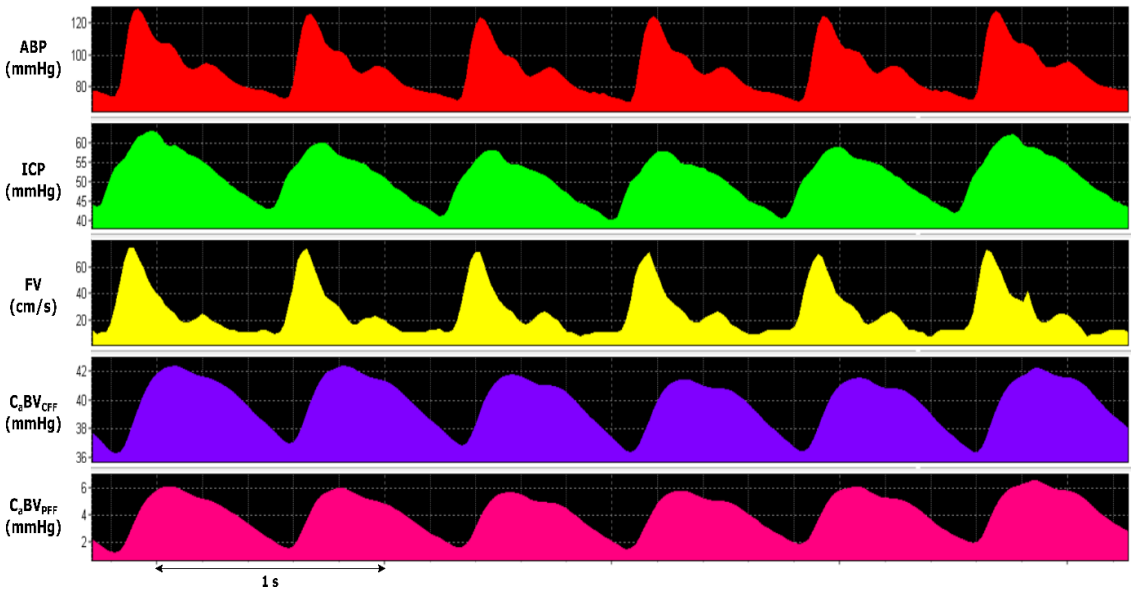

The time delay between the FV and ABP signals is estimated as a median ± IQR of 10 ± 15 ms (derived from the distance between the site of ABP measurement and MCA). The pulse amplitude of C_aBV_{CFF} is greater than C_aBV_{PFF}.

ABP (mmHg), arterial blood pressure; ICP (mmHg), intracranial pressure; FV (cm/s), cerebral blood flow velocity; C_aBV_{CFF} (mmHg), estimator of pulsatile arterial blood volume calculated using constant flow forward; C_aBV_{PFF} (mmHg), estimator of pulsatile arterial blood volume calculated using pulsatile flow forward.

Patient population

Two cohorts of patients from the previously described database of 446 adult TBI patients (Section 4.1.2) (median age of patients: 30 years (IQR: 18–78), with 75% being male) were analysed in this study.

The first cohort consisted of patients undergoing an induced rise in ABP producing rises in CPP levels (N=16). The second cohort consisted of patients in whom ICP plateau waves were identified as sudden and spontaneous increases in ICP (and pulse amplitude of ICP), during which CPP and FV dropped with a relatively stable ABP (N=14, in a total of 21 plateau waves identified).

Clinical monitoring and data collection

The implemented clinical monitoring included ABP, ICP and FV as described in Section 4.2.1. CPP and derived physiological parameters were calculated as described in Section 4.2.3. $nCPP_s$ was calculated as described above.

For the patients undergoing induced rises in ABP, one hour of baseline modalities were recorded (baseline phase), then CPP was controlled with an infusion of norepinephrine adjusted to reach and maintain the desired CPP constant during the recording (plateau phase). Mean CPP at baseline and plateau phases were 69±6 mmHg and 92±4 mmHg, respectively. This patient cohort has been previously studied by Steiner et al. [222] assessing cerebral autoregulation with PET (positron-emission tomography) at different CPP levels.

For patients presenting ICP plateau waves, the recordings were also divided into baseline (before the onset of plateau waves) and plateau (during plateau of plateau waves) phases.

All parameters were calculated and averaged for both baseline and plateau phases.

Statistical analysis

The data were tested for normal distribution using the Shapiro-Wilk test and are presented as median (IQR). Data distributions were non-parametric. All plateau waves identified were treated as independent events. To assess the performance of the proposed method, the

correlation coefficient in the time domain (R) was calculated between direct CPP and $nCPP_s$ for both induced rises in ABP and plateau waves cohorts. R values in the time domain were obtained for individual patients and then averaged within each cohort. The Spearman correlation coefficient was calculated for mean values between CPP and $nCPP_s$ considering the difference (delta (Δ - the magnitude of changes)) between the baseline and plateau phases for both patient cohorts. The Fisher z-transformation was used to test whether ΔR values between CPP and $nCPP_s$ were significantly different in the two populations analysed.

To assess the prediction ability of the model, the area under the of a receiver operating characteristic analysis was calculated. To integrate this assessment for both patient cohorts, the prediction threshold chosen was determined as the median value of the absolute difference (absolute Δ) between the plateau and baseline phases for the two cohorts together to provide a consistent statistical assessment. The threshold obtained was ΔCPP ≥23.2 mm Hg. This test permits, independently of the direction of changes in CPP, to assess whether $nCPP_s$ can predict the magnitude of these changes reliably.

Results

Table 7.1 presents values of the physiological variables and $nCPP_s$ estimator assessed. Figure 7.3 and Figure 7.4 demonstrate examples of changes in ABP, ICP, CPP and $nCPP_s$ in the patient cohorts undergoing induced ABP increase and ICP plateau waves, respectively.

The averaged correlation (mean ± SD) in the time domain between CPP and $nCPP_s$ for patients undergoing induced rises in ABP was 0.95±0.07, and 0.86±0.14 during ICP plateau waves. Δ correlations between mean values of CPP and $nCPP_s$ were 0.73 ($p=0.002$) and 0.78 ($p<0.001$), respectively for induced rises in ABP and ICP plateau waves cohorts (Figure 7.5). The Fisher z-transformation did not indicate statistically significant difference between these two Δ correlation coefficients ($z=-0.32$ ($p=0.75$)).

The four estimators forming $nCPP_s$ differed in their correlations in the time domain with direct CPP during plateau waves. The estimators using CVR_2 correlated better with CPP than

estimators using CVR_1: R=0.49 and R=-0.16, for estimators using CVR_1 & C_{aCFF} and CVR_1 & C_{aPFF}, respectively.

Table 7.1. Values of the physiological variables and $nCPP_s$ estimator assessed for measurements at baseline and plateau phases.

	Induced rise in ABP (N=16 patients)		**Plateau waves (N=21 waves)**	
	Baseline	**Plateau**	**Baseline**	**Plateau**
ABP	86.92 (91.19-81.08)	110.9 (114.4-107.1)	91.21 (97.97-83.00)	90.77 (94.05-78.00)
FV	59.03 (69.51-49.23)	72.56 (81.84-53.40)	47.51 (64.92-42.84)	35.87 (60.46-30.70)
ICP	13.93 (19.00-11.53)	15.19 (20.60-12.70)	25.08 (28.76-16.81)	48.26 (53.86-38.07)
CPP	73.19 (76.68-68.80)	93.25 (96.93-92.17)	66.35 (74.04-58.24)	41.74 (47.91-35.29)
$nCPP_s$	82.73 (85.41-78.53)	109.85 (113.15-103.04)	72.82 (83.27-64.40)	61.97 (69.01-54.04)

ABP (mmHg), arterial blood pressure; FV (cm/s), cerebral blood flow velocity; ICP (mmHg), intracranial pressure; CPP (mmHg), cerebral perfusion pressure; $nCPP_s$ (mmHg), non-invasive cerebral perfusion pressure according to the spectral method.

In contrast, estimators using CVR_2 & C_{aCFF} and CVR_2 & C_{aPFF} presented R=0.79 and R=0.82, respectively. Such differences were not observed in the cohort undergoing induced ABP rises ($R \geq 0.80$ for all estimators).

Being the average of the four possible estimators using the proposed model, $nCPP_s$ presented better correlation in the time domain with CPP in comparison to single estimators in all cases but for the estimator using CVR_1 & C_{aCFF} in patients undergoing induced ABP rises (R=0.95 and R=0.96, respectively for $nCPP_s$ and estimator using CVR_1 & C_{aCFF}). The same findings were observed considering Δ correlations (R=0.73 (p=0.002) and R=0.81 (p=0.0002), respectively for $nCPP_s$ and estimator using CVR_1 & C_{aCFF}).

ROC analysis of the combined threshold for CPP prediction ($\Delta CPP \geq 23.2$) in both patient cohorts revealed that $nCPP_s$ had an AUC of 0.71 (95% confidence interval: 0.58-0.88) (Figure 7.6).

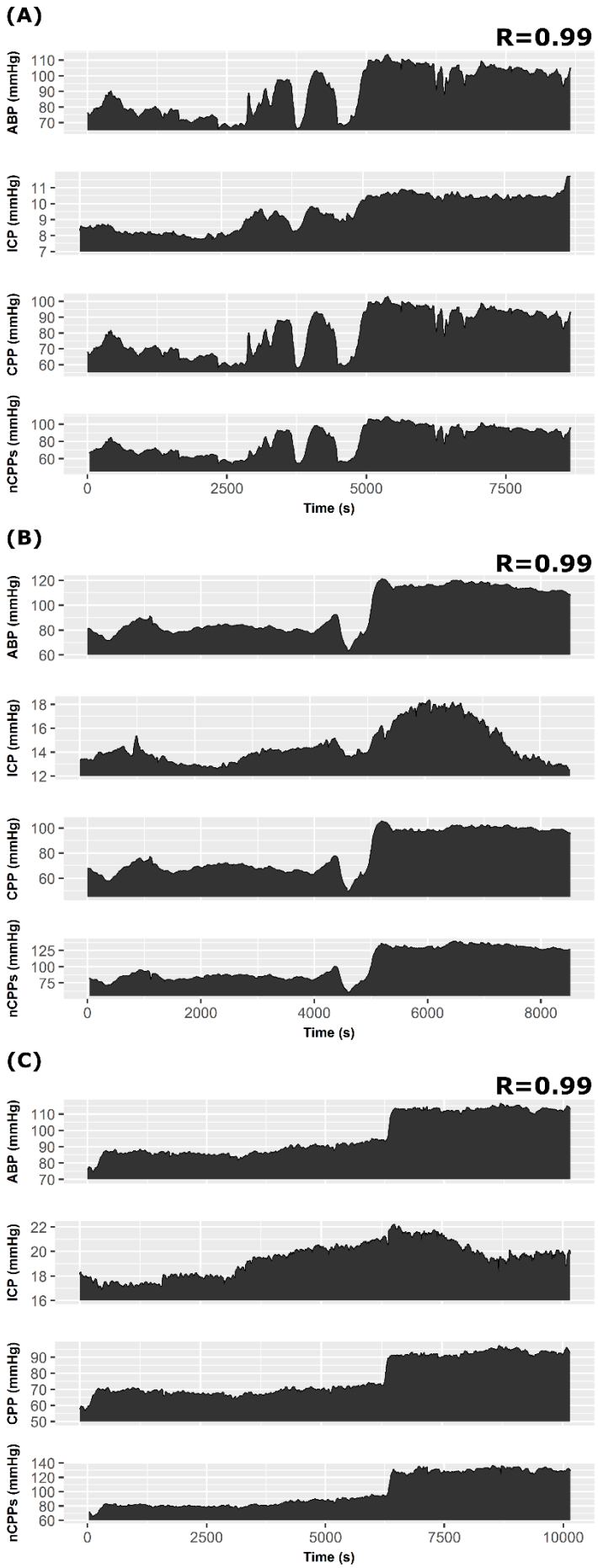

Figure 7.3. Example of individual cases (A, B, C) showing the correlation in the time domain between $nCPP_s$ and CPP (R) in patients with induced rises in ABP. Baseline and rise in ABP phases are distinguishable in the recordings. ABP (mmHg), arterial blood pressure; ICP (mmHg), intracranial pressure; CPP (mmHg), cerebral perfusion pressure; $nCPP_s$ (mmHg), non-invasive cerebral perfusion pressure according to the spectral method; R, correlation coefficient in the time domain.

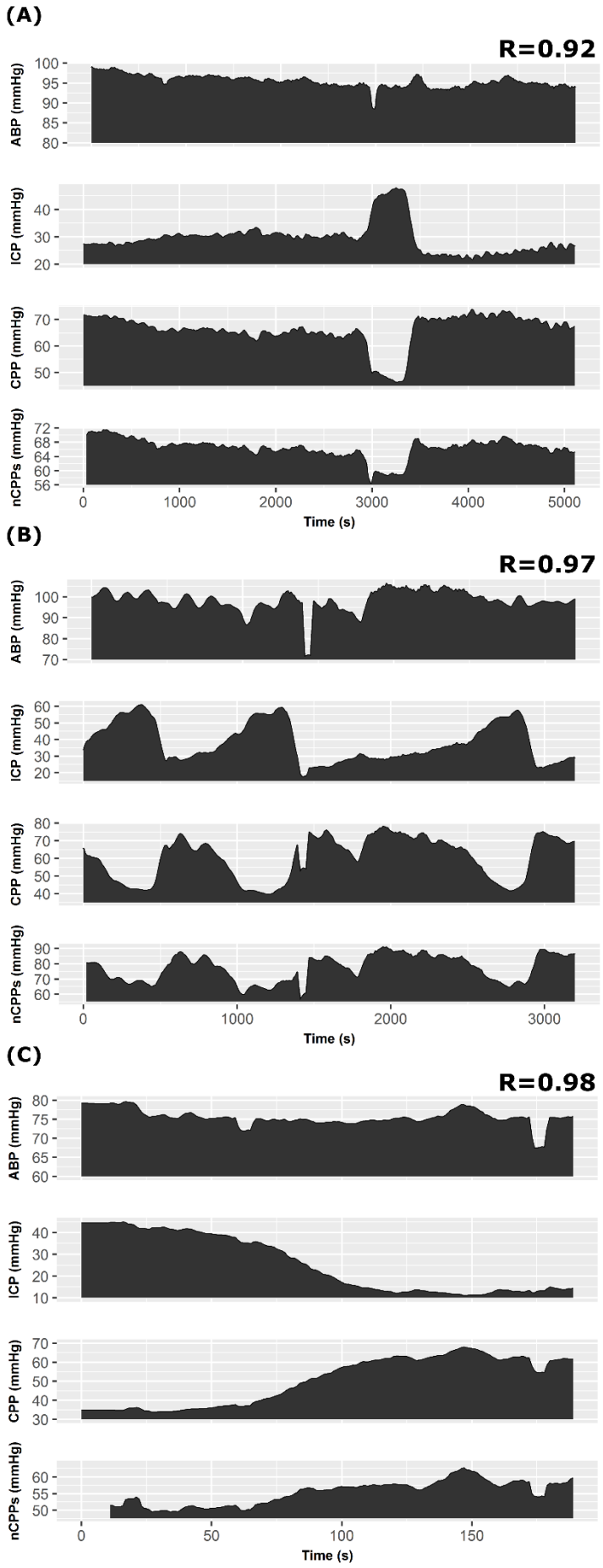

Figure 7.4. Example of individual cases (A, B, C) showing the correlation in the time domain between $nCPP_s$ and CPP (R) in patients presenting ICP plateau waves. Baseline and plateau phases for these rises in ICP (and consequent decrease in CPP) are demonstrated in the recordings. ABP (mmHg), arterial blood pressure; ICP (mmHg), intracranial pressure; CPP (mmHg), cerebral perfusion pressure; $nCPP_s$ (mmHg), non-invasive cerebral perfusion pressure according to the spectral method; R, correlation coefficient in the time domain.

Figure 7.5. Correlation plots between the magnitude of changes (Δ) of both CPP and $nCPP_s$ in the induced rises in ABP (A) and plateau waves (B) cohorts. In both cases, $nCPP_s$ could detect the magnitude of changes in CPP reliably (R>0.70).

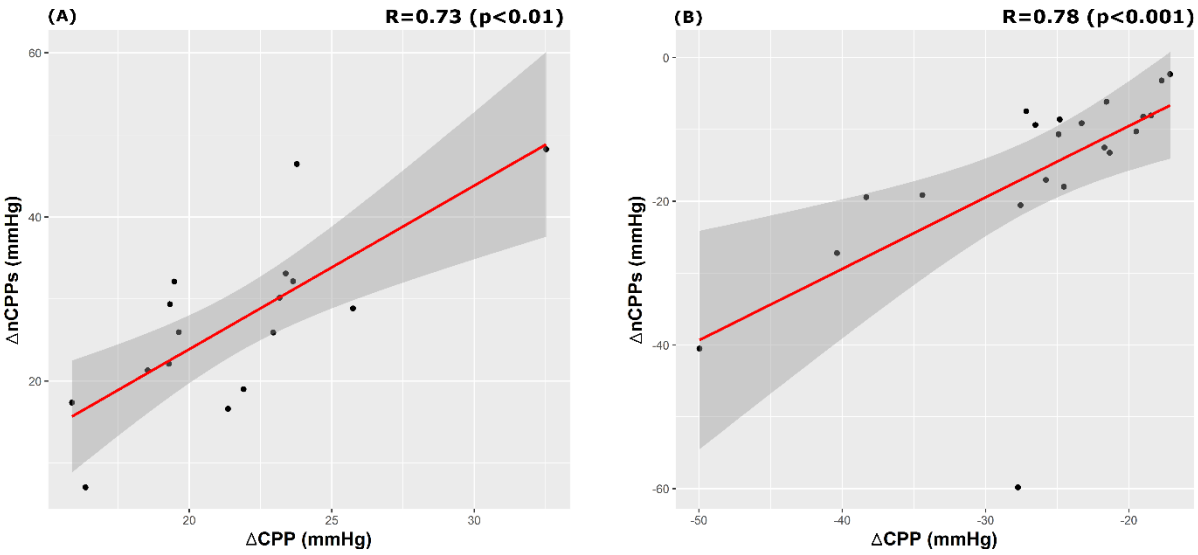

CPP (mmHg), cerebral perfusion pressure; $nCPP_s$ (mmHg), non-invasive cerebral perfusion pressure according to the spectral method; R, Spearman correlation coefficient; Δ, mean difference between plateau and baseline phases.

Figure 7.6. Receiver operating characteristic (ROC) curve for prediction of CPP changes using the combined threshold of 23.2 mmHg. AUC of 0.711 (95% CI: 0.543-0.878) demonstrates reasonable prediction ability for $nCPP_s$.

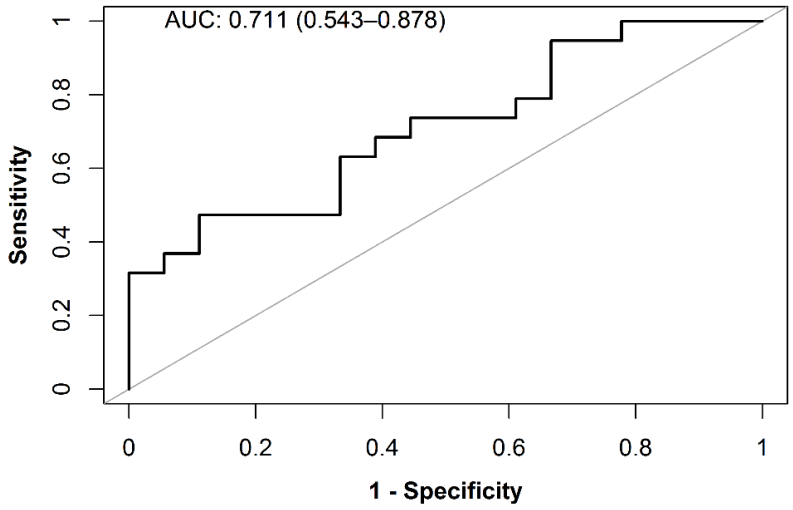

AUC, area under ROC curve; CPP, cerebral perfusion pressure; $nCPP_s$, non-invasive cerebral perfusion pressure according to the spectral method.

Discussion

The proposed spectral nCPP method estimates CPP by accounting for changes in pulsatile cerebral blood volume based on a simplified hydrodynamic model of CBF and CSF dynamics. The spectral feature of the method has some advantages: it creates partial independence from the inaccuracy associated with zeroing the ABP transducer at heart level and partially eliminates the issue of the time delay between peripheral ABP and FV in the MCA. The dynamical model of CSF and cerebral blood circulation proposed by Ursino and Lodi [89,139] has also been modified by other authors to incorporate changes in cerebral blood volume and adapted to nICP o nCPP estimations. $nICP_{Heldt}$ [36] described in Section 3.3.3 is one example. Similarly to this method, $nCPP_s$ produces patient-specific CPP estimates and does not require calibration datasets.

The $nCPP_s$ method was evaluated in two different conditions associated with changes in cerebral perfusion pressure: I) increases in CPP following a rise in ABP caused by the administration of vasopressor; II) spontaneous decrease in CPP caused by cerebral vasodilation during ICP plateau waves. In both conditions, $nCPP_s$ replicated changes of CPP in the time domain reliably (Figure 7.3 and Figure 7.4). However, the estimators forming $nCPP_s$ using CVR expressed as the ratio between ABP and FV presented weaker or even negative correlations with CPP during plateau waves; these were the ones using $CVR_1 \cdot C_{aCFF}$ and $CVR_1 \cdot C_{aPFF}$, with this remark especially denoted in the latter.

This could be related to the fact that in cases in which the source of changes in cerebrovascular resistance is ICP (like in plateau waves), the ratio between mean ABP and FV (CVR_1) cannot detect it effectively. Considering a relatively constant ABP and mainly a decrease in the diastolic component of FV during plateau waves [141], CVR_1 increases, whereas, in reality, cerebrovascular resistance decreases due to vasodilation. In contrast, estimators using CVR_2 (ratio between pulse amplitude of ABP and FV) performed better, since it can detect changes in FV amplitude caused by ICP increases. Therefore, cerebrovascular resistance decreases in this case, which is realistic.

The magnitude of changes observed in $nCPP_s$ also presented strong correlations with direct CPP considering both patient populations. This indicates that independently of its degree of accuracy, $nCPP_s$ was reliable to detect the magnitude of changes in CPP (Figure 7.5).

Moreover, $nCPP_s$ demonstrated reasonable AUC for prediction of CPP changes ≥23.2 in both patient cohorts analysed jointly (AUC = 0.71) (Figure 7.6).

In the $nCPP_s$ model, only CVR_2 provides complete independence from ABP transducer zeroing, and only the *CFF* model eliminates the issue of time delay. Consequently, both issues still appear in an averaged, partial way in $nCPP_s$.

The averaging approach applied to produce $nCPP_s$ has advantages and disadvantages. It is advantageous by approximating the different features of the estimators to yield a method that is versatile in several conditions associated with derangements in cerebral haemodynamics. This characteristic resulted in a better correlation in the time domain between $nCPP_s$ and single estimators in the plateau waves cohort. In contrast, in other circumstances, the averaging approach may suppress specific characteristics of an estimator. This can be observed in the cohort undergoing induced rises in ABP, in which the estimator using CVR_1 & C_{aCFF} presented a better correlation in comparison to $nCPP_s$.

Nevertheless, considering the two population cohorts together, in this assessment $nCPP_s$ generally performed better than single CPP estimators alone.

8 CONCLUSIONS

8.1 Accuracy of TCD-based nICP monitoring methods

This section provides general conclusions about the assessment of TCD-based nICP methods in a variety of clinical conditions with differing physiological mechanisms associated with ICP changes (Chapter 5).

Among the four methods compared, the black box model ($nICP_{BB}$) had the best performance to estimate ICP in a prospective cohort of TBI patients. However, to replicate changes in ICP in the time domain, the method based on pulsatility index ($nICP_{PI}$) had the best performance. A new method based on averaging the best estimators ($nICP_{BB}$ and methods based on diastolic FV and critical closing pressure ($nICP_{FVd}$ and $nICP_{CrCP}$) - $nICP_{Av}$), demonstrated better performance for ICP prediction. However, in other assessments, $nICP_{Av}$ was not considered since it did not show any noticeable improvement in comparison to single methods. The overall 95% confidence interval for ICP prediction presented by TCD-based nICP methods in this assessment was estimated around 10 mmHg.

During infusion tests, ICP changes were estimated with only moderate correlations by the nICP methods. $nICP_{PI}$ had the best performance for predicting changes in ΔICP during infusion test, followed by $nICP_{BB}$. Vasogenic components of ICP appeared to be easier to estimate with TCD-based nICP methods than the component related to increased CSF circulation.

In the assessment considering ICP plateau waves, the nICP methods were remarkably accurate to detect relative changes in ICP across time. Furthermore, they presented high performance to rule out intracranial hypertension and identify ICP changes related to plateau waves.

Among the four nICP methods evaluated, $nICP_{BB}$ has demonstrated the overall best performances. Table 5.8 summarises the measures of accuracy presented by all methods in different clinical conditions. However, the estimation of ICP absolute values is limited at the current state of development for all nICP methods. This inaccuracy is suggested to be associated with the matter of non-specific nICP calibrations.

In respect to ICP accuracy, it is known that even the standard invasive techniques might not comply with the specified limits for error [120,215,223], particularly using epidural and intraparenchymal microtransducers [215]. Thus, it is debatable whether these accuracy requirements are realistic for all sorts of ICP monitoring. In view of this, an important concept that should be stressed is ICP not solely "as a number", once dynamical features of this parameter, such as its waveform and relative changes in time, are fundamental for a proper assessment of the clinical state of the patient [165].

Therefore, despite the intrinsic limitations and inaccuracy to predict ICP mean absolute values, TCD-based nICP methods may have a potential clinical utility since this technique allows a non-invasive assessment of cerebral circulation dynamics as ICP changes in the time domain. These features also allow tracking nICP changes in real-time in a variety of clinical settings (emergency rooms, ambulatories, operating theatres). This is one of the advantages of transcranial Doppler ultrasonography and may become particularly useful as a primary assessment tool in centres where ICP monitoring is not routinely applied or unavailable. It may also suit patients in whom invasive ICP monitoring may not be clearly indicated (mild closed head injury, for example) or contraindicated (coagulopathy, for instance).

Given these conclusions, hypothesis I cannot be confirmed in all clinical conditions studied (like during CSF infusion tests). A finite error of 10 mmHg has been determined for TBI patients, in which vasogenic waves of ICP appeared to be reliably replicated by TCD-based nICP methods.

8.2 Feasibility of TCD-based monitoring of nICP and cerebral haemodynamics

The feasibility of nICP monitoring was assessed in conditions in which the knowledge of intracranial pressure and cerebral haemodynamics could help explain many of the pathological states observed clinically (Chapter 6).

In the study assessing the presence of interhemispheric pressure gradients, the ability of TCD-based nICP to identify these patterns could represent a suitable tool in the management of TBI patients with closed head injury presenting midline shift. As it has been suggested, the interhemispheric nCPP difference showed a significant correlation with midline shift, suggesting that in TBI patients with brain's structural asymmetry, CPP is greater on the side of brain expansion, acting as the driving force to shift brain structures.

In patients with acute liver failure, different patterns of cerebral haemodynamics could be identified non-invasively during orthotopic liver transplant using a TCD-derived multimodal approach englobing nICP, nCPP, and other cerebral haemodynamics parameters. Generally, the results indicated an alteration of cerebral autoregulation, normal ICP and decreasing CPP during the transplant surgery.

The assessment of patients undergoing shoulder surgery in the beach-chair position demonstrated significant cerebral haemodynamics changes in patients with no indications of previous neurological impairment. The findings suggest that this surgical setting caused an alteration of cerebral haemodynamics, especially impairment of cerebral blood flow autoregulation. Left untreated, a significant reduction in cerebral blood flow may result in brain ischaemia and postoperative neurologic damage.

Overall, these findings confirm hypothesis II and demonstrate the feasibility of TCD-based monitoring of nICP and cerebral haemodynamics in a variety of clinical settings. In this scenario, multiparameter TCD assessment may provide an early detection of the onset of cerebrovascular derangements and potentially guide their clinical management.

8.3 Assessment of the spectral nCPP method

The novel method for nCPP monitoring proposed in this thesis has been validated in two different clinical conditions presenting changes in cerebral perfusion pressure. Such changes were associated with pharmacologically-induced rises in ABP resulting in CPP increases, and changes related to ICP increases of vasogenic origin (plateau waves of ICP) resulting in CPP decrease (Chapter 7).

In both conditions, the proposed spectral nCPP method could identify changes in CPP across time reliably, and the magnitude of these changes expressed in mmHg was reasonable. The prediction ability to detect changes in CPP was acceptable.

In the context of monitoring CPP in the time domain, these features confirm hypothesis III and confer reliability to monitoring CPP dynamics with $nCPP_s$. Furthermore, there is a need for prospective studies to validate and determine the accuracy of the method in traumatic brain injury and other conditions requiring neurocritical care. For this assessment, it is essential that the ABP transducer be zeroed at the level of the head (auditory meatus) to provide an accurate measurement of CPP.

9 DIRECTIONS OF FUTURE RESEARCH

Development of nICP/nCPP monitoring methods

Among the TCD-based methods discussed throughout this thesis, a recurrent issue regarding their estimation accuracy was the manner these methods were formed, i.e., whether they were derived from specific or general formation datasets. Although, in principle, a model based on general formation datasets should be able to englobe most of the pathophysiological events occurring in a certain population, the sample size required to form such a model needs to be extensively representative. This could represent a major limitation factor since the precision of a method would be subjective to its formation sample size.

This downside could be overcome by the application of model-based methods capable of replicating physiological phenomena, such as $nCPP_s$ presented previously. Once it does not require a formation dataset, the estimates produced by the method are individual-specific. Nevertheless, the precision of the method would be subjective to the input parameters assigned to the model. From this premise, another issue that arises is which combination of input parameters would be best to simulate cerebral pathophysiological events.

At the current state of development for nICP/nCPP monitoring methods, there is not an ideal model. However, with the advancements in computational simulation, mostly applying the concept of machine learning, the physiological model-based methods could be considered the most promising on this field. Moreover, recent improvements in TCD devices, such as robotic probes that allow automated insonation of the middle cerebral artery and auto-correction in time may open new perspectives to making long-term nICP/nCPP monitoring achievable.

Applications of nICP/nCPP monitoring

Transcranial Doppler ultrasonography has the potential to be used as an alternative diagnostic tool for the assessment of cerebral haemodynamics rather than costly and potentially risky investigations such as invasive ICP monitoring. Nevertheless, the range of TCD applications has been limited mostly to neurocritical care settings.

In many clinical conditions outside this environment, there is a void for neurologic assessment in the unconscious patient. In patients who are not undergoing brain surgery and neurocritical care, invasive monitoring that breaches the skull surgically is seldom feasible, and clinicians rely on periodic, limited assessments. Even in medical conditions in which the brain is regularly and significantly affected, such as hypoxic and metabolic encephalopathies, sepsis, refractory status epilepticus, an effective non-invasive monitoring regime has not been established yet. In these conditions, it would be ideal to monitor cerebral haemodynamics continuously, applying a TCD multiparameter assessment in association with other monitoring modalities like near infrared spectroscopy (NIRS), electroencephalography (EEG), optic nerve sheath diameter measurement (ONSD).

Techniques like ONSD measurement, parallelly investigated in the course of this thesis, may provide a better estimate of the absolute value of ICP than TCD does [224]. Furthermore, the combination of ONSD and venous TCD-derived parameters showed an improved accuracy than ONSD alone [224]. In preliminary unpublished findings, the 95% CI for prediction of ICP obtained with the combination of ONSD and venous TCD presented similar values described by Ragauskas et al. [225] ($< \pm 9$ mmHg), whose non-invasive method has been reported as having the closest accuracy to direct ICP. This method is based on a two-depth high-resolution transcranial Doppler insonation of the ophthalmic artery and does not require calibration since it relies on the equilibrium between blood flow pulsations in the intracranial and extracranial segments of the ophthalmic artery [226]. However, it can be limited in clinical practice because it requires a special two-depth TCD device and highly skilled transcranial Doppler operator with the anatomical knowledge to identify the specific location of the intracranial and extracranial segments of the ophthalmic artery. On the other hand, ONSD and venous TCD is methodologically easy, quick and repeatable [227].

As demonstrated in this thesis, TCD monitoring can provide a reliable assessment of cerebral haemodynamics, including intracranial pressure, cerebral perfusion pressure, cerebral

autoregulation. The association of these methods, alongside neurological and cerebral oxygenation assessments (EEG and NIRS, respectively) and other predictors of ICP (like ONSD and venous TCD), may provide a comprehensive multimodal assessment of the brain functions. This approach could guide oriented therapies to patients with suspicion of neurological disorders in a variety of clinical settings.

10 REFERENCES

1. Monro, A. (1783). Observations on the structure and functions of the nervous system: illustrated with tables. Edinburgh.

2. Wilson, M.H. (2016). Monro-Kellie 2.0: The dynamic vascular and venous pathophysiological components of intracranial pressure. J. Cereb. Blood Flow Metab. 36, 1338–1350.

3. Kellie. (1824). Appearances Observed in the Dissection of Two Individuals; Death from Cold and Congestion of the Brain. Tr. Med.-Chir. Soc. Edinburgh 1.

4. Magendie, F. (1842). Recherches anatomique et physiologique sur le liquide cephalo-rachidien ou cerebro-spinal. Paris: Me´ quignon-Marvis fils.

5. Burrows, G. (1848). On Disorders of the Cerebral Circulation and on the Connection between Affections of the Brain and Diseases of the Heart. Philadelphia, PA, USA: Lea & Blanchard.

6. Cushing, H. (1926). The Third Circulation in Studies in Intracranial Physiology and Surgery. London: Oxford University Press.

7. Czosnyka, M., and Pickard, J.D. (2004). Monitoring and interpretation of intracranial pressure. J. Neurol. Neurosurg. Psychiatry 75, 813–821.

8. Cardim, D., Robba, C., Donnelly, J., Bohdanowicz, M., Schmidt, B., Damian, M., Varsos, G. V, Liu, X., Cabeleira, M., Frigieri, G., Cabella, B., Smieleweski, P., Mascarenhas, S., and Czosnyka, M. (2015). Prospective study on non-invasive assessment of ICP in head injured patients: comparison of four methods. J. Neurotrauma .

9. Carney, N., Totten, A.M., O'Reilly, C., Ullman, J.S., Hawryluk, G.W.J., Bell, M.J., Bratton, S.L., Chesnut, R., Harris, O.A., Kissoon, N., Rubiano, A.M., Shutter, L., Tasker, R.C., Vavilala, M.S., Wilberger, J., Wright, D.W., and Ghajar, J. (2016). Guidelines for the Management of Severe Traumatic Brain Injury, Fourth Edition. Neurosurgery 19, 1.

10. Surgeons., B.T.F.A.A. of N.S.C. of N. (2007). Guidelines for the Management of Severe Traumatic Brain Injury 3rd Edition. J. Neurosurg. 24, Suppl, S1-106.

11. Hanlo, P.W., Peters, R.J.A., Gooskens, R.H.J.M., Heethaar, R.M., Keunen, R.W.M., Van Huffelen, A.C., Tulleken, C.A.F., and Willemse, J. (1995). Monitoring intracranial dynamics by transcranial Doppler - A new Doppler index: Trans Systolic Time. Ultrasound Med. Biol. 21, 613–621.

12. Ueno, T., Ballard, R.E., Shuer, L.M., Cantrell, J.H., Yost, W.T., and Hargens, A.R. (1998). Noninvasive measurement of pulsatile intracranial pressure using ultrasound. Acta Neurochir. Suppl. 71, 66–69.

13. Ballestero, M.F.M., Frigieri, G., Cabella, B.C.T., de Oliveira, S.M., and de Oliveira, R.S. (2017). Prediction of intracranial hypertension through noninvasive intracranial pressure waveform analysis in pediatric hydrocephalus. Child's Nerv. Syst. 33, 1517–1524.

14. Bollela, V.R., Frigieri, G., Vilar, F.C., Spavieri, D.L., Tallarico, F.J., Tallarico, G.M., Andrade, R.A.P., de Haes, T.M., Takayanagui, O.M., Catai, A.M., and Mascarenhas, S. (2017). Noninvasive intracranial pressure monitoring for HIV-associated cryptococcal meningitis. Brazilian J. Med. Biol. Res. = Rev. Bras. Pesqui. medicas e Biol. 50, e6392.

15. Michaeli, D., and Rappaport, Z.H. (2002). Tissue resonance analysis; a novel method for noninvasive monitoring of intracranial pressure. Technical note. J. Neurosurg. 96, 1132–1137.

16. Ragauskas, A., Daubaris, G., Ragaisis, V., and Petkus, V. (2003). Implementation of non-invasive brain physiological monitoring concepts. Med. Eng. Phys. 25, 667–678.

17. Querfurth, H.W., Lieberman, P., Arms, S., Mundell, S., Bennett, M., and van Horne, C. (2010). Ophthalmodynamometry for ICP prediction and pilot test on Mt. Everest. BMC Neurol. 10, 106.

18. Geeraerts, T., Launey, Y., Martin, L., Pottecher, J., Vigué, B., Duranteau, J., and Benhamou, D. (2007). Ultrasonography of the optic nerve sheath may be useful for detecting raised intracranial pressure after severe brain injury. Intensive Care Med. 33, 1704–1711.

19. Reid, A., Marchbanks, R.J., Bateman, D.E., Martin, A.M., Brightwell, A.P., and Pickard, J.D. (1989). Mean intracranial pressure monitoring by a non-invasive audiological technique: a pilot study. J. Neurol. Neurosurg. Psychiatry 52, 610–612.

20. Shimbles, S., Dodd, C., Banister, K., Mendelow, A.D., and Chambers, I.R. (2005). Clinical comparison of tympanic membrane displacement with invasive intracranial pressure measurements. Physiol. Meas. 26, 1085–1092.

21. Frank, A.M., Alexiou, C., Hulin, P., Janssen, T., Arnold, W., and Trappe, A.E. (2000). Non-invasive measurement of intracranial pressure changes by otoacoustic emissions (OAEs)--a report of preliminary data. Zentralbl. Neurochir. 61, 177–80.

22. Alperin, N.J., Lee, S.H., Loth, F., Raksin, P.B., and Lichtor, T. (2000). MR-Intracranial pressure (ICP): a method to measure intracranial elastance and pressure noninvasively by means of MR imaging: baboon and human study. Radiology 217, 877–85.

23. Bartusis, L., Zakelis, R., Daubaris, G., Ragauskas, A., Rutkauskas, S., Matijosaitis, V., and Preiksaitis, A. (2012). Ophthalmic artery as a sensor for non-invasive intracranial pressure measurement electronic system. Elektron. ir Elektrotechnika 122, 45–48.

24. Zhao, Y.L., Zhou, J.Y., and Zhu, G.H. (2005). Clinical experience with the noninvasive ICP monitoring system., in: *Acta Neurochirurgica, Supplementum*. pps. 351–355.

25. Schmidt, B., Klingelhöfer, J., Schwarze, J.J., Sander, D., and Wittich, I. (1997). Noninvasive Prediction of Intracranial Pressure Curves Using Transcranial Doppler Ultrasonography and Blood Pressure Curves. Stroke 28, 2465–2472.

26. Schmidt, B., Czosnyka, M., and Klingelhöfer, J. (2002). Clinical applications of a non-invasive ICP monitoring method. Eur. J. Ultrasound 16, 37–45.

27. Bellner, J., Romner, B., Reinstrup, P., Kristiansson, K.A., Ryding, E., and Brandt, L. (2004). Transcranial Doppler sonography pulsatility index (PI) reflects intracranial pressure (ICP). Surg. Neurol. 62, 45–51.

28. Figaji, A.A., Zwane, E., Fieggen, A.G., Siesjo, P., and Peter, J.C. (2009). Transcranial Doppler pulsatility index is not a reliable indicator of intracranial pressure in children with severe traumatic brain injury. Surg. Neurol. 72, 389–394.

29. Kashif, F.M., Heldt, T., and Verghese, G.C. (2008). Model-based estimation of intracranial pressure and cerebrovascular autoregulation. Comput. Cardiol. 35, 369–372.

30. Schmidt, B., Czosnyka, M., Schwarze, J.J., Sander, D., Gerstner, W., Lumenta, C.B., and Klingelhöfer, J. (2000). Evaluation of a method for noninvasive intracranial pressure assessment during infusion studies in patients with hydrocephalus. J. Neurosurg. 92, 793–800.

31. Schmidt, B., Czosnyka, M., Raabe, A., Yahya, H., Schwarze, J.J., Sackerer, D., Sander, D., and Klingelhöfer, J. (2003). Adaptive noninvasive assessment of intracranial pressure and cerebral autoregulation. Stroke 34, 84–89.

32. Asil, T., Uzunca, I., Utku, U., and Berberoglu, U. (2003). Monitoring of Increased Intracranial

Pressure Resulting From Cerebral Edema With Transcranial Doppler Sonography in Patients With Middle Cerebral Artery Infarction. J Ultrasound Med 22, 1049–1053.

33. Voulgaris, S.G., Partheni, M., Kaliora, H., Haftouras, N., Pessach, I.S., and Polyzoidis, K.S. (2005). Early cerebral monitoring using the transcranial Doppler pulsatility index in patients with severe brain trauma. Med. Sci. Monit. 11, CR49-R52.

34. Steinbach, G.C., Macias, B.R., Tanaka, K., Yost, W.T., and Hargens, A.R. (2005). Intracranial pressure dynamics assessed by noninvasive ultrasound during 30 days of bed rest. Aviat. Sp. Environ. Med. 76, 85–90.

35. Prunet, B., Asencio, Y., Lacroix, G., Montcriol, A., Dagain, A., Cotte, J., Esnault, P., Boret, H., Meaudre, E., and Kaiser, E. (2012). Noninvasive detection of elevated intracranial pressure using a portable ultrasound system. Am. J. Emerg. Med. 30, 936–941.

36. Kashif, F.M., Verghese, G.C., Novak, V., Czosnyka, M., and Heldt, T. (2012). Model-Based Noninvasive Estimation of Intracranial Pressure from Cerebral Blood Flow Velocity and Arterial Pressure. Sci. Transl. Med. 4, 129ra44-129ra44.

37. Wakerley, B., Yohana, K., Luen Teoh, H., Tan, C.W., Chan, B.P.L., and Sharma, V.K. (2014). Non-invasive intracranial pressure monitoring with transcranial Doppler in a patient with progressive cerebral venous sinus thrombosis. J. Neuroimaging 24, 302–4.

38. Wakerley, B.R., Kusuma, Y., Yeo, L.L.L., Liang, S., Kumar, K., Sharma, A.K., and Sharma, V.K. (2014). Usefulness of transcranial doppler-derived cerebral hemodynamic parameters in the noninvasive assessment of intracranial pressure. J. Neuroimaging , 1–6.

39. Cardim, D., Robba, C., Bohdanowicz, M., Donnelly, J., Cabella, B., Liu, X., Cabeleira, M., Smielewski, P., Schmidt, B., and Czosnyka, M. (2016). Non-invasive Monitoring of Intracranial Pressure Using Transcranial Doppler Ultrasonography: Is It Possible? Neurocrit. Care .

40. Reid, J.M., and Spencer, M.P. (1972). Ultrasonic Doppler technique for imaging blood vessels. Science (80-.). 176, 1235–1236.

41. Aaslid, R., Markwalder, T.M., and Nornes, H. (1982). Noninvasive transcranial Doppler ultrasound recording of flow velocity in basal cerebral arteries. J. Neurosurg. 57, 769–774.

42. Aaslid, R. (1986). Transcranial Doppler Sonography., in: Vienna, R.A. (ed). . New York, NY, USA: Springer, pps. 22–38.

43. Moppett, I.K., and Mahajan, R.P. (2004). Transcranial Doppler ultrasonography in anaesthesia and intensive care. Br. J. Anaesth. Br J Anaesth 93, 710–24.

44. Marinoni, M., Ginanneschi, A., Forleo, P., and Amaducci, L. (1997). Technical limits in transcranial Doppler recording: Inadequate acoustic windows. Ultrasound Med. Biol. 23, 1275–1277.

45. Tsivgoulis, G., Alexandrov, A. V., and Sloan, M.A. (2009). Advances in transcranial Doppler ultrasonography. Curr. Neurol. Neurosci. Rep. 9, 46–54.

46. Bouzat, P., Oddo, M., and Payen, J.-F. (2014). Transcranial Doppler after traumatic brain injury: is there a role? Curr. Opin. Crit. Care 20, 153–60.

47. Toole, J.. (1984). Cerebrovascular Disorders, 3rd ed. New York, 1-18 p.

48. Lindegaard, K.F., Lundar, T., Wiberg, J., Sjoberg, D., Aaslid, R., and Nornes, H. (1987). Variations in middle cerebral artery blood flow investigated with noninvasive transcranial blood velocity measurements. Stroke 18, 1025–1030.

49. Dahl, A., Lindegaard, K.F., Russell, D., Nyberg-Hansen, R., Rootwelt, K., Sorteberg, W., and

Nornes, H. (1992). A comparison of transcranial Doppler and cerebral blood flow studies to assess cerebral vasoreactivity. Stroke. 23, 15–19.

50. Matta, B., and Czosnyka, M. (2010). Transcranial Doppler Ultrasonography in Anesthesia and Neurosurgery., in: Cotrell, J.E., and Young, W.L. (eds). *Cottrell and Young'S Neuroanesthesia*, 5th ed. Elsevier, pps. 131–146.

51. Gosling, R.G., and King, D.H. (1974). Arterial assessment by Doppler-shift ultrasound. Proc. R. Soc. Med. 67, 447–9.

52. De Riva, N., Budohoski, K.P., Smielewski, P., Kasprowicz, M., Zweifel, C., Steiner, L.A., Reinhard, M., Fábregas, N., Pickard, J.D., and Czosnyka, M. (2012). Transcranial doppler pulsatility index: What it is and what it isn't. Neurocrit. Care 17, 58–66.

53. Nicoletto, H.A., and Burkman, M.H. (2009). Transcranial Doppler series part III: interpretation. Am. J. Electroneurodiagnostic Technol. 49, 244–59.

54. Nicoletto, H.A., and Burkman, M.H. (2009). Transcranial Doppler series part IV: case studies. Am. J. Electroneurodiagnostic Technol. 49, 342–60.

55. Tegeler, C.H., Crutchfield, K., Katsnelson, M., Kim, J., Tang, R., Passmore Griffin, L., Rundek, T., and Evans, G. (2013). Transcranial doppler velocities in a large, healthy population. J. Neuroimaging 23, 466–472.

56. Steiger, H.J. (1981). Carotid Doppler hemodynamics in posttraumatic intracranial hypertension. Surg. Neurol. 16, 459–61.

57. Chan, K.H., Miller, J.D., Dearden, N.M., Andrews, P.J., and Midgley, S. (1992). The effect of changes in cerebral perfusion pressure upon middle cerebral artery blood flow velocity and jugular bulb venous oxygen saturation after severe brain injury. J. Neurosurg. 77, 55–61.

58. Homburg, A.M., Jakobsen, M., and Enevoldsen, E. (1993). Transcranial Doppler recordings in raised intracranial pressure. Acta Neurol. Scand. 87, 488–493.

59. Martin, N.A., Patwardhan, R. V, Alexander, M.J., Africk, C.Z., Lee, J.H., Shalmon, E., Hovda, D.A., and Becker, D.P. (1997). Characterization of cerebral hemodynamic phases following severe head trauma: hypoperfusion, hyperemia, and vasospasm. J. Neurosurg. 87, 9–19.

60. McQuire, J.C., Sutcliffe, J.C., and Coats, T.J. (1998). Early changes in middle cerebral artery blood flow velocity after head injury. J.Neurosurg. 89, 526–532.

61. Moreno, J.A., Mesalles, E., Gener, J., Tomasa, A., Ley, A., Roca, J., and Fernández-Llamazares, J. (2000). Evaluating the outcome of severe head injury with transcranial Doppler ultrasonography. Neurosurg. Focus 8, e8.

62. Rainov, N.G., Weise, J.B., and Burkert, W. (2000). Transcranial Doppler sonography in adult hydrocephalic patients. 34-38 p.

63. Behrens, A., Lenfeldt, N., Ambarki, K., Malm, J., Eklund, A., and Koskinen, L.O. (2010). Transcranial doppler pulsatility index: Not an accurate method to assess intracranial pressure. Neurosurgery 66, 1050–1057.

64. Brandi, G., Béchir, M., Sailer, S., Haberthür, C., Stocker, R., and Stover, J.F. (2010). Transcranial color-coded duplex sonography allows to assess cerebral perfusion pressure noninvasively following severe traumatic brain injury. Acta Neurochir. (Wien). 152, 965–972.

65. Melo, J.R.T., Di Rocco, F., Blanot, S., Cuttaree, H., Sainte-Rose, C., Oliveira-Filho, J., Zerah, M., and Meyer, P.G. (2011). Transcranial Doppler can predict intracranial hypertension in children with severe traumatic brain injuries. Childs. Nerv. Syst. 27, 979–84.

66. Zweifel, C., Czosnyka, M., Carrera, E., de Riva, N., Pickard, J.D., and Smielewski, P. (2012).

Reliability of the blood flow velocity pulsatility index for assessment of intracranial and cerebral perfusion pressures in head-injured patients. Neurosurgery 71, 853–61.

67. O'Brien, N.F., Maa, T., and Reuter-Rice, K. (2015). Noninvasive screening for intracranial hypertension in children with acute, severe traumatic brain injury. J. Neurosurg. Pediatr. , 1–6.

68. Robba, C., Donnelly, J., Bertuetti, R., Cardim, D., Sekhon, M.S., Aries, M., Smielewski, P., Richards, H., and Czosnyka, M. (2015). Doppler Non-invasive Monitoring of ICP in an Animal Model of Acute Intracranial Hypertension. Neurocrit. Care .

69. Miller JD, Teasdale GM, R., and JO, et al. (eds). (1986). Estimation of cerebral perfusion pressure from arterial blood pressure and transcranial Doppler recordings., in: *Intracranial Pressure VI*. Berlin: SpringerVerlag, pps. 226–229.

70. Greenfield, J.C., and Tindall, G.T. (1965). Effect of acute increase in intracranial pressure on blood flow in the internal carotid artery of man. J. Clin. Invest. 44, 1343–51.

71. Czosnyka, M., Matta, B.F., Smielewski, P., Kirkpatrick, P.J., and Pickard, J.D. (1998). Cerebral perfusion pressure in head-injured patients: a noninvasive assessment using transcranial Doppler ultrasonography. J. Neurosurg. 88, 802–808.

72. Chan, K.H., Miller, J.D., Dearden, N.M., Andrews, P.J., and Midgley, S. (1992). The effect of changes in cerebral perfusion pressure upon middle cerebral artery blood flow velocity and jugular bulb venous oxygen saturation after severe brain injury. J Neurosurg 77, 55–61.

73. Schmidt, E.A., Czosnyka, M., Gooskens, I., Piechnik, S.K., Matta, B.F., Whitfield, P.C., and Pickard, J.D. (2001). Preliminary experience of the estimation of cerebral perfusion pressure using transcranial Doppler ultrasonography. J. Neurol. Neurosurg. Psychiatry 70, 198–204.

74. Gura, M., Silav, G., Isik, N., and Elmaci, I. (2012). Noninvasive estimation of cerebral perfusion pressure with transcranial doppler ultrasonography in traumatic brain injury. Turk. Neurosurg. 22, 411–415.

75. Rasulo, F.A., Bertuetti, R., Robba, C., Lusenti, F., Cantoni, A., Bernini, M., Girardini, A., Calza, S., Piva, S., Fagoni, N., and Latronico, N. (2017). The accuracy of transcranial Doppler in excluding intracranial hypertension following acute brain injury: a multicenter prospective pilot study. Crit. Care 21, 44.

76. Edouard, A.R., Vanhille, E., Le Moigno, S., Benhamou, D., and Mazoit, J.-X. (2005). Non-invasive assessment of cerebral perfusion pressure in brain injured patients with moderate intracranial hypertension. Br. J. Anaesth. 94, 216–21.

77. Belfort, M.A., Tooke-Miller, C., Varner, M., Saade, G., Grunewald, C., Nisell, H., and Herd, J.A. (2000). Evaluation of a noninvasive transcranial Doppler and blood pressure-based method for the assessment of cerebral perfusion pressure in pregnant women. Hypertens. pregnancy 19, 331–40.

78. Varsos, G. V, Kolias, A.G., Smielewski, P., Brady, K.M., Varsos, V.G., Hutchinson, P.J., Pickard, J.D., and Czosnyka, M. (2015). A noninvasive estimation of cerebral perfusion pressure using critical closing pressure. J. Neurosurg. , 11.

79. Nichol, J., Girling, F., Jerrard, W., Claxton, E.B., and Burton, A.C. (1951). Fundamental instability of the small blood vessels and critical closing pressures in vascular beds. Am. J. Physiol. 164, 330–44.

80. Czosnyka, M., Richards, H., Pickard, J.D., Harris, N., and Iyer, V. (1994). Frequency-dependent properties of cerebral blood transport - An experimental study in anaesthetized rabbits. Ultrasound Med. Biol. 20, 391–399.

81. Michel, E., Hillebrand, S., vonTwickel, J., Zernikow, B., and Jorch, G. (1997). Frequency

dependence of cerebrovascular impedance in preterm neonates: a different view on critical closing pressure. J. Cereb. Blood Flow Metab. 17, 1127–1131.

82. Puppo, C., Camacho, J., Yelicich, B., Moraes, L., Biestro, A., and Gomez, H. (2012). Bedside study of cerebral critical closing pressure in patients with severe traumatic brain injury: a transcranial Doppler study. Acta Neurochir. Suppl. 114, 283–288.

83. Varsos, G. V., Richards, H., Kasprowicz, M., Budohoski, K.P., Brady, K.M., Reinhard, M., Avolio, A., Smielewski, P., Pickard, J.D., and Czosnyka, M. (2013). Critical closing pressure determined with a model of cerebrovascular impedance. J. Cereb. Blood Flow Metab. 33, 235–43.

84. Kasuga, Y., Nagai, H., Hasegawa, Y., and Nitta, M. (1987). Transmission characteristics of pulse waves in the intracranial cavity of dogs. J. Neurosurg. 66, 907–914.

85. Marmarelis P, M. V. (1978). Analysis of Physiological Systems. New York: Plenum Press, 1-221 p.

86. Czosnyka, M., Smielewski, P., Kirkpatrick, P., Menon, D.K., and Pickard, J.D. (1996). Monitoring of Cerebral Autoregulation in Head-Injured Patients. Stroke 27, 1829–1834.

87. Rosner, M.J., and Becker, D.P. (1984). Origin and evolution of plateau waves. Experimental observations and a theoretical model. J. Neurosurg. 60, 312–324.

88. Muizelaar, J.P., Ward, J.D., Marmarou, A., Newlon, P.G., and Wachi, A. (1989). Cerebral blood flow and metabolism in severely head-injured children. Part 2: Autoregulation. J. Neurosurg. 71, 72–76.

89. Ursino, M., and Lodi, C.A. (1997). A simple mathematical model of the interaction between intracranial pressure and cerebral hemodynamics. J. Appl. Physiol. 82, 1256–69.

90. Xu, P., Kasprowicz, M., Bergsneider, M., and Hu, X. (2010). Improved noninvasive intracranial pressure assessment with nonlinear kernel regression. IEEE Trans. Inf. Technol. Biomed. 14, 971–978.

91. Lin, C.-J. (2001). Formulations of Support Vector Machines: A Note from an Optimization Point of View. Neural Comput. 13, 307–317.

92. Cai, D., He, X., and Han, J. (2007). Spectral regression for efficient regularized subspace learning., in: *Proceedings of the IEEE International Conference on Computer Vision*. .

93. Melgani, F., and Bazi, Y. (2008). Classification of electrocardiogram signals with support vector machines and particle swarm optimization. IEEE Trans. Inf. Technol. Biomed. 12, 667–677.

94. Douglas M. Bates, D.G.W. (2007). Nonlinear Regression Analysis and Its Applications -. Wiley [cited 2015 Sep 9] Available from: http://eu.wiley.com/WileyCDA/WileyTitle/productCd-0470139005.html.

95. Hu, X., Nenov, V., Bergsneider, M., and Martin, N. (2006). A Data mining framework of noninvasive intracranial pressure assessment. Biomed. Signal Process. Control 1, 64–77.

96. Kim, S., Scalzo, F., Bergsneider, M., Vespa, P., Martin, N., and Hu, X. (2012). Noninvasive intracranial pressure assessment based on a data-mining approach using a nonlinear mapping function. IEEE Trans. Biomed. Eng. 59, 619–626.

97. Kim, S., Hamilton, R., Pineles, S., Bergsneider, M., and Hu, X. (2013). Noninvasive intracranial hypertension detection utilizing semisupervised learning. IEEE Trans. Biomed. Eng. 60, 1126–1133.

98. Hanlo, P.W., Gooskens, R.H.J.M., Nijhuis, I.J.M., Faber, J.A.J., Peters, R.J.A., van Huffelen,

A.C., Tulleken, C.A.F., and Willemse, J. (1995). Value of transcranial Doppler indices in predicting raised ICP in infantile hydrocephalus - A study with review of the literature. Child's Nerv. Syst. 11, 595–603.

99. Czosnyka, M., Smielewski, P., Piechnik, S., Schmidt, E.A., Al-Rawi, P.G., Kirkpatrick, P.J., and Pickard, J.D. (1999). Hemodynamic characterization of intracranial pressure plateau waves in head-injured patients. J. Neurosurg. 91, 11–9.

100. Varsos, G. V., Richards, H.K., Kasprowicz, M., Reinhard, M., Smielewski, P., Brady, K.M., Pickard, J.D., and Czosnyka, M. (2014). Cessation of diastolic cerebral blood flow velocity: The role of critical closing pressure. Neurocrit. Care 20, 40–48.

101. Donnelly, J., Czosnyka, M., Harland, S., Varsos, G. V., Cardim, D., Robba, C., Liu, X., Ainslie, P.N., and Smielewski, P. (2017). Cerebral haemodynamics during experimental intracranial hypertension. J. Cereb. Blood Flow Metab. 37, 694–705.

102. Budohoski, K.P., Schmidt, B., Smielewski, P., Kasprowicz, M., Plontke, R., Pickard, J.D., Klingelhöfer, J., and Czosnyka, M. (2012). Non-invasively estimated ICP pulse amplitude strongly correlates with outcome after TBI. Acta Neurochir. Suppl. 114, 121–5.

103. Czosnyka, M., Brady, K., Reinhard, M., Smielewski, P., and Steiner, L.A. (2009). Monitoring of cerebrovascular autoregulation: Facts, myths, and missing links. Neurocrit. Care 10, 373–386.

104. Czosnyka, M., Smielewski, P., Kirkpatrick, P., Menon, D.K., and Pickard, J.D. (1996). Monitoring of cerebral autoregulation in head-injured patients. Stroke 27, 1829–1834.

105. Czosnyka, M., Smielewski, P., Piechnik, S., Steiner, L. a, and Pickard, J.D. (2001). Cerebral autoregulation following head injury. J. Neurosurg. 95, 756–763.

106. Sorrentino, E., Diedler, J., Kasprowicz, M., Budohoski, K.P., Haubrich, C., Smielewski, P., Outtrim, J.G., Manktelow, A., Hutchinson, P.J., Pickard, J.D., Menon, D.K., and Czosnyka, M. (2012). Critical thresholds for cerebrovascular reactivity after traumatic brain injury. Neurocrit. Care 16, 258–266.

107. Tiecks, F.P., Lam, A.M., Aaslid, R., and Newell, D.W. (1995). Comparison of Static and Dynamic Cerebral Autoregulation Measurements. Stroke 26, 1014–1019.

108. Panerai, R.B., White, R.P., Markus, H.S., and Evans, D.H. (1998). Grading of cerebral dynamic autoregulation from spontaneous fluctuations in arterial blood pressure. Stroke. 29, 2341–2346.

109. Aaslid, R., Blaha, M., Sviri, G., Douville, C.M., and Newell, D.W. (2007). Asymmetric dynamic cerebral autoregulatory response to cyclic stimuli. Stroke 38, 1465–1469.

110. Zeiler, F.A., Donnelly, J., Calviello, L., Menon, D., Smieleweski, P., and Czosnyka, M. (2017). Pressure Autoregulation Measurement Techniques in Adult TBI, Part I: A Scoping Review of Intermittent/Semi-Intermittent Methods. J. Neurotrauma , neu.2017.5085.

111. Steiner, L., Czosnyka, M., and Piechnik, S. (2002). Continuous monitoring of cerebrovascular pressure reactivity allows determination of optimal cerebral perfusion pressure in patients with traumatic brain injury. Crit. Care .

112. Aries, M.J.H., Czosnyka, M., Budohoski, K.P., Steiner, L.A., Lavinio, A., Kolias, A.G., Hutchinson, P.J., Brady, K.M., Menon, D.K., Pickard, J.D., and Smielewski, P. (2012). Continuous determination of optimal cerebral perfusion pressure in traumatic brain injury. Crit Care Med 40, 2456–63.

113. Czosnyka, M., Smielewski, P., Kirkpatrick, P., Laing, R.J., Menon, D., and Pickard, J.D. (1997). Continuous assessment of the cerebral vasomotor reactivity in head injury.

Neurosurgery 41, 11-7-9.

114. Hosmer, D., and Lameshow, S. (1989). Applied Logistic Regression. New York: John Wiley & Sons.

115. Robin, A.X., Turck, N., Hainard, A., Lisacek, F., Sanchez, J., Müller, M., and Xavierrobinunigech, M.X.R. (2013). Package " pROC ." 1-71 p.

116. Menon, D.K. (1999). Cerebral protection in severe brain injury: physiological determinants of outcome and their optimisation. Br. Med. Bull. 55, 226–258.

117. Chan, K.H., Miller, J.D., Dearden, N.M., Andrews, P.J., and Midgley, S. (1992). The effect of changes in cerebral perfusion pressure upon middle cerebral artery blood flow velocity and jugular bulb venous oxygen saturation after severe brain injury. J. Neurosurg. 77, 55–61.

118. Czosnyka, M., Richards, H.K., Whitehouse, H.E., and Pickard, J.D. (1996). Relationship between transcranial Doppler-determined pulsatility index and cerebrovascular resistance: an experimental study. J. Neurosurg. 84, 79–84.

119. Popovic, D., Khoo, M., and Lee, S. (2009). Noninvasive monitoring of intracranial pressure. Recent Pat. Biomed. Eng. 2, 165–179.

120. Koskinen, L.O.D., and Olivecrona, M. (2005). Clinical experience with the intraparenchymal intracranial pressure monitoring Codman microsensor system. Neurosurgery 56, 693–697.

121. Eide, P.K., and Sorteberg, W. (2010). Simultaneous measurements of intracranial pressure parameters in the epidural space and in brain parenchyma in patients with hydrocephalus. J. Neurosurg. 113, 1317–25.

122. Cardim, D., Czosnyka, M., Donnelly, J., Robba, C., Cabella, B.C.T., Liu, X., Cabeleira, M.T., Smielewski, P., Haubrich, C., Garnett, M.R., Pickard, J.D., and Czosnyka, Z. (2016). Assessment of non-invasive ICP during CSF infusion test: an approach with transcranial Doppler. Acta Neurochir. (Wien). 158, 279–87.

123. Weerakkody, R.A., Czosnyka, M., Schuhmann, M.U., Schmidt, E., Keong, N., Santarius, T., Pickard, J.D., and Czosnyka, Z. (2011). Clinical assessment of cerebrospinal fluid dynamics in hydrocephalus. Guide to interpretation based on observational study. Acta Neurol. Scand. 124, 85–98.

124. Katzman, R., and Hussey, F. (1970). A simple constant-infusion manometric test for measurement of CSF absorption. I. Rationale and method. Neurology 20, 534–44.

125. Czosnyka, Z.H., Czosnyka, M., Whitfield, P.C., Donovan, T., Pickard, J.D., Milhorat, T.H., Selman, W.R., Gjerris, F., and Juhler, M. (2002). Cerebral autoregulation among patients with symptoms of hydrocephalus. Neurosurgery 50, 526–533.

126. Chin, K.Y., and Panerai, R.B. (2012). Comparative study of Finapres devices. Blood Press. Monit. 17, 171–8.

127. Stokes, D.N., Clutton-Brock, T., Patil, C., Thompson, J.M., and Hutton, P. (1991). Comparison of invasive and non-invasive measurement of continuous arterial pressure using the Finapres. Br. J. Anaesth. 67, 26–35.

128. Sloan, M.A., Alexandrov, A. V, Tegeler, C.H., Spencer, M.P., Caplan, L.R., Feldmann, E., Wechsler, L.R., Newell, D.W., Gomez, C.R., Babikian, V.L., Lefkowitz, D., Goldman, R.S., Armon, C., Hsu, C.Y., and Goodin, D.S. (2004). Assessment: transcranial Doppler ultrasonography: report of the Therapeutics and Technology Assessment Subcommittee of the American Academy of Neurology. Neurology 62, 1468–1481.

129. Schmidt, E.A., Czosnyka, Z., Momjian, S., Czosnyka, M., Bech, R.A., and Pickardl, J.D. (2005). Intracranial baroreflex yielding an early Cushing response in human., in: *Acta*

Neurochirurgica, Supplementum. pps. 253–256.

130. Cardim, D., Schmidt, B., Robba, C., Donnelly, J., Puppo, C., Czosnyka, M., and Smielewski, P. (2016). Transcranial Doppler Monitoring of Intracranial Pressure Plateau Waves. Neurocrit. Care , 1–9.

131. Lundburg, N. (1960). Continuous recording and control of ventricular fluid pressure in neurosurgical practice. Acta Psychiatr. Scand. Suppl. 36, 1–193.

132. Janny, P. (1950). La Pression Intracranienne Chez l'Homme.

133. Avezaat, C.J., van Eijndhoven, J.H., and Wyper, D.J. (1979). Cerebrospinal fluid pulse pressure and intracranial volume-pressure relationships. J. Neurol. Neurosurg. Psychiatry 42, 687–700.

134. Hayashi, M., Handa, Y., Kobayashi, H., Kawano, H., Ishii, H., and Hirose, S. (1991). Plateau-wave phenomenon (I). Correlation between the appearance of plateau waves and CSF circulation in patients with intracranial hypertension. Brain 114 (Pt 6, 2681–91.

135. Hayashi, M., Kobayashi, H., Kawano, H., Yamamoto, S., and Maeda, T. (1984). Cerebral blood flow and ICP patterns in patients with communicating hydrocephalus after aneurysm rupture. J Neurosurg 61, 30–36.

136. Hayashi, M., Ishii, H., Handa, Y., Kobayashi, H., Kawano, H., and Kabuto, M. (1987). Role of the medulla oblongata in plateau-wave development in dogs. J. Neurosurg. 67, 97–101.

137. Renier, D., Sainte-Rose, C., Marchac, D., and Hirsch, J.F. (1982). Intracranial pressure in craniostenosis. J. Neurosurg. 57, 370–377.

138. Castellani, G., Zweifel, C., Kim, D.-J., Carrera, E., Radolovich, D.K., Smielewski, P., Hutchinson, P.J., Pickard, J.D., and Czosnyka, M. (2009). Plateau waves in head injured patients requiring neurocritical care. Neurocrit. Care 11, 143–150.

139. Ursino, M., and Di Giammarco, P. (1991). A mathematical model of the relationship between cerebral blood volume and intracranial pressure changes: the generation of plateau waves. Ann. Biomed. Eng. 19, 15–42.

140. Schmidt, B., Czosnyka, M., Schwarze, J.J., Sander, D., Gerstner, W., Lumenta, C.B., Pickard, J.D., and Klingelhöfer, J. (1999). Cerebral vasodilatation causing acute intracranial hypertension: a method for noninvasive assessment. J. Cereb. Blood Flow Metab. 19, 990–996.

141. Czosnyka, M., Smielewski, P., Piechnik, S., Schmidt, E.A., Al-Rawi, P.G., Kirkpatrick, P.J., and Pickard, J.D. (1999). Hemodynamic characterization of intracranial pressure plateau waves in head-injury patients. J. Neurosurg. 91, 11–19.

142. Mindermann, T. (1999). Pressure gradients within the central nervous system. J. Clin. Neurosci. 6, 464–466.

143. Gambardella, G., D'Avella, D., and Tomasello, F. (1992). Monitoring of brain tissue pressure with a fiberoptic device. Neurosurgery 31, 918-21–2.

144. Sahuquillo, J., Poca, M.A., Arribas, M., Garnacho, A., and Rubio, E. (1999). Interhemispheric supratentorial intracranial pressure gradients in head-injured patients: are they clinically important? J. Neurosurg. 90, 16–26.

145. Wolfla, C.E., Luerssen, T.G., and Bowman, R.M. (1997). Regional brain tissue pressure gradients created by expanding extradural temporal mass lesion. J. Neurosurg. 86, 505–10.

146. Wolfla, C.E., Luerssen, T.G., Bowman, R.M., and Putty, T.K. (1996). Brain tissue pressure gradients created by expanding frontal epidural mass lesion. J. Neurosurg. 84, 642–7.

147. Turner, J.M., Gibson, R.M., McDowall, D.G., and Nahhas, F. (1975). Further Experiences with Extradural Pressure Monitoring., in: *Intracranial Pressure II*. Berlin, Heidelberg: Springer Berlin Heidelberg, pps. 397–402.

148. Marshall, L.F., Zovickian, J., Ostrup, R., and Seelig, J.M. (1986). Multiple Simultaneous Recordings of ICP in Patients with Acute Mass Lesions., in: *Intracranial Pressure VI*. Berlin, Heidelberg: Springer Berlin Heidelberg, pps. 184–186.

149. Chambers, I.R., Kane, P.J., Signorini, D.F., Jenkins, A., and Mendelow, A.D. (1998). Bilateral ICP monitoring: its importance in detecting the severity of secondary insults. Acta Neurochir. Suppl. 71, 42–3.

150. Mindermann, T., Reinhardt, H., and Gratzl, O. (1992). Significant lateralisation of supratentorial ICP after blunt head trauma. Acta Neurochir. (Wien). 116, 60–1.

151. Mindermann, T., and Gratzl, O. (1998). Interhemispheric pressure gradients in severe head trauma in humans. Acta Neurochir. Suppl. 71, 56–58.

152. Weaver, D.D., Winn, H.R., and Jane, J.A. (1982). Differential intracranial pressure in patients with unilateral mass lesions. J. Neurosurg. 56, 660–665.

153. Symon, L., Pasztor, E., Branston, N.M., and Dorsch, N.W. (1974). Effect of supratentorial space-occupying lesions on regional intracranial pressure and local cerebral blood flow: an experimental study in baboons. J. Neurol. Neurosurg. Psychiatry 37, 617–26.

154. Patel, H.C., Menon, D.K., Tebbs, S., Hawker, R., Hutchinson, P.J., and Kirkpatrick, P.J. (2002). Specialist neurocritical care and outcome from head injury. Intensive Care Med. 28, 547–553.

155. Lawrence F. Marshall, Sharon Bowers Marshall, Melville R. Klauber, Marjan van Berkum Clark, Howard M. Eisenberg, John A. Jane, Thomas G. Luerssen, Anthony Marmarou, and Mary A. Foulkes. (1991). A new classification of head injury based on computerized tomography. J. Neurosurg. 75, S14–S20.

156. Valadka, A.B., Gopinath, S.P., and Robertson, C.S. (2000). Midline shift after severe head injury: pathophysiologic implications. J. Trauma 49, 1-8-10.

157. Miller, J.D., Peeler, D.F., Pattisapu, J., and Parent, A.D. (1987). Supratentorial pressures. Part I: Differential intracranial pressures. Neurol. Res. 9, 193–7.

158. Lee, J.H., Kelly, D.F., Oertel, M., McArthur, D.L., Glenn, T.C., Vespa, P., Boscardin, W.J., and Martin, N. a. (2001). Carbon dioxide reactivity, pressure autoregulation, and metabolic suppression reactivity after head injury: a transcranial Doppler study. J. Neurosurg. 95, 222–232.

159. Villalba, N., Sonkusare, S.K., Longden, T.A., Tran, T.L., Sackheim, A.M., Nelson, M.T., Wellman, G.C., and Freeman, K. (2014). Traumatic Brain Injury Disrupts Cerebrovascular Tone Through Endothelial Inducible Nitric Oxide Synthase Expression and Nitric Oxide Gain of Function. J. Am. Heart Assoc. 3, e001474–e001474.

160. Werner, C., and Engelhard, K. (2007). Pathophysiology of traumatic brain injury. Br. J. Anaesth. 99, 4–9.

161. DeWitt, D.S., and Prough, D.S. (2003). Traumatic cerebral vascular injury: the effects of concussive brain injury on the cerebral vasculature. J. Neurotrauma 20, 795–825.

162. Schmidt, E.A., Czosnyka, M., Steiner, L.A., Balestreri, M., Smielewski, P., Piechnik, S.K., Matta, B.F., and Pickard, J.D. (2003). Asymmetry of pressure autoregulation after traumatic brain injury. J. Neurosurg. 99, 991–998.

163. Kumar, A., Schmidt, E.A., Hiler, M., Smielewski, P., Pickard, J.D., and Czosnyka, M. (2005).

Asymmetry of critical closing pressure following head injury. J. Neurol. Neurosurg. Psychiatry 76, 1570–1573.

164. Varsos, G. V., Kasprowicz, M., Smielewski, P., and Czosnyka, M. (2014). Model-based indices describing cerebrovascular dynamics. Neurocrit. Care 20, 142–157.

165. Czosnyka, M., Smielewski, P., Timofeev, I., Lavinio, A., Guazzo, E., Hutchinson, P., and Pickard, J.D. (2007). Intracranial pressure: more than a number. Neurosurg. Focus 22, E10.

166. Blei, A.T. (2007). Brain edema in acute liver failure: Can it be prevented? Can it be treated? J. Hepatol. 46, 564–569.

167. Blei, A.T. (2005). The pathophysiology of brain edema in acute liver failure. Neurochem. Int. 47, 71–77.

168. Ott, P., and Vilstrup, H. (2014). Cerebral effects of ammonia in liver disease: current hypotheses. Metab. Brain Dis. 29, 901–911.

169. Bernal, W., Hyyrylainen, A., Gera, A., Audimoolam, V.K., McPhail, M.J.W., Auzinger, G., Rela, M., Heaton, N., O'Grady, J.G., Wendon, J., and Williams, R. (2013). Lessons from look-back in acute liver failure? A single centre experience of 3300 patients. J. Hepatol. 59, 74–80.

170. Chan, G., Taqi, A., Marotta, P., Levstik, M., McAlister, V., Wall, W., and Quan, D. (2009). Long-term outcomes of emergency liver transplantation for acute liver failure. Liver Transplant. 15, 1696–1702.

171. Tan, W.-F., Steadman, R.H., Farmer, D.G., Hong, J.C., Busuttil, R.W., Apinyachon, W., and Xia, V.W. (2012). Pretransplant neurological presentation and severe posttransplant brain injury in patients with acute liver failure. Transplantation 94, 768–74.

172. Iwatsuki, S., Stieber, A.C., Marsh, J.W., Tzakis, A.G., Todo, S., Koneru, B., Makowka, L., Gordon, R.D., and Starzl, T.E. (1989). Liver transplantation for fulminant hepatic failure. Transplant. Proc. 21, 2431–4.

173. Bismuth, H., Samuel, D., Gugenheim, J., Castaing, D., Bernuau, J., Rueff, B., and Benhamou, J.P. (1987). Emergency liver transplantation for fulminant hepatitis. Ann. Intern. Med. 107, 337–41.

174. Emond, J.C., Aran, P.P., Whitington, P.F., Broelsch, C.E., and Baker, A.L. (1989). Liver transplantation in the management of fulminant hepatic failure. Gastroenterology 96, 1583–1588.

175. Vickers, C., Neuberger, J., Buckels, J., McMaster, P., and Elias, E. (1988). Transplantation of the liver in adults and children with fulminant hepatic failure. J. Hepatol. 7, 143–50.

176. Larsen, F.S., Ejlersen, E., Hansen, B.A., Knudsen, G.M., Tygstrup, N., and Secher, N.H. (1995). Functional loss of cerebral blood flow autoregulation in patients with fulminant hepatic failure. J. Hepatol. 23, 212–217.

177. Keays, R.T., Alexander, G.J., and Williams, R. (1993). The safety and value of extradural intracranial pressure monitors in fulminant hepatic failure. J. Hepatol. 18, 205–9.

178. Lidofsky, S.D., Bass, N.M., Prager, M.C., Washington, D.E., Read, A.E., Wright, T.L., Ascher, N.L., Roberts, J.P., Scharschmidt, B.F., and Lake, J.R. (1992). Intracranial pressure monitoring and liver transplantation for fulminant hepatic failure. Hepatology 16, 1–7.

179. Karvellas, C.J., Fix, O.K., Battenhouse, H., Durkalski, V., Sanders, C., Lee, W.M., and U S Acute Liver Failure Study Group. (2014). Outcomes and complications of intracranial pressure monitoring in acute liver failure: a retrospective cohort study. Crit. Care Med. 42, 1157–67.

180. Bratton, S.L., Chestnut, R.M., Ghajar, J., McConnell Hammond, F.F., Harris, O.A., Hartl, R.,

Manley, G.T., Nemecek, A., Newell, D.W., Rosenthal, G., Schouten, J., Shutter, L., Timmons, S.D., Ullman, J.S., Videtta, W., Wilberger, J.E., and Wright, D.W. (2007). Guidelines for the management of severe traumatic brain injury. IX. Cerebral perfusion thresholds. J. Neurotrauma 24 Suppl 1, S59-64.

181. Bindi, M.L., Biancofiore, G., Esposito, M., Meacci, L., Bisà, M., Mozzo, R., Urbani, L., Catalano, G., Montin, U., and Filipponi, F. (2008). Transcranial Doppler Sonography is Useful for the Decision-Making at the Point of Care in Patients with Acute Hepatic Failure: A Single Centre's Experience. J. Clin. Monit. Comput. 22, 449–452.

182. Abdo, A., Pérez-Bernal, J., Hinojosa, R., Porras, F., Castellanos, R., Gómez, F., Gutiérrez, J., Castellanos, A., Leal, G., Espinosa, N., and Gómez-Bravo, M. (2015). Cerebral Hemodynamics Patterns by Transcranial Doppler in Patients With Acute Liver Failure. Transplant. Proc. 47, 2647–2649.

183. Ardizzone, G., Arrigo, A., Panaro, F., Ornis, S., Colombi, R., Distefano, S., Jarzembowski, T.M., and Cerruti, E. (2004). Cerebral hemodynamic and metabolic changes in patients with fulminant hepatic failure during liver transplantation. Transplant. Proc. 36, 3060–3064.

184. Ardizzone, G., Arrigo, A., Panaro, F., Centanaro, M., Demartini, M., Pellizzari, A., Cifelli, A., Jarzembowsky, T.M., Valente, U., and Siani, C. (2004). Modifications of cerebral vascular resistance and autoregulation after graft reperfusion during human orthotopic liver transplantation. Transplant. Proc. 36, 1473–1478.

185. Abdo, A., López, O., Fernández, A., Santos, J., Castillo, J., Castellanos, R., González, L., Gómez, F., and Limonta, D. (2003). Transcranial Doppler sonography in fulminant hepatic failure. Transplant. Proc. 35, 1859–1860.

186. Raschke, R.A., Curry, S.C., Rempe, S., Gerkin, R., Little, E., Manch, R., Wong, M., Ramos, A., and Leibowitz, A.I. (2008). Results of a protocol for the management of patients with fulminant liver failure. Crit. Care Med. 36, 2244–2248.

187. Maloney, P.R., Mallory, G.W., Atkinson, J.L.D., Wijdicks, E.F., Rabinstein, A.A., and Van Gompel, J.J. (2016). Intracranial Pressure Monitoring in Acute Liver Failure: Institutional Case Series. Neurocrit. Care 25, 86–93.

188. Keays, R., Potter, D., O'Grady, J., Peachey, T., Alexander, G., and Williams, R. (1991). Intracranial and cerebral perfusion pressure changes before, during and immediately after orthotopic liver transplantation for fulminant hepatic failure. Q J Med 79, 425–433.

189. Detry, O., Arkadopoulos, N., Ting, P., Kahaku, E., Margulies, J., Arnaout, W., Colquhoun, S.D., Rozga, J., and Demetriou, A.A. (1999). Intracranial pressure during liver transplantation for fulminant hepatic failure. Transplantation 67, 767–70.

190. Peruto, C.M., Ciccotti, M.G., and Cohen, S.B. (2009). Shoulder Arthroscopy Positioning: Lateral Decubitus Versus Beach Chair. Arthrosc. J. Arthrosc. Relat. Surg. 25, 891–896.

191. Trentman, T.L., Fassett, S.L., Thomas, J.K., Noble, B.N., Renfree, K.J., and Hattrup, S.J. (2011). More hypotension in patients taking antihypertensives preoperatively during shoulder surgery in the beach chair position. Can. J. Anaesth. 58, 993–1000.

192. Buhre, W., Weyland, A., Buhre, K., Kazmaier, S., Mursch, K., Schmidt, M., Sydow, M., and Sonntag, H. (2000). Effects of the sitting position on the distribution of blood volume in patients undergoing neurosurgical procedures. Br. J. Anaesth. 84, 354–7.

193. Bhatti, M.T., and Enneking, and F.K. (2003). Visual Loss and Ophthalmoplegia After Shoulder Surgery. Anesth. Analg. , 899–902.

194. Morandi, X., Riffaud, L., Amlashi, S.F.A., and Brassier, G. (2004). Extensive spinal cord infarction after posterior fossa surgery in the sitting position: case report. Neurosurgery 54,

1512-5-6.

195. Pohl, A., and Cullen, D.J. (2005). Cerebral ischemia during shoulder surgery in the upright position: a case series. J. Clin. Anesth. 17, 463–469.

196. Friedman, D.J., Parnes, N.Z., Zimmer, Z., Higgins, L.D., and Warner, J.J.P. (2009). Prevalence of cerebrovascular events during shoulder surgery and association with patient position. Orthopedics 32.

197. Weber, S.C., Abrams, J.S., and Nottage, W.M. (2002). Complications associated with arthroscopic shoulder surgery. Arthroscopy 18, 88–95.

198. Yadeau, J.T., Casciano, M., Liu, S.S., Edmonds, C.R., Gordon, M., Stanton, J., John, R., Shaw, P.M., Wilfred, S.E., and Stanton, M. (2011). Stroke, regional anesthesia in the sitting position, and hypotension: a review of 4169 ambulatory surgery patients. Reg. Anesth. Pain Med. 36, 430–5.

199. Papadonikolakis, A., Wiesler, E.R., Olympio, M.A., and Poehling, G.G. (2008). Avoiding catastrophic complications of stroke and death related to shoulder surgery in the sitting position. Arthroscopy 24, 481–2.

200. Drummond, J.C., Lee, R.R., and Howell, J.P. (2012). Focal cerebral ischemia after surgery in the "beach chair" position: the role of a congenital variation of circle of Willis anatomy. Anesth. Analg. 114, 1301–3.

201. McCulloch, T.J., Liyanagama, K., and Petchell, J. (2010). Relative hypotension in the beach-chair position: Effects on middle cerebral artery blood velocity. Anaesth. Intensive Care 38, 486–491.

202. Hanouz, J.-L., Fiant, A.-L., and Gérard, J.-L. (2016). Middle cerebral artery blood flow velocity during beach chair position for shoulder surgery under general anesthesia. J. Clin. Anesth. 33, 31–36.

203. Laflam, A., Joshi, B., Brady, K., Yenokyan, G., Brown, C., Everett, A., Selnes, O., McFarland, E., and Hogue, C.W. (2015). Shoulder Surgery in the Beach Chair Position Is Associated with Diminished Cerebral Autoregulation but No Differences in Postoperative Cognition or Brain Injury Biomarker Levels Compared with Supine Positioning. Anesth. Analg. 120, 176–185.

204. Strebel, S., Lam, A.M., Matta, B., Mayberg, T.S., Aaslid, R., and Newell, D.W. (1995). Dynamic and static cerebral autoregulation during isoflurane, desflurane, and propofol anesthesia. Anesthesiology 83, 66–76.

205. Grathwohl, K.W., Black, I.H., Spinella, P.C., Sweeney, J., Robalino, J., Helminiak, J., Grimes, J., Gullick, R., and Wade, C.E. (2008). Total Intravenous Anesthesia Including Ketamine versus Volatile Gas Anesthesia for Combat-related Operative Traumatic Brain Injury. Anesthesiology 109, 44–53.

206. Summors, A.C., Gupta, A.K., and Matta, B.F. (1999). Dynamic cerebral autoregulation during sevoflurane anesthesia: a comparison with isoflurane. Anesth. Analg. 88, 341–345.

207. Gupta, S., Heath, K., and Matta, B.F. (1997). Effect of incremental doses of sevoflurane on cerebral pressure autoregulation in humans. Br J Anaesth 79, 469–472.

208. Schlünzen, L., Cold, G.E., Rasmussen, M., and Vafaee, M.S. (2006). Effects of dose-dependent levels of isoflurane on cerebral blood flow in healthy subjects studied using positron emission tomography. Acta Anaesthesiol. Scand. 50, 306–312.

209. Hug Jr., C.C., McLeskey, C.H., Nahrwold, M.L., Roizen, M.F., Stanley, T.H., Thisted, R.A., Walawander, C.A., White, P.F., Apfelbaum, J.L., and Grasela, T.H. (1993). Hemodynamic effects of propofol: Data from over 25,000 patients. Anesth. Analg. 77, S21–S29.

210. Smith, J.J., Porth, C.M., and Erickson, M. (1994). Hemodynamic response to the upright posture. J. Clin. Pharmacol. 34, 375–386.

211. Pin-On, P., Schroeder, D., and Munis, J. (2013). The hemodynamic management of 5177 neurosurgical and orthopedic patients who underwent surgery in the sitting or "beach chair" Position without incidence of adverse neurologic events. Anesth. Analg. 116, 1317–1324.

212. Buget, M.I., Atalar, A.C., Edipoglu, I.S., Sungur, Z., Sivrikoz, N., Karadeniz, M., Saka, E., Kucukay, S., and Senturk, M.N. (2016). Patient State Index e alterações do fluxo sanguíneo cerebral durante artroscopia do ombro em posição de cadeira de praia. Brazilian J. Anesthesiol. 66, 470–474.

213. Czosnyka, M., SR, W., and R, J. (2015). Calculation of cerebral perfusion pressure in the management of traumatic brain injury: joint position statement by the councils of the Neuroanaesthesia and Critical Care Society of Great Britain and Ireland (NACCS) and the Society of British Neurological Surgeons (SBNS). Br. J. Anaesth. 115, 487–488.

214. Van Aken, H., and Miller, E. (2000). Deliberate hypotension., in: Miller, R. (ed). *Anesthesia*, 5th ed. New York: Churchill Livingstone, pps. 1470–90.

215. Zacchetti, L., Magnoni, S., Di Corte, F., Zanier, E.R., and Stocchetti, N. (2015). Accuracy of intracranial pressure monitoring: systematic review and meta-analysis. Crit. Care 19, 420.

216. Schmidt, E.A., Czosnyka, M., Matta, B.F., Gooskens, I., Piechnik, S., and Pickard, J.D. (2000). Non-invasive cerebral perfusion pressure (nCPP): evaluation of the monitoring methodology in head injured patients. Acta Neurochir. Suppl. 76, 451–2.

217. Czosnyka, M., Piechnik, S., Richards, H.K., Kirkpatrick, P., Smielewski, P., and Pickard, J.D. (1997). Contribution of mathematical modelling to the interpretation of bedside tests of cerebrovascular autoregulation. J. Neurol. Neurosurg. Psychiatry 63, 721–31.

218. Avezaat, C.J.J., and van Eijndhoven, J.H.M. (1986). The role of the pulsatile pressure variations in intracranial pressure monitoring. Neurosurg. Rev. 9, 113–120.

219. Balédent, O., Gondry-Jouet, C., Stoquart-Elsankari, S., Bouzerar, R., Le Gars, D., and Meyer, M.E. (2006). Value of phase contrast magnetic resonance imaging for investigation of cerebral hydrodynamics. J. Neuroradiol. 33, 292–303.

220. Stoquart-ElSankari, S., Lehmann, P., Villette, A., Czosnyka, M., Meyer, M.-E., Deramond, H., and Bal?dent, O. (2009). A Phase-Contrast MRI Study of Physiologic Cerebral Venous Flow. J. Cereb. Blood Flow Metab. 29, 1208–1215.

221. Panerai, R.B. (2003). The critical closing pressure of the cerebral circulation. Med. Eng. Phys. 25, 621–632.

222. Steiner, L.A., Coles, J.P., Johnston, A.J., Chatfield, D.A., Smielewski, P., Fryer, T.D., Aigbirhio, F.I., Clark, J.C., Pickard, J.D., Menon, D.K., and Czosnyka, M. (2003). Assessment of Cerebrovascular Autoregulation in Head-Injured Patients. Stroke 34.

223. Eide, P.K., Park, E.-H., and Madsen, J.R. (2010). Arterial blood pressure vs intracranial pressure in normal pressure hydrocephalus. Acta Neurol. Scand. 122, 262–9.

224. Robba, C., Cardim, D., Tajsic, T., Pietersen, J., Bulman, M., Donnelly, J., Lavinio, A., Gupta, A., Menon, D.K., Hutchinson, P.J.A., and Czosnyka, M. (2017). Ultrasound non-invasive measurement of intracranial pressure in neurointensive care: A prospective observational study. PLOS Med. 14, e1002356.

225. Koskinen, L.O.D., Malm, J., Zakelis, R., Bartusis, L., Ragauskas, A., and Eklund, A. (2016). Can intracranial pressure be measured non-invasively bedside using a two-depth Doppler-technique? J. Clin. Monit. Comput. , 1–9.

226. Ragauskas, A., Bartusis, L., Piper, I., Zakelis, R., Matijosaitis, V., Petrikonis, K., and Rastenyte, D. (2014). Improved diagnostic value of a TCD-based non-invasive ICP measurement method compared with the sonographic ONSD method for detecting elevated intracranial pressure. Neurol. Res. 36, 607–14.

227. Schoser, B.G., Riemenschneider, N., and Hansen, H.C. (1999). The impact of raised intracranial pressure on cerebral venous hemodynamics: a prospective venous transcranial Doppler ultrasonography study. J. Neurosurg. 91, 744–749.